2022

Transient Experimental Study of a Latent Heat Thermal Energy Storage in a Phase Change Material-Air-Liquid Heat Exchanger

Serena Askar
University of Windsor

Transient experimental study of a latent heat thermal energy storage in a phase
change material-air-liquid heat exchanger

By

Serena Askar

A Dissertation
Submitted to the Faculty of Graduate Studies
through the Department of Mechanical, Automotive, and Materials Engineering
in Partial Fulfillment of the Requirements for
the Degree of Doctor of Philosophy
at the University of Windsor

Windsor, Ontario, Canada

2022

Transient experimental study of a latent heat thermal energy storage in a phase change material-air-liquid heat exchanger

by

Serena Askar

APPROVED BY:

_____
G. Jarjoura, External Examiner
Dalhousie University

_____
X. Nie
Department of Mechanical, Automotive, and Materials Engineering

_____
N. Zamani
Department of Mechanical, Automotive, and Materials Engineering

_____
G. Nasif
Department of Mechanical, Automotive, and Materials Engineering

_____
A. Fartaj, Advisor
Department of Mechanical, Automotive, and Materials Engineering

September 6, 2022

DECLARATION OF CO-AUTHORSHIP/PREVIOUS PUBLICATION

I.   Co-Authorship

I hereby declare that this dissertation incorporates the findings of an experimental research with the supervision of Professor A. Fartaj at the University of Windsor. This work is a collaboration with Dr. S. Fotowat and Mr. M. Momeni. I confirm that I am the primary author and have the credit authorship contribution in conceptualization, methodology, data curation, validation, investigation, writing- original draft, writing - review & editing, data analysis, visualization, results interpretation, and graphing. Professor Fartaj contributed to supervision, conceptualization, visualization, methodology, writing - review & editing. The contributions of Dr. Fotowat was in the assistance of running experiments and review the journal papers providing comments and suggestions for the first published journal paper and the second under review journal paper. Mr. Momeni's contribution is in the review and editing of the second paper (accepted) with comments and suggestions.

 I am aware of the University of Windsor Senate Policy on Authorship and I certify that I have properly acknowledged the contribution of other researchers to my dissertation, and have obtained written permission from each of the co-author(s) to include the above material(s) in my dissertation.

I certify that, with the above qualification, this dissertation, and the research to which it refers, is the product of my own work.

II.   Previous Publication

This dissertation includes [2] original papers that have been previously published/submitted to journals for publication, as follows:

Publication title/Full citation	Status
Serena Askar, Shahram Fotowat, Amir Fartaj, 2021, "Transient experimental investigation of airside heat transfer in a crossflow heat exchanger". Applied Thermal Engineering, Volume 199, 117516, ISSN 1359-4311, https://doi.org/10.1016/j.applthermaleng.2021.117516.	Published, Permission granted and included in Appendix B

Serena Askar, Shahram Fotowat, Mahdi Momeni, Amir Fartaj, 2022, "Transient experimental study of a latent heat thermal energy storage in a heat exchanger for effective thermal management". Journal of Energy Storage, EST-D-22-01786, ref. # EST_105680.	Accepted

I certify that I have obtained a written permission from the copyright owner(s) to include the above published material in my dissertation. I certify that the above material describes work completed during my registration as a graduate student at the University of Windsor.

III.   General

I declare that, to the best of my knowledge, my dissertation does not infringe upon anyone's copyright nor violate any proprietary rights and that any ideas, techniques, quotations, or any other material from the work of other people included in my dissertation, published or otherwise, are fully acknowledged in accordance with the standard referencing practices. Furthermore, to the extent that I have included copyrighted material that surpasses the bounds of fair dealing within the meaning of the Canada Copyright Act, I certify that I have obtained a written permission from the copyright owner to include such material in my dissertation.

I declare that this is a true copy of my dissertation, including any final revisions, as approved by my dissertation committee and the Graduate Studies office, and that this dissertation has not been submitted for a higher degree to any other University or Institution.

ABSTRACT

The increase in energy consumption and the demand for effective thermal management systems necessitate the search for enhanced heat exchangers with high thermal performance, lower weight, and compact sizes. Crossflow heat exchangers are a key component in the thermal management system of many industries such as HVAC, automotive, etc. Generally, heat exchangers are characterized based on their steady state operating conditions. However, a transient analysis helps predict the behavior of heat exchangers when they experience variations in their operational conditions in terms of fluid flow rate and temperature.

Thermal management and thermal comfort can be achieved through active and passive cooling or heating. The transient analysis of active air heating and cooling provides an insight on the response of the heat exchanger to the imposed variations and the time duration in reaching final steady state conditions. On the other hand, passive air cooling represented by a latent heat thermal energy storage offers a solution to provide thermal comfort to occupants for short periods of time. The increasing interest in the thermal energy storage is due to the rising demands for energy, increasing cost, and environmental and economic concerns which need an efficient utilization of existing energy sources and a reduction in energy consumption. A phase change material PCM is introduced as a latent heat thermal energy storage offering a clean compact thermal storage technology that provides extended thermal comfort with possible environmental and energy savings.

The dynamic response of a cross flow heat exchanger subjected to airside mass velocity changes is studied. The transient air heating and cooling performance of the heat exchanger due to step changes in airside mass velocity ratios is examined using

dimensional and dimensionless parameters. Results are shown in terms of fluids heat transfer rates, dimensionless outlet temperatures, heat transfer coefficient, Colburn j-factor, and Nusselt number. A generalized empirical correlation to predict the airside Nusselt number as a function of air mass velocity ratio was derived for each of the cases. The results demonstrate that both fluids response is not instantaneous to the step imposed and the magnitude of the step has a dissimilar effect on each fluid's response time. The increase in the step change results in higher fluids response time.

Passive air cooling is studied due to the implementation of the start-stop function in many vehicles for fuel savings and the increasing demand for electric and hybrid vehicles which require a solution to provide extended passenger thermal comfort. An experimental investigation of an innovative PCM-air-liquid meso heat exchanger to extend the thermal comfort in a vehicle during short periods of engine shutdown is presented. Extended surfaces (fins) are placed inside the PCM medium and integrated throughout the whole heat exchanger to enable and improve the transfer of thermal energy between the PCM and the air. The effect of air mass flow rate variation on the PCM discharging time is discussed. A comparison of heat transfer when using PCM to no PCM case revealed a 120 kJ released from the PCM during the discharging process. Furthermore, doubling the air mass flow rate resulted in a 29% decrease in the cumulative energy transferred to the air. The current experimental results indicate that the use of PCM extends the airside cooling time by more than 4 minutes, thus provides additional thermal comfort. The presented dynamic results along with the PCM efficient thermal energy storing and releasing processes offer a productive thermal management, energy, and environmental savings.

DEDICATION

Dedicated to

my family,

who offers me a continuous support

ACKNOWLEDGEMENTS

TABLE OF CONTENTS

LIST OF TABLES

LIST OF FIGURES

LIST OF APPENDICES

NOMENCLATURE/ ABBREVIATIONS

A	Area [m^2]
A$_a$	Total airside heat transfer area [m^2]
A$_{Fin}$	Fin area [m^2]
A$_{a,min}$	Airside minimum free flow area [m^2]
C	Wall heat capacity rate [kJ/kg.K]
c$_p$	Fluid heat capacity rate [kJ/kg.K]
C.V.	Control volume
DAQ	Data acquisition system
DI water	Deionized water
D$_{a,hyd}$	Airside hydraulic diameter [m]
dE	Energy change [kJ]
dU	Internal energy change [kJ]
G	Mass velocity [kg/m^2.s]
GR	Mass velocity ratio $\left(\dfrac{G_{a,final,steady\ state}}{G_{a,initial,steady\ state}}\right)$
H	Height (m)
h	Heat transfer coefficient [kW/m^2.K]
H^o	Latent heat of fusion (kJ/kg)
j	Colburn j factor
k	Fluid thermal conductivity [kW/m.K]
L	Fin parameter [m]
M	Heat exchanger wall mass [kg]
$\dot{m}$	Fluid mass flow rate [kg/s]
Nu	Nusselt number
Nu(t)	Transient Nusselt number
P	pressure [pa]

Pr	Prandtl number
PTD	Pressure Transducer
$\dot{Q}$	Heat transfer rate [kW]
Re	Reynolds number
RSS	Root Sum Square
RTD	Resistance Temperature Detector
S	Fin parameter
St	Stanton number
T	Temperature [°C]
T^*	Dimensionless temperature
$T^*(t)$	Transient dimensionless temperature
t	Time [s]
t_{fin}	Fin thickness [m]
t^*	Dimensionless time
V	velocity [m/s]
Z	Characteristic length (m)
∞	Final, steady state

Greek letters

Δ	Change in variable, final-initial
ε	Effectiveness
μ	Fluid dynamic viscosity [N. s/m^2]
ρ	Density [kg/m^3]
η	Efficiency

Subscripts

a	Air
avg	Average

b	Bulk
cum	Cumulative
f	Final
g	Glycol (50/50 ethylene glycol-water mixture)
l	Liquid
min	Minimum
norm	Normalized
HT	Heat transfer
HX	Heat Exchanger
w	DI Water
i	Inlet
o	Outlet
s	Surface

CHAPTER 1

INTRODUCTION

The continuous development in economy worldwide is faced by a strong demand of energy supply. According to the International Energy Outlook [1], a 50% world energy consumption growth between the years of 2020 and 2050 is projected by the U.S. Energy Information Administration (EIA). The challenges represented by the current limitation in energy resources, the fluctuation of their prices, and the significant effect of energy utilization on global warming, have motivated researchers to develop alternatives and use energy sources to avert from technologies with high environmental impact or higher cost. This is due to the posing risks of the increase in energy use on global warming and climate change. These risks are due to the greenhouse gases GHG released as a result of fuel burning such as in the transportation section. The transportation section in Canada is considered to be the second highest sector in energy use after industrial, Figure 1.1. It also contributes to the emissions and has a 28% increase in the transportation GHG emissions in Canada between the years of 2000 to 2019 [2].
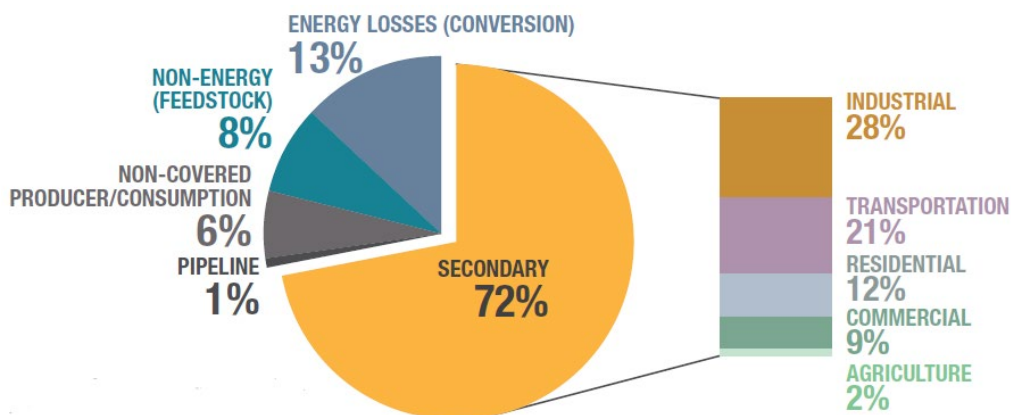
Figure 1.1. Primary and secondary energy use by sector, 2018 [2]

The availability of many energy resources is faced by the continuous increase of energy consumption. Therefore, efficient utilization of the existing energy resources is highly promoted. In industries such as automotive, some systems such as the Heating, ventilation, and Air Conditioning HVAC system consume large amount of energy and contribute to the GHG emissions. Air conditioners in a vehicle are referred to as Mobile Air

Conditioning MAC. It is predicted that by 2050, the energy use from MAC systems may reach more than 5.7 million oil barrels each day [3]. In addition to MAC contribution to GHG emission from its energy consumption, it also reduces the driving range of the electric vehicle. However, a MAC system is important to provide thermal comfort to vehicle occupants. Enhancement of the thermal management system in a vehicle has a significant impact on safety, fuel consumption, range, and the thermal comfort of passengers. Therefore, efficient thermal management and control is necessary to balance the required thermal comfort of the passengers and the energy consumption of the MAC system. The technology nowadays has not yet reached a point to fully eliminate the dependency on fossil fuels. For this regard, it is important to perform good energy management to ensure long lasting fuel reserves especially with the rising environmental concerns.

Vehicle thermal management represented by a MAC system gained more interest over the years in its enhancement and new technologies. This is due to the concerns of energy consumption, environmental impact, weight and size reductions, the new features added to the car, and the increasing demand on electric cars. A thermal management system in a vehicle is responsible to provide thermal comfort to the occupants. Thermal comfort is a condition in which humans are satisfied with the thermal environment. The term thermal comfort is influenced by many factors such as measurable factors: air temperature, relative humidity, air velocity, and radiant temperature as well as personal factors such as clothing and activity level Simion et. al. [4]. In the automotive industry, manufacturers are committed to increase the thermal comfort for passengers. They ensure the use of an air conditioning system to provide air heating, cooling, and ventilation. The HVAC technology plays an important role in facilitating the comfort environment for the passenger cabin.

One of the vital components utilized for heat transfer in a thermal management system is the heat exchanger which is designed to perform certain requirements by transferring thermal energy between two or more fluids at different temperatures. Heat exchangers in a system may perform different needs such as heating, cooling, recovering heat, evaporation, condensation, control a fluid in a process, etc. There exist different types of heat exchangers that are commonly used in current systems, shell and tube, automotive radiator, condenser, heater core, etc. Shah and Sekulic [5] classified heat exchangers into many categories

based on transfer process, number of fluids, surface compactness, construction, flow arrangement, and heat transfer mechanism.

Surface compactness is one of the classifications of heat exchangers which is characterized by higher area density defined as the heat transfer surface area per unit volume. The higher area density combined with the small hydraulic diameter, used for the fluid to flow in, result in enhanced efficiency within a smaller volume compared to conventional heat exchangers. A compact liquid-gas heat exchanger has a 400 m^2/m^3 surface area density or higher. On the other hand, a heat exchanger is called a meso heat exchanger if it has a surface area density of higher than 3000 m^2/m^3 or a hydraulic diameter between 100 μm and 1 mm. These types of compact heat exchangers provide advantages over conventional heat exchangers and can find many applications such as aerospace, cryogenic, power plants, automobiles, and others.

Many industries rely on the existence of heat exchangers; therefore, a necessity has been driven to enhance their effectiveness and reduce their cost and energy consumption. Researchers reported different enhancement methods of heat transfer such as the use of extended surfaces, nanofluids, turbulence promoters, surface fluid vibration, etc. Siddeque et. al. [6], Picón-Núñez [7], and Steinke and Kandlikar [8]. The early work of Bergles et. al. [9] organized these techniques into two groups, active and passive and generated a database for the enhancement methods on convective heat transfer available in the literature. The advancement in technology made it possible to manufacture channels with very small diameters thus diverting from the large diameter tubes. This advancement provides a solution to the heat exchangers weight and size concern with enhanced heat transfer rate.

1.1. Transient Heat Transfer in Heat Exchangers

The vast majority of heat exchangers' thermal performance evaluation focuses on steady state operation. Typically, a thermal system is designed considering steady state or based on a maximum load. This design results in an oversized heat exchanger and more power consumption. In addition to that, in many applications, heat exchangers experience a variation in their inlet operating conditions and therefore, they do not work according to

their design requirements. Many systems have the heat exchanger as one component of a complex process, consequently, any perturbation in the inlet conditions leads to unpredictable results in the performance of not only the heat exchanger but also the other components connected to it in the system. Common scenarios where load variations affect the steady operating condition of the heat exchanger are startup, shut down, accidents, and failures. An example where a change in the operating conditions can occur in real applications is in the automotive air heating or cooling system. A blower fan in an air distribution system of a vehicle where the heater core and the evaporator housing are located is turned on suddenly to a low, medium, or high level to achieve occupants' thermal comfort during hot or cold weather, the inlet mass flow rate entering the heat exchanger is changed. This sudden change from an initial steady state creates a transient behavior and affects the outlet air temperature entering the passenger compartment. Additionally, some new design vehicles are equipped with double, triple, or quad climate control zones that allow not only the driver but also the passengers to control their side of the blower speed.

A transient condition can affect the heat transfer and cause a thermal stress issue which if increased can cause a mechanical failure. For this regard, a dynamic performance investigation is necessary not only to study the behavior of these devices under inlet condition variations and choose the suitable design but also to have a better control of the thermal system in general. Transient analysis allows the prediction and control of the fluids outlet temperatures in response to a change in the inlet conditions whether temperature or mass flow rate of the working fluids. The dynamic analysis of the heat exchanger quantifies the response time of the outlet temperatures to the change imposed which can be beneficial to predict the time to reach the steady state condition. Additionally, this analysis assists in analyzing the effect of the imposed change on the heat exchanger performance. The transient heat transfer can be characterized by dimensional and dimensionless parameters. One of these parameters is Nusselt number which represents the dimensionless heat transfer coefficient as a quantitative characteristic of convective heat transfer.

1.2. Thermal Energy Storage

While transient analysis provides an understanding of the heat exchanger thermal behavior and predicts the fluids outlet temperature, an efficient solution to sustain extra cooling load

and damp the variation in the temperature due to transient changes is required. The search for innovative methods to provide sustainable thermal comfort has led to the introduction of the Thermal Energy Storage, TES, Yang et. al. [10]. There exist three types of thermal energy storage: sensible, latent, and thermochemical. Sensible energy storage involves a temperature change without a phase change, while thermochemical energy storage involves a thermal reaction which the heat generated from it is stored. Through the integration of a Phase Change Material, PCM, in a heat exchanger, a latent heat thermal energy storage, LHTES, works on storing/releasing the heat to alleviate a peak energy load or provide extra cooling and heating for thermal processes Elarem et. al. [11].

A latent heat thermal energy storage with PCM provides a cost-effective solution to reduce energy consumption by releasing the stored energy through the exchange of heat from the PCM to the process fluid. PCM can work to reliably extend the period of operation when the main coolant experiences a short period of shut down which minimizes the need for a source of power or batteries and results in energy savings. Such application can be found in the vehicles equipped with an automatic start-stop function. When a vehicle stops at a red light, not only the engine stops working but the air-conditioning compressor as well. Since this is a short period of time while the car is stopped, a PCM can be used to provide that extra cooling time and achieve a comfortable temperature level in the passenger cabin.

A phase change material, PCM, is a material that transforms its phase between liquid and solid where it absorbs and releases thermal energy during its freezing and melting processes at a constant temperature. A sensible heat involves the transition with a temperature change while the temperature does not change during a latent heat transition. When a PCM melts, it absorbs energy and the bond between the atoms gets loose and the material transforms from the solid state to the liquid state. While in freezing it is the opposite, the PCM releases energy and the molecules arrange themselves to form the solid phase. This energy is called the latent heat of fusion. Each PCM is characterized with a latent heat of fusion which controls the amount of energy to be absorbed or released along with the PCM mass. While the melting and freezing rates are controlled by the operating conditions.

The heating process of a PCM can be found in Figure 1.2. In this figure, the transformation from solid to liquid starts with a subcooled liquid that receives energy until it reaches its

5

melting point through sensible heating. At his point, the material continues to be heated and experiences a phase change to liquid at constant temperature. Thereafter, the liquid heating results in the material reaching its boiling point at an increased temperature. When the boiling point is reached, the liquid experiences a phase change to vapor. However, this change in phase is controlled by the latent heat of vaporization and any further heating is considered sensible heating.
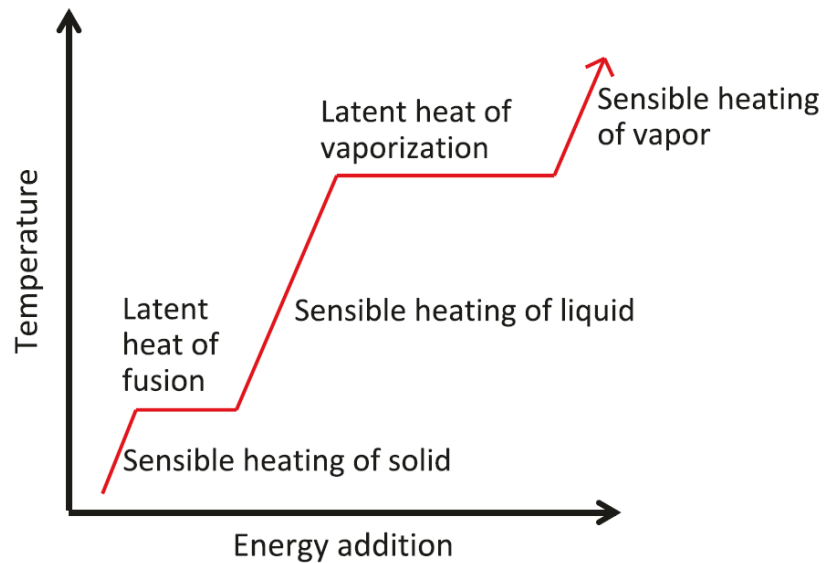
Figure 1.2. PCM heating process [12]

1.2.1. PCM Classification

Various types of PCMs exist in a variety of different range of temperatures, however, they all can be categorized within three different groups: organic, inorganic, and eutectic. This classification is presented by Sharma et. al. [13] and can be found in Fig. 1.3. A brief explanation of the main categories of PCM can be shown as follows.

6
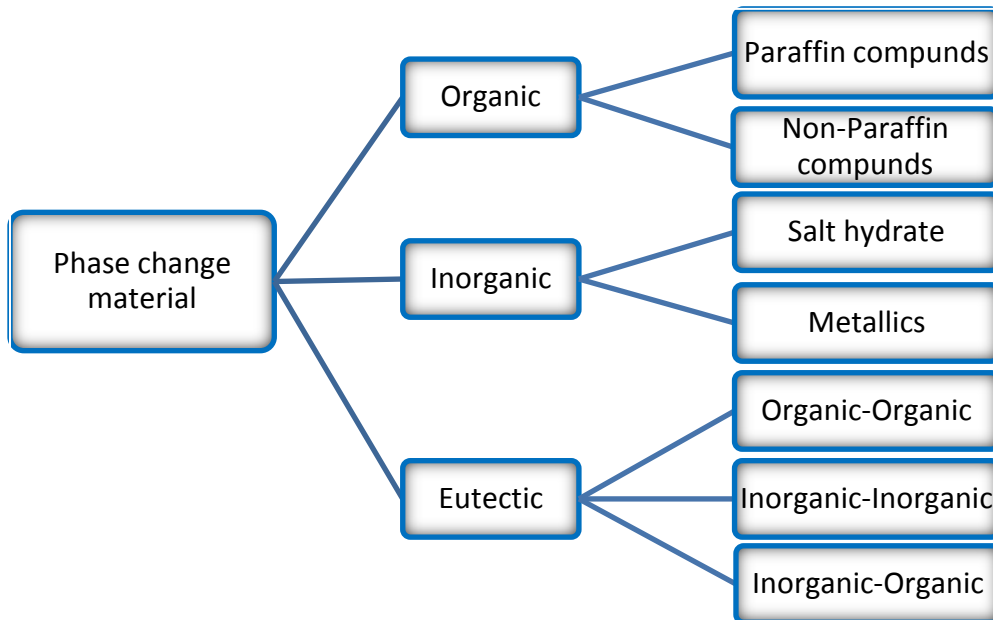
Figure 1.3. PCM classification [13]

1.2.1.1. Organic PCMs

This is the most common type of PCM such as paraffin, fatty acids and polyethylene glycol. Paraffin is widely investigated in thermal management applications due to its availability, affordability, and feasibility. Organic PCMs possess high latent heat that makes it possible to store a large amount of energy using a small mass. They can be used with many materials without deteriorating them and have a good repeatability for multiple cycles with no effect to their performance. They also show a physical and chemical stability. The drawback with this type of PCM is the low thermal conductivity that can result in a reduced effectiveness.

1.2.1.2. Inorganic PCMs

This type of PCM comprised of salt hydrates and metallics. They possess thermal stability over repeated cycles and are commonly used with applications that require a high melting temperature. Inorganic PCMs have a high thermal conductivity compared to the organic PCMs and their phase change occur faster than the organics. The drawbacks of inorganics lie in their phase change irreversibility in which they need to be stirred or to add chemicals. Another issue is they can be corroded when left to the environment or interacted with the housing materials.

1.2.1.3. Eutectic

Eutectic is a compound that is comprised of two or more types which can be organics, inorganics, or both and possesses a single melting temperature. The advantage of this type of PCM is the ability to control its melting point by changing the weight percentage of the components added. Their solidification or melting occurs without any phase segregation or supercooling Atinafu et. al. [14].
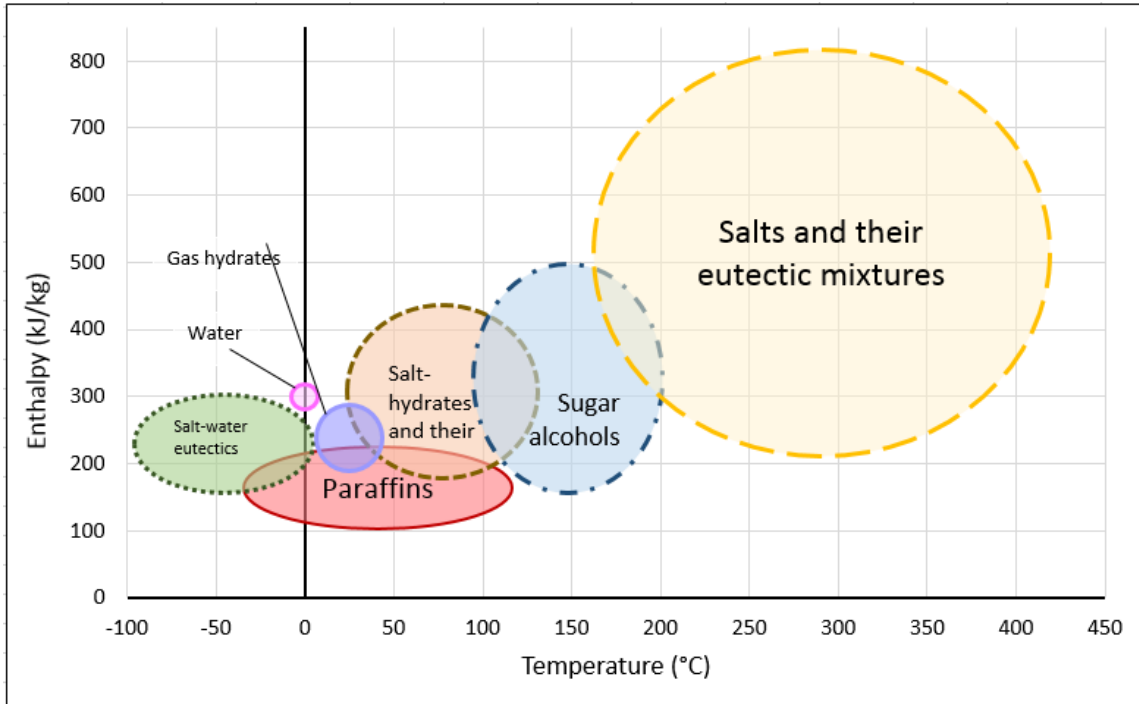
Figure 1.4. Various PCM groups melting temperature range [15]

1.2.2. Comparison of Different PCMs Types

A PCM can fall into one of the above-mentioned groups. Each group has its advantages and disadvantages and choosing a specific PCM will take these characteristics into consideration along with the application temperature range and other factors. A list of comparison of different PCM groups is shown in Table 1.1.

Table 1.1. PCM groups advantages and disadvantages

PCM type	Advantages	Disadvantages
Organic	✓ Chemical stability [16] ✓ Effective repeated thermal cycles ✓ Available in a wide temperature range ✓ Compatible with other materials ✓ Nontoxic ✓ Noncorrosive [17]	❖ Low thermal conductivity ❖ High cost ❖ Large volume change [17] ❖ Flammable ❖ Low heat of fusion [16]
Inorganic	✓ Lower cost ✓ High heat of fusion [18] ✓ High melting point range ✓ High thermal conductivity ✓ Nonflammable	❖ Many thermal cycles reduce effectiveness ❖ Supercooling and subcooling ❖ Corrosive ❖ Phase segregation [18] ❖ Incompatibility issues
Eutectics	✓ Lower cost ✓ Sharp melting temperature ✓ Large volumetric storage density [19]	❖ Corrosivity ❖ Limited melting temperature range ❖ Low thermal conductivity [20]

1.2.3. PCM Applications

PCM is gaining more interest due to many reasons including the increased cost of energy utilization, environmental concern, and space and weight limitation. Thermal energy storage with PCM is used for energy efficiency as well as thermal comfort. There is a variety of PCM applications as an energy storage due to the wide range of temperatures utilized in many systems. Some of these applications include the use of PCM in buildings for cooling purposes. Phase change materials can be used for cooling in a building envelope, HVAC unit, and solar system. It works on storing energy and releasing it thus

reduces peak load and results in smaller HVAC unit Souayfane et. al. [21]. A PCM can be employed as a thermal energy storage in solar systems to store thermal energy for later use. PCM can find an application in the protection of food, medical supplies, electronics, etc. at their desired temperature during transportation. Another application is in the transportation of refrigerated trucks to minimize the peak heat transfer rate and maintain the refrigeration equipment working for a longer period of time. Depending on the temperature range of the application, a PCM can be integrated in a system such as electronics. It works on absorbing the heat at peaks and emits it thus results in minimization of the cooling system.

1.2.4. PCM Selection Criteria

Phase change materials exist in a wide temperature range of melting and freezing. Choosing a PCM for a specific application depends on the PCM characteristics. The following presents some consideration points to value when selecting a specific type of PCM. Three aspects can set a selection criterion when choosing a PCM: thermal, chemical, and economical.

1.2.5. PCM Thermal Characteristics

The thermal characteristics of the PCM can include latent heat of fusion, thermal conductivity, density, and melting temperature range. The latent heat of fusion is an important factor for selecting a PCM since its unit is in (J/g). High energy storage capacity is required in order to store higher amount of thermal energy through using a minimum quantity of the material. A high thermal conductivity is important for heat transfer performance therefore, researchers are continuously investigating different methods to enhance the PCM thermal conductivity.

1.2.5.1. Chemical Characteristics

A phase change material is expected to undergo many melting and freezing cycles. Through a DSC test, the reliability of the PCM to continuously absorb and release energy without any effect to its performance is assessed. The degradation of PCM can occur over the many repeated cycles it experiences; therefore, it is important to choose a PCM that

maintains its chemical and thermal stability after many melting and solidification processes. For health and safety considerations, the selected PCM should show no corrosivity, toxicity, explosivity and possess low flammability.

1.2.5.2. Economical Characteristics

Economical consideration is represented by the PCM cost, availability, and compatibility. The PCM cost can affect its feasibility in different applications. The integration of a specific type of PCM in an application requires the availability of that PCM at an affordable cost. While cost and availability are important factors, the compatibility of the PCM with the housing material is crucial.

1.3. Motivation

Dynamic analysis is a great tool to characterize the transient heat transfer and provide a prediction on the response of the heat exchanger. The experimental investigation of the transient behavior of a cross flow heat exchanger is of great importance due to its use in many industries. The integration of PCM in a heat exchanger as a latent heat thermal energy storage has gained significant research interest due to its capability to provide cooling and heating without the reliance on a power source or a battery. The transient analysis and the PCM incorporation in the heat exchanger can offer some advantages which are summarized below,

- o The dynamic analysis under inlet conditions perturbations presents a prediction of the thermal behavior of the heat exchanger as a result to a sudden change.
- o The prediction of the fluids' outlet temperature response and behavior due to transient changes and the use of PCM in heat exchangers assists in achieving a continuous and uninterrupted occupants' thermal comfort.
- o Sizing of HVAC unit for average thermal load instead of peak thermal load.
- o Size reduction when space is limited and cooling with a process fluid cannot be utilized.
- o Energy savings and less use of power or battery for example in vehicles. Less reliance on fuel and energy conservation.
- o Storing thermal energy according to the temperature required by the application.
- o Thermal cycle repeatability without an impact on PCM effectiveness.
- o Storing energy at peak periods for a later use.

The motivation to perform this work can be summarized in the following points,

- Lack of available data on transient analysis of heat exchangers with airside flow rate perturbations, especially experimental data for air cooling.
- Majority of the published work focused on the liquid side inside the tube/channel rather than the airside due to the complexity of the airside circuit and the need for a state-of-the-art highly equipped experimental setup to perform such analysis.

- The increasing demand for electric and hybrid vehicles, the incorporation of climate control features such as start stop function, and the need to extend thermal comfort such as in a vehicle's passenger compartment during short period of shutdown.

- The search for an existing source of energy that doesn't impact the environment yet provide energy and fuel savings.

- The rising concern for space and weight limitations in many applications.

- Lack of experimental studies that involve a cross flow heat exchanger with two working fluids (air and ethylene glycol/water mixture) besides PCM.

For all the aforementioned reasons, this experimental work is of importance and need as it provides an insight and a solution to real life problems resulting in power and energy savings.

1.4. Objectives

Heat exchangers are typically analyzed using steady state conditions. However, perturbations in fluids' inlet conditions can occur due to many reasons. A change in a fluid's inlet flow rate or temperature affects the thermal process and heat exchanger. Due to the fact that heat exchangers are generally part of a thermal system, this effect can lead to undesirable consequences to the subsequent parts connected to the heat exchanger. Majority of the published transient works related to cross flow heat exchangers are based on liquid side variations inside the tube. In view of the shortage of available studies on the dynamic behavior of cross flow heat exchangers with perturbations in airside mass velocity for air cooling and heating, the current work is presented. Therefore, an experimental study of the dynamic behavior of a cross flow heat exchanger due to airside mass velocity variations is investigated. The main objectives of this work are listed below,

> Present an insight into the transient thermal behavior of cross flow heat exchangers when airside is subjected to an inlet condition change.
> Experimentally investigate the dynamic behavior of a compact heat exchanger for air cooling and heating using different inlet mass velocity ratios.
> Discuss the effect of a sudden step change of a fluid inlet condition on the heat transfer and fluid flow of the heat exchanger using different dimensional and dimensionless parameters.
> Analyze the factors that affect the response time of the heat exchanger to the steps imposed.
> Develop generalized empirical correlations to predict the airside Nusselt number with respect to air inlet mass velocity ratios for both cases of air heating and cooling.
> Generate a database for future researchers on experimental transient heat transfer due to airside inlet conditions variation.

The use of a PCM in enhancing and providing a sustainable energy system is important to the efficiency of the system. This is due to the capability of the PCM to manage heat and provide cooling energy in an effective way. For this regard, the current study proposes the use of a PCM as a reliable cold thermal energy storage solution. While significant effort is shown in the published literature into developing and presenting different thermal energy

storages, there remains however a scarcity of published experimental work dealing with the incorporation of PCM in a crossflow heat exchanger. The present study tackles the lack of available experimental data problem and present a solution for thermal comfort of occupants through fulfilling the following objectives,

> Conduct experiments using a PCM as a latent heat thermal energy storage for extended thermal comfort in a compact cross flow heat exchanger to solve the limited space and weight concern in applications.
> Examine the effect of different air mass flow rates on the PCM discharge time.
> Assess the PCM optimal performance using effectiveness.
> Study the repeatability of the PCM charging and discharging through short periods working and idles.
> Evaluate the advantage of using PCM to provide thermal comfort when compared to a no PCM case for the case of air cooling.
> Compare the effect of the air mass flow rate and liquid mass flow rate change on the discharging process of the PCM.

In order to successfully achieve the proposed objectives, a flow chart is presented as in the following to show a step-by-step guide as in Figure 1.5.

| Title | Transient experimental study of a latent heat thermal energy storage in a phase change material-air-liquid heat exchanger |

| 1 | • Comprehensive literature review |

| 2 | • Find the gaps in research and formulate the problem |

| 3 | • Outline motivation and objectives and identify a method of approach |

| 4 | • Obtain necessary equipement and measuring devices to run the experiements |

| 5 | • Implement modifications to the experimental setup to accomodate the transient and PCM testings |

| 6 | • Run experimental tests to preset the operating conditions |

| 7 | • Conduct experiments and record data |

| 8 | • Analyze data, develp correlations, and compare results with published works |

| 9 | • Publish journal papers of the composed results |

| 10 | • Write, submit, and defend the dissertation |

Figure 1.5. Research goals achievement flow chart

CHAPTER 2
LITERATURE SURVEY

Heat exchangers are employed in a variety of applications and their main use is to accomplish thermal management and maintain thermal comfort. A typical design of heat exchangers is based on their steady state operating conditions. This means that the inlet temperatures and flow rates of the working fluids remain constant and do not experience any variation with time. Steady state numerical, analytical, and experimental investigations on different types of heat exchangers are well established and presented.

2.1. Heat Transfer Enhancement

There are many studies on the thermal performance of heat exchangers that include modifying the working fluid properties, using different heat exchanger orientations, changing the geometry surface, and adding extended surfaces with varying the fin parameters. Enhancing the heat transfer and obtaining better thermal performance in a heat exchanger by adding another equipment which needs an additional source of energy is considered costly and increases the weight and size of the thermal unit. Therefore, alternative methods have been suggested. One of these methods is the use of nanofluids to enhance the heat transfer in cross flow heat exchangers Albadr [22]. Huminic and Huminic [23] have presented a review study on the use of nanofluids in heat exchangers. They have divided their paper in two sections where the first one summarizes the enhancement in fluid properties and Nusselt number. While the other section focuses on the use of nanofluids in different types of heat exchanger.

Heat transfer enhancement can also be accomplished considering different tube/channel sizes and shapes. The effect of different channel diameters in a thin slab has been investigated by Ismail et. al. [24]. The heat transfer coefficient, pressure drop, and Nusselt number have been shown to increase or decrease according to the slab length/channel diameter ratio. Adding extended surfaces to the heat exchanger has shown to increase the heat transfer by increasing the heat transfer area. Fin shapes. Sizes, and orientation are investigated with their effect on heat transfer in a heat exchanger Moorthy et. al. [25], Basavarajappa et. al. [26], and Altwieb et. al. [27]. The effect of geometrical parameters

on the heat exchanger thermal performance was examined by Kuehndel et. al. [28] and Erec et. al. [29].

2.2. Airside Steady State Thermal Performance

Cross flow heat exchangers with airside thermal performance evaluation focus have been examined by many researchers at steady state conditions. Siddiqui et. al. [30] have experimentally studied the effect of different operating conditions on the airside heat transfer and fluid flow characteristics of a compact CFHX. They have compared airside Nusselt number to a published literature and derived correlations for the case of air heating. Junqi et. al. [31] experimentally evaluated the airside thermal performance in a crossflow heat exchanger. They have used the effectiveness-NTU method to study the effect of fin parameters on the thermal performance of the heat exchanger. Empirical correlations were presented for Colburn j and friction factors.

An examination of the heat transfer and fluid flow of a cross flow heat exchanger under steady state conditions was done by Dasgupta et. al. [32]. Their experimental work resulted in airside heat transfer and thermal resistance evaluation along with an obtained correlation for Nusselt number as a function of Reynolds number. Waltrich et. al. [33] presented an evaporator design where the heat transfer coefficient experienced an enhancement due to minimizing the free flow area. Experiments were conducted to analyze the thermal behavior of the alternative evaporator design and present a method to predict the heat transfer and pressure drop without any further fitting parameters. The presented model compared reasonably with the experimental data. The airside heat transfer coefficient in a crossflow heat exchanger was determined experimentally and numerically by Taler [34]. He obtained the fluids' average heat transfer coefficients using a new method based on the nonlinear least squares.

2.3. Transient Study of Heat Exchangers

Many researchers have studied the dynamic change in either one fluid or both fluids inlet conditions and their effect on the thermal performance and outlet parameters of the heat exchanger. A transient response of a counter flow heat exchanger with temperature variation of one of the fluids was studied numerically by Bunce [35]. The transient behavior

was modeled using a commercial software and the effects of the different variables such as geometry and process were examined. A transient response of a double pipe heat exchanger subjected to fluid flow rate change was numerically and experimentally analyzed by Lachi et. al. [36]. A model was developed to predict the response of the heat exchanger. Their results show a decrease in time constant due to the increase in flow rate which results in a faster response of the heat exchanger.

Yin and Jensen [37] analytically examined the heat exchanger transient performance due to a fluid's temperature or mass flow rate perturbations. The working fluids used were a single-phase fluid and a constant temperature fluid. They have concluded that their model can be used for a heat exchanger regardless of the flow arrangement. However, further study for the two fluids in a single phase has to be investigated. Transient analysis of a plate type heat exchanger due to a temperature perturbation was investigated by Srihari and Das [38]. Two types of plate heat exchangers, U and Z types were analyzed and compared with and without flow maldistribution under the transient change. Dynamic parameters such as initial delay time, response time, and time constant were evaluated. A model was created and verified with experimental data to predict these parameters.

2.3.1. Transient Analysis of Cross Flow Heat Exchangers-Temperature Changes

Dynamic investigation of heat exchangers has gained noteworthy interest in recent years for applications that involve mostly heating or cooling to control the outlet temperature of the fluid. A number of researchers have reported studies on the transient analysis of CFHXs. Much of them explored the effect of the variations of the fluid's inlet temperatures and channel/tube mass flow rate on the dynamic performance of the heat exchanger. Abdallah and Rooke [39] examined the thermal response of a liquid-gas cross flow heat exchanger due to a step change in liquid temperature and derived analytical expressions for the liquid and gas outlet temperatures. They have compared their analytical solution to the available numerical methods and found good agreement. Chen and Chen [40] worked on developing a numerical work to analyze the transient response of a CFHX with finite wall heat capacity. They have expressed fluids outlet temperatures as well as the wall temperature in terms of the variation of the inlet temperature of the primary fluid.

Likewise, numerical analysis of a cross flow heat exchanger by Syed and Idem [41] considered a step change to the minimum capacity rate fluid inlet temperature. They have reported a time lag on the stepped fluid unlike the other fluid which responded instantaneously to the change. Also, they have found that the higher the NTU value, the higher the time needed to reach steady state condition. Gogus and Ataer [42] numerically and experimentally studied the transient response of a CFHX subjected to step changes in the liquid temperature. A model was developed and verified to predict the thermal behavior of the crossflow heat exchanger considering the existence of fins.

Ataer [43] studied the transient analytical modeling of a cross flow heat exchanger with step change in the hot fluid inlet temperature by deriving energy equations for both fluids and obtaining the outlet temperature variations with respect to time. He has characterized the heat exchanger behavior by time delay, time constant, and gain while comparing his results to experimental and numerical results found in [44]. Later on, Silaipillayarputhur and Idem [45] numerically studied the effect of the step change in inlet temperature and flow rate of the minimum capacity rate fluid on the transient performance of multi pass cross flow heat exchanger. They have solved the energy equations for both fluids as well as the wall and discussed the response of both fluids. Their results have been compared with published work [46] for different flow arrangements yielding the conclusion of adding more passes to cross and counter flow arrangements improved the steady state transfer performance. Moreover, the crossflow arrangement showed an improved thermal response time when three or more passes were used compared to the other arrangements. Vaisi et. al. [47] numerically studied the transient behavior of a CFHX with fluids' temperature step change. The response of each fluid to reach the steady state as well as the effect of the step magnitude on the time constant were examined. Furthermore, the delay time for each fluid was discussed.

2.3.2. Transient Analysis of Cross Flow Heat Exchangers-Flow Changes

An early work on improving the control capability of cross flow heat exchangers using transient analysis started in mid-sixties targeting applications in HVAC and automotive fields. The research work studied the effect of variations in the inlet flow rate of the internal fluid inside the tube on both fluids' outlet temperatures as well as the response time of the

heat exchanger for air heating. Pearson et. al. [48] have studied the dynamic response of the air outlet temperature in a conventional CFHX due to changes in water flow rate. They have solved a first order dynamic model and compared their results to their experimental and numerical findings. Fotowat et. al. [49] have studied the transient response of a minichannel cross flow heat exchanger when the channel flow rate is subjected to step changes. They have analyzed different step magnitudes and their effect on the outlet temperature response of both fluids. Askar et. al. [50] have experimentally studied the effect of air mass flow rate step changes on a compact CFHX performance for air heating. They have characterized the thermal response of the heat exchanger and obtained a derived empirical correlation for Nusselt number prediction due to different air mass flow rate steps imposed.

Mishra et. al. [51] have investigated the transient temperature response of a CFHX due to fluids temperature and flow rate variations. In their numerical study, hot fluid flow rate step and ramp changes were considered. They found that the exit temperatures increased when the hot fluid flow had the higher variation while decreased when the cold fluid flow rate changes were larger. Transient experimental characterization of a cross flow heat exchanger with liquid and air temperature and flow rate perturbations was investigated by Del Valle and Ortega [52]. Their results show that the increase in water flow rate raises the outlet water temperature. Furthermore, perturbations in water flow rate presented no delay in exit temperatures response.

Transient cooling response in data centers using CFHXs was studied by Gao et. al. [53]. Fluids' flow rates were subjected to step and ramp changes to examine the effect of the thermal response of the heat exchanger. Their numerical results investigated the fluids' exit temperature response, the time constant, and the step magnitude effect on the transient response of the heat exchanger. The transient thermal behavior of a cross flow heat exchanger used in a data center was examined numerically and experimentally by Erden [54]. He developed a model and verified it with experimental data for transient prediction of the heat exchanger subjected to different variations including airflow. Del Valle et. al. [55] numerically modeled the transient response of a CFHX used in data centers due to perturbations in inlet water temperature and flow rate. They have performed experiments

to validate their model and found good agreement for the flow rate variations case. However, the model faced some limitations for the temperature step changes.

Gao et. al. [56] worked on the prediction of the transient response for a cross flow heat exchanger by numerically solving a thermal dynamic model. They have studied different combination of variations, air inlet temperature and water flow rate change, air inlet temperature and air flow rate change, air inlet temperature variation along with a combination of air and water mass flow rate change, and both fluids inlet mass flow rate change. Their results have shown that the effect of mass flow rate variation on the outlet temperature response is faster than the temperature variation. In addition, the combination cases resulted in an unexpected thermal performance such as overshooting of the outlet temperatures.

2.4. Thermal Energy Storage

A latent heat thermal energy storage is a technology that allows the storage of energy using a medium and releasing this energy when needed through heat transfer with a working fluid. Their many benefits and the ability to store large amounts of energy with a small size make them attractive alternatives for applications such as cooling or heating where space is limited. Different thermal energy storage technologies including sensible and latent were reviewed comprehensively by Sarbu and Sebarchievici [57]. While various applications of thermal energy storage for heating and cooling were examined and reviewed by Chavan et. al. [58].

A material that can store large amount of thermal energy and is characterized by a high energy density is referred to as a phase change material. Many researchers have focused on investigating and reporting different enhancement techniques to improve the PCM thermal properties. Wang et. al. [59] have prepared a phase change material with an aluminum nitride additive to enhance its thermal conductivity. They investigated the thermal energy storage performance through a cycle of storing and releasing thermal energy. Their experiments resulted in a PCM that is characterized by high thermal conductivity but a decrease in the latent heat. Fan and Khodadadi [60] have presented a review of experimentally and numerically studies review on methods to improve the PCM

thermal conductivity. They reviewed different metal inserts as promoters on a variety of PCMs. Teng and Yu [61] have investigated experimentally the use of different types of additives into an organic PCM working as a thermal energy storage to enhance its thermal characteristics. They have found that the use of titania in a PCM resulted in an enhanced storage performance and extended phase change temperature range.

The increase in thermal conductivity of a PCM for a better thermal energy storage was explored by Ji et. al. [62]. Their use of graphite foams resulted in an PCM enhanced thermal conductivity that can be used for different applications such as automotive and buildings. Sivasamy et. al. [63] have reviewed different enhancement techniques to improve the thermal performance of the energy storage. various types of thermal conductivity enhancement methods have been presented and applications of thermal energy storage have been discussed.

2.4.1. Thermal Energy Storage in Heat Exchangers

The use of PCM in heat exchangers have found an increasing interest due to the many applications where thermal management is required. Al-Mudhafar et. al. [64] have investigated the effect of fins in a shell and tube heat exchanger on the thermal performance of a PCM. A comparison of the used T-type fin with a longitudinal fin revealed that the T-type fins have resulted in a reduced melting time. They have also found that the fin geometry plays an important role on the melting of the PCM. Li et. al. [65] have numerically studied the fin number and location on the melting process of an energy storage heat exchanger. The heat exchanger investigated was a double tube positioned horizontally. They have found that fin positioning has a higher effect than fin number in heat transfer and performance enhancement of the heat exchanger. Additionally, fin location has reduced the melting time considerably compared to the case of no fins.

A numerical investigation of PCM melting in a triplex tube heat exchanger was done by Mat et. al. [66]. Their study examined heating with PCM using different fin positions such as internal, external, and both sides fin positions. A comparison of the performance of the PCM with both sides fins and without fins resulted in shorter melting time than no fins. Their numerical models were verified with experimental data and found good agreement.

An investigation of the performance of a plate heat exchanger with PCM was experimentally done by Kumar et. al. [67]. The increase in the fluid's flow rate or temperature led to an enhanced efficiency for the case of melting while no effect was shown during solidification. Recommendations for future performance enhancement for the plate heat exchanger with PCM were discussed. Kalapala and Devanuri [68] reviewed two types of energy storage heat exchangers, shell and tube and a triple concentric tube. Their work involved operating conditions investigation of temperature and mass flow rate of the working fluid, geometry consideration such as the ratio of the shell and tube diameters, heat exchanger orientation, fins, and positioning of the tubes. They provided recommendations for an enhanced heat transfer in the LHTES heat exchangers studied based on the design, geometry, and operating conditions.

Lu et. al. [69] have studied the thermal performance of a LHTES in a shell and a tube with fins. The melting and solidification characteristics were assessed using a paraffin PCM. Higher fluid flow rates showed a significant reduction in the charging time. while higher fluid temperature reduced the discharging time. Promoppatum et. al. [70] have studied the use of PCM in a crossflow shell and tube heat exchanger for HVAC applications. A model validated by experiments was used to examine the heat transfer characteristics. They explored the parameters that affect the thermal performance such as geometry and operating conditions. Through a dispersion of aluminum in the PCM, its thermal conductivity was enhanced and as a result, the thermal performance was improved.

There is an increasing interest in utilizing PCM in heat exchangers as a thermal energy storage for various applications due to the energy supply and environmental concerns. Herbinger et. al. [71] have numerically investigated the thermal performance of a PCM-air heat exchanger as a thermal energy storage in HVAC applications. Their results show the dependency of the heat transfer rate on the airside temperature and velocity as well as the channel diameter. They have found that the small channel size along with the high inlet temperature increase the heat transfer, while less significant effect was found from the inlet velocity. A PCM in a finned tube was experimentally researched by Rahimi et. al. [72]. The melting and solidification processes were examined based on the effect of varying the fluid's temperature and flow rate. The fin effect on these processes was also considered.

They concluded that the existence of the fins and the flow regime significantly influence the melting time. Additionally, the solidification process is affected by the fluid flow rate variation.

Energy improvement with a TES was investigated by Medrano et. al. [73]. The charging and discharging processes were evaluated for different heat exchangers. Using the average thermal power, the compact heat exchanger is concluded to be the most adequate to store heat for real applications. Amagour et. al. [74] have experimentally studied a compact finned-tube heat exchanger as a TES. The fluid flow rate effect on the phase transition process and the TES effectiveness was considered. They have found that the mass flow rate possessed higher significant effect than temperature on the TES effectiveness. They also concluded that higher flow rates resulted in lower system effectiveness and faster phase transition.

Koukou et. al. [75] have investigated a LHTES unit using different organic PCMs in a staggered heat exchanger. They observed that fluid flow rate change presented an effect on the charging and discharging processes, however, the heat transfer mechanism showed the highest effect. Wang et. al. [76] have designed a climate control system with LHTES to provide heating to electric and hybrid vehicles' compartment. Their design targeted a 20% extension in the winter driving range.

2.5. Summary of The Literature Survey

The transient analysis of heat exchangers has found great interest due to its importance in controllability and thermal management. In the past, researchers have depended on the steady state conditions to design and analyze heat exchangers. Therefore, most of the work published on heat exchangers have dealt with steady state conditions due to the complexity of performing the dynamic analysis. Studies on cross flow heat exchangers have reported the effect of geometry of the tubes, channel sizes, and orientation on heat transfer and heat exchanger performance such as, Horvat et. al. [77], Mosa [78], Ismail et al. [79], Mangrulkar et. al. [80], and Mohanan et. al. [81]. While research related to the fluid inside the tube/channel can be found in Mesbah [82], Quaiyum [83], and Ghachem et al. [84]. Meanwhile, the focus in crossflow heat exchangers on airside was investigated by Junqi et.

al. [31], Paeng et al. [85], Siddiqui et. al. [30], Das Gupta et. al. [32], Waltrich et. al. [33], Fotowat [86], and Taler [34].

While transient analysis of heat exchangers is of interest to many researchers, their work involved the use of conventional heat exchanger Bunce [35], Lachi et. al. [36], Yin and Jensen [37], Srihari and Das [38]. On the other hand, dynamic analysis of cross flow heat exchangers, in particular, studied the heat exchanger performance and response due to a fluid's inlet temperature change such as, Abdallah and Rooke [39], Chen and Chen [40], Syed and Idem [41], Gogus and Ataer [42], Ataer [43], Silaipillayarputhur and Idem [45], and Vaisi et. al. [47]. However, for the case of flow variations, the reported research main emphasis was on the liquid inside the tube/channel of the heat exchanger Pearson et. al. [48], Fotowat et al. [49], Mishra et. al. [51], Del Valle and Ortega [52], Gao et. al. [53], and Erden [54]. It is observed that most of the transient analysis was represented using numerical or analytical analysis while less can be found using experimental work.

2.6. Scope of the Current Work

Several published articles have been thoroughly reviewed and reported in this study. The results of their work are also discussed in the above sections. In light of the previous published work and to fill in the gap in the research, the response of a compact finned meso heat exchanger was experimentally investigated. An experimental setup that is capable of accommodating different experimental sets of operating conditions was used to study the transient response of the heat exchanger. This setup was designed and developed to accommodate the heating and cooling modes of operation. Many equipment and devices are connected to the setup for measurement and recording.

The transient part of this study was achieved through the variation in the inlet mass velocity of the airside which flows perpendicular to the channel length. A thermal wind tunnel that is capable of running different airside flow rates at a wide range of temperatures was used. The heat exchanger response to the flow rate steps imposed was reported and discussed. The effect of the variation of airside flow rate on the thermal performance and heat transfer in the heat exchanger was analyzed. The aluminum heat exchanger consists of many channels distributed evenly in a thin slab. Correlations for airside Nusselt number

prediction in the cases of air heating and cooling were derived. The working fluids for the transient analysis involved air and water having all the inlet conditions constant except for the airside flow rate which was varied in a step form.

For the case of the thermal energy storage in the meso heat exchanger using a PCM, a modification was done to the experimental setup to run these experiments. The main working fluids were air and 50/50 ethylene glycol-water mixture along with the PCM as the latent heat thermal energy storage. Several cases of air flow rates and their effect on the storage performance were introduced. A comparison case study of the heat exchanger response time with and without PCM was made. Repeatability and effectiveness of the thermal energy storage was also investigated.

The outcome of this study will enrich the transient database and provide researchers with the required knowledge needed for the efficient design and control of heat exchangers. The results from this work will facilitate the prediction of the outlet temperature response to the changes in the inlet conditions and the response time for the heat exchanger to reach the steady state after the imposed variations. The correlations developed will offer a great prediction on the heat transfer necessary to manage a thermal system through the use of a heat exchanger. The thermal management accomplished via the thermal energy storage will attain savings in energy and fuel with low environmental impact. The use of PCM to store and release cold thermal energy assists in reaching occupants thermal comfort for an intermittent operation. The design of the heat exchanger makes it attractive for many applications due to its compactness and high heat transfer. While the use of PCM offers a source of energy that is available, cost effective, and environmentally friendly.

CHAPTER 3

EXPERIMENTAL SETUP

The experimental work discussed in this chapter was carried out in the Thermal management laboratory at the university of Windsor. This advanced lab features many different types of equipment, measuring devices, and test specimens. The focus of this laboratory is on running experiments that involve thermal management and thermal comfort such as heat transfer in heat exchangers and the use of PCM as a latent heat thermal energy storage along with other experiments related to solar energy and vehicle battery management. The major components of this sophisticated system include closed and open loop thermal wind tunnels with a built-in heat exchanger, chillers, heaters, water supply system, test section with tested heat exchanger, and a Data Acquisition System DAQ. The experimental setup with its main components can be shown in Fig. 3.1.

Figure 3.1. Experimental Setup

The experiments in this study are divided into transient air heating, transient air cooling, and air cooling using thermal energy storage. Therefore, the experimental setup is modified according to each experiment. Modifications are made to two main circuits in the system which are the airside and the liquid side circuits to accommodate the heating or cooling mode. A detailed description of each circuit can be found in the following sections.

3.1. Airside Loop

Conditioned air is supplied through an open loop thermal wind tunnel that encompasses a built-in heat exchanger for air temperature control. This wind tunnel is designed to have a thick wall of 1cm and a contraction ratio of 6.25. It has a test section in its middle top part that is detachable and can be adjusted to incorporate different heat exchangers. The air velocities in the wind tunnel vary in a wide range as well as the air temperature. The wind tunnel has an in-built ga to liquid CFHX for temperature control. This heat exchanger is located in the upstream of the air flow where it supplies conditioned air to the test section.

Air enters a thermally insulated open wind tunnel at ambient temperature and is forced into the test section by means of a blower. A blower is attached to the wind tunnel along with a controller to accommodate a wide range of air mass flow rate. The flow of air is considered uniform through the wind tunnel due to the use of a honeycomb mesh and a set of screens. Air temperatures at the inlet and the outlet are measured using 2 thermocouple grids. A total of 9 T-type thermocouples are placed in a grid at the inlet section of the airside and 18 thermocouples grid at the outlet as shown in Figure 3.2. Calibrated thermocouple probes are installed and connected to the multi-Channel data acquisition system for measurement readings and recordings. The relative humidity of air is also monitored and recorded via a humidity sensor attached at the inlet and outlet of the test section.

(a)   (b)
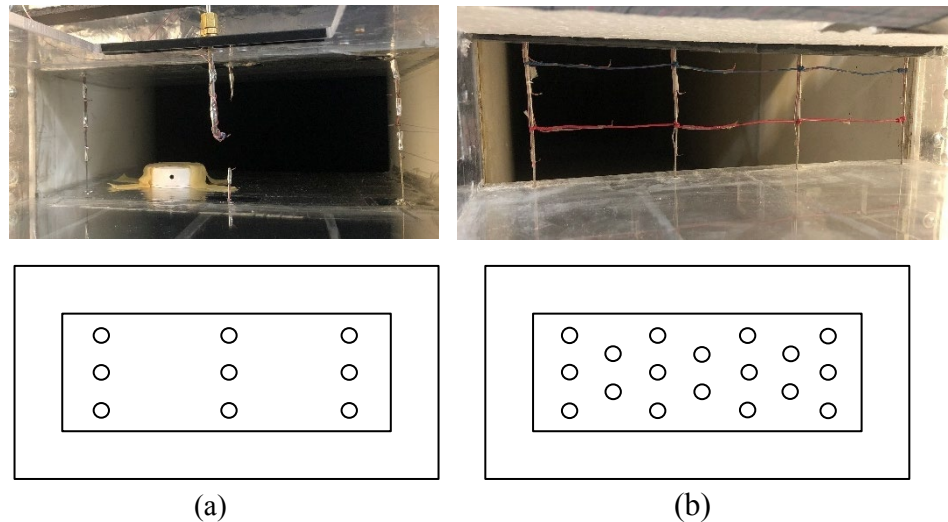
Figure 3.2. Air thermocouple grids (a) Inlet and (b) Outlet

Air enters the thermal wind tunnel at room temperature, therefore, attaining the required air inlet temperature below or above room temperature needs some system modifications.

3.1.1. Air Heating Experiments

Pipes that supply hot and cold city water are connected to the inbuilt heat exchanger. A mixing valve is installed to allow the control of the amount of each of the streams. The mixture of these two hot and cold streams passes through to the inbuilt heat exchanger and exchange the heat with the incoming air at room temperature. This heat exchange process achieves the desired air inlet temperature supplied to the test section. After exchanging the heat with the air, the city water is sent to drain.

3.1.2. Air Cooling Experiments

Air at room temperature is pre-dehumidified before entering the wind tunnel. The pre-dehumidification is to ensure no condensation effect takes place. A circuit comprising an inbuilt gas to liquid heat exchanger, a heater, a plate heat exchanger, and a pump is used to obtain the air inlet temperature. The city supplies hot and cold water. However, the exchange of air with hot city water alone in the inbuilt heat exchanger is not adequate to yield the desired air temperature. Therefore, a main inlet tank supplies DI-water at room temperature to the heater. Afterwards, a pump draws this heated DI-water and passes it through a plate heat exchanger where it exchanges heat with the city water supply. A mixing valve controls the amount of hot and cold city water needed to exchange the heat with the DI-water from the heater. As a result, a hot DI-water at a specified temperature is passed to the inbuilt heat exchanger. The heat transfer that occurs between the two fluids provides the desired inlet air temperature entering the test section. Figure 3.3 illustrates the inlet air temperature set loop.

Figure 3.3. Inbuilt heat exchanger air temperature control loop

3.2. Test Chamber

The test section is located at the wind tunnel top center part and houses the cross flow meso heat exchanger. Since polycarbonate is known for its lightweight, transparency, and a very good thermal resistance, it is used to fabricate the test chamber with a 0.25″ thickness. It has dimensions of 4″x12″x 24″ in a rectangular cross-section. All test chamber outer sides are well insulated to ensure no heat transfer to or from the environment. There are top inlet and outlet doors to provide accessibility to the inner part of the test section. The test section is designed with thick walls to ensure no heat transfer with the surrounding. There is an extra insulation all around the test section to ensure a complete insulation and minimization of any heat transfer between the chamber and the surroundings.

The test chamber is made detachable using screws to the wind tunnel for replacement, maintenance, or modification. The entrance to this section has a Pitot static tube placed at the center of the airflow and connected to a Differential Pressure Transducer PTD to provide air velocity measurement through static and total pressures difference. Velocity profile measurement is achieved using 5 ports on the test section inlet side. There are two other ports located in the test section center inlet and exit front walls which are used to provide pressure reading across the heat exchanger. A total of 30 thermocouples are

distributed evenly at the slab and serpentine inlet/outlet of the meso heat exchanger to provide surface temperature measurements.

3.3. Meso Heat Exchanger

The heat exchanger in this study is situated in the center of the test chamber with a perfect fit from the top and the bottom. This heat exchanger is a serpentine finned compact liquid-gas cross flow exchanger with a header and a manifold at the inlet and outlet. It is constructed of aluminum material with dimensions of 304.8 X 101.6 mm and a height of 101.6 mm. The heat exchanger has 5 aluminum flat thin slabs of 2mm thickness with an alternate flow direction and a surface area density β of 4000 m^2/m^3. Each slab incorporates 68 channels that are 1mm diameter distributed evenly along the flat slab and run through the serpentine bend leading to a total of 4 serpentines. The schematic of the heat exchanger is shown in Figure 3.4 and a section of the slab with the minichannels is shown in Figure 3.5.
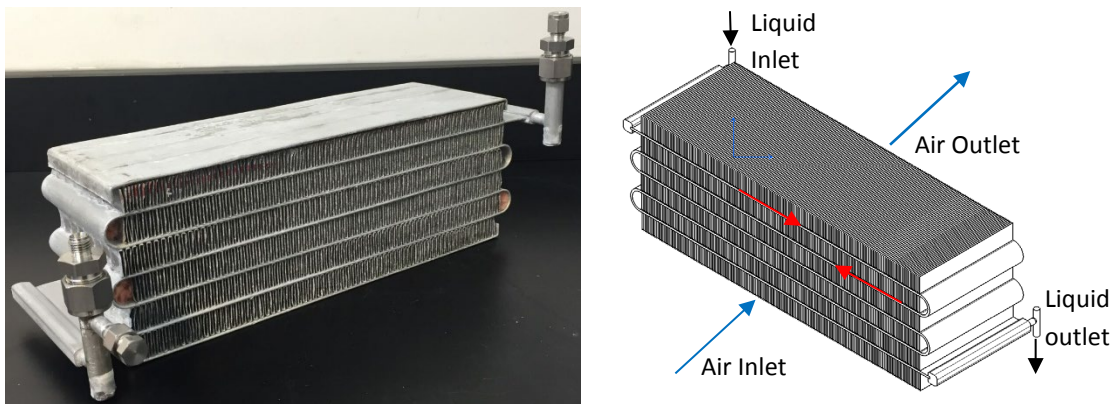
Figure 3.4. Meso heat exchanger

A list with the specifications of the heat exchanger is found in Table 3.1. Each slab has a set of aluminum fins that run parallel to the air flow along the depth of the heat exchanger. This heat exchanger is a one circuit exchanger with 5 passes. The fins are located between slabs and connected to them to allow heat transfer from the slab to the fins. There are 12 fins per 25.4 mm and the fins have a total length of 304.8 mm along the slab which make the total fin number in one row to 144. These rows were sealed from all directions to ensure no PCM leak happens during the experimental runs. Several thermocouples are distributed inside the PCM and on the slabs and serpentines surfaces to monitor and record the heat exchanger surface and PCM temperatures.

Table 3.1. Heat exchanger specifications

Compact heat exchanger	Specifications
Number of serpentines	4
Number of slabs	5
Thickness of slab	0.002 m
Material of the slab	Aluminum
Width of slab	0.1 m
Number of channels in a slab	68
Channel diameter	0.001 m
Fin height	0.018 m
Fin density	12 fins/in
Fins material	Aluminum
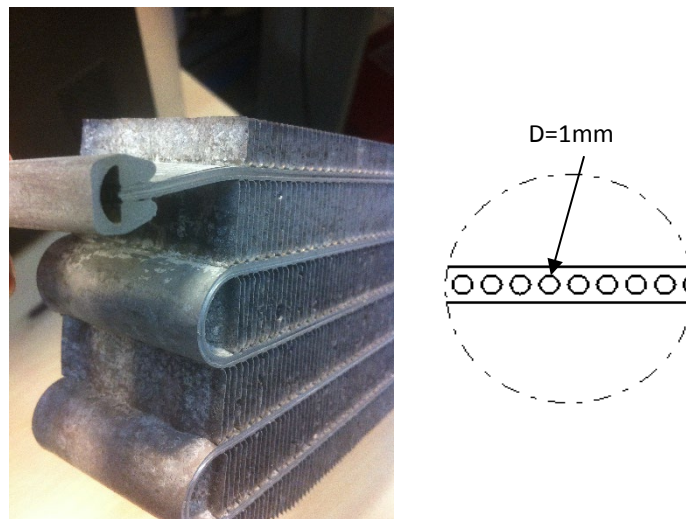
Figure 3.5. Slab with minichannels

3.4. Liquid Side Loop

The liquid side main components are a chiller, heater, pumps, liquid tanks, pipes, fittings, and hoses along with temperature and pressure gauges distributed along the inlet and outlet lines to monitor the temperature and pressure of the liquid. This loop differs in components depending on the heat transfer mode it is used for such as air heating or cooling. The flow of the liquid that passes through the meso heat exchanger is accurately determined and monitored via an inline Coriolis mass flow meter. It provides measurements of mass flow rate and temperature of the liquid with an uncertainty of ±0.1%. A variable speed gear pump was used to deliver steady state flow of the liquid and can handle different types of

liquids depending on their viscosity. The liquid mass flow rate is controlled by changing the frequency of an electric motor attached to the pump (more information can be found in appendix B).

3.4.1. Air Heating Experiments

For the case of air heating, the liquid side loop consists of two circuits: primary and secondary circuits as shown in Figure 3.6. DI water at room temperature is drawn from the main supply tank by the gear pump and is distributed into two portions. One portion is allowed to pass to the meso heat exchanger where its quantity is controlled by a needle valve. Another portion is heated by the incoming hot water from the secondary circuit via the brazed plate heat exchangers. Two common brazed plate heat exchangers are placed between the primary and secondary circuits to assist in providing a desired liquid inlet temperature.

The secondary water circuit comprises a tank, a gear pump, and an inline heater. In this circuit, the gear pump draws the water from the tank to the inline heater. The main purpose of using the secondary circuit is to assist in achieving the desired controllable DI water temperature flowing to the meso heat exchanger. The water exits the brazed plate exchangers and returns to the tank while, the DI water flows to the meso exchanger and is mixed with the first portion from the primary supply tank to obtain the desired DI water temperature going to the test section. Precise needle valves assist in controlling the amount of hot DI water and room temperature DI water mixture.

The amount of DI water that flows through the meso heat exchanger is measured and monitored by an inline Coriolis type mass flow meter. Additionally, Resistant Temperature Detectors RTDs and PTDs are used to measure the temperature and pressure of the inlet/outlet DI water. These measurements are recorded and stored through the DAQ system for processing using the NI LabView software.

1.	DI water source tank
2.	Gear pump
3.	Brazed plate heat exchangers
4.	Inlet liquid PTD
5.	Inlet liquid RTD
6.	Meso heat exchanger
7.	Outlet liquid PTD
8.	Outlet liquid RTD
9.	Inline mass flow meter
10.	DI water return tank
11.	Pitot static tube
12.	Data acquisition system
13.	Thermal wind tunnel
14.	Honeycomb straightener
15.	Flow net
16.	Hydraulic motor and fan
17.	Air filter
18.	Inbuilt heat exchanger
19.	Hot water city supply
20.	Needle control valve
21.	Cold water city supply
22.	Mixing valve
23.	Drainer
24.	Secondary water source tank
25.	Gear pump
26.	Heater
27.	Pressure gauge
28.	Temperature gauge

Figure 3.6. Schematic diagram of the experimental setup (heating)

3.4.2. Air Cooling Experiments

There are two types of the main working liquids used inside the channels of the heat exchanger for air cooling experiments, a DI-water for the transient air cooling and a 50/50 Ethylene Glycol (EG)-water mixture for the PCM experiments. The main reason for using the latter in the PCM experiments is to obtain a low liquid temperature to charge the PCM. Both experiments share the same liquid side main components: supply tank, gear pump, chiller, control valves, inline Coriolis mass flow meter, RTD, PTD, and pressure and temperature gauges as seen in Figure 3.7. The liquid mass flow rate was kept constant by means of a pump controller. The pump draws the working liquid from the supply tank at room temperature where it passes through the chiller to be cooled then transferred to an inlet tank to maintain it at a stabilized liquid temperature. Afterwards, the cooled liquid is passed to the test section meso heat exchanger. This working liquid had two purposes depending on the type of the experiment: cooling the air and charging the PCM.
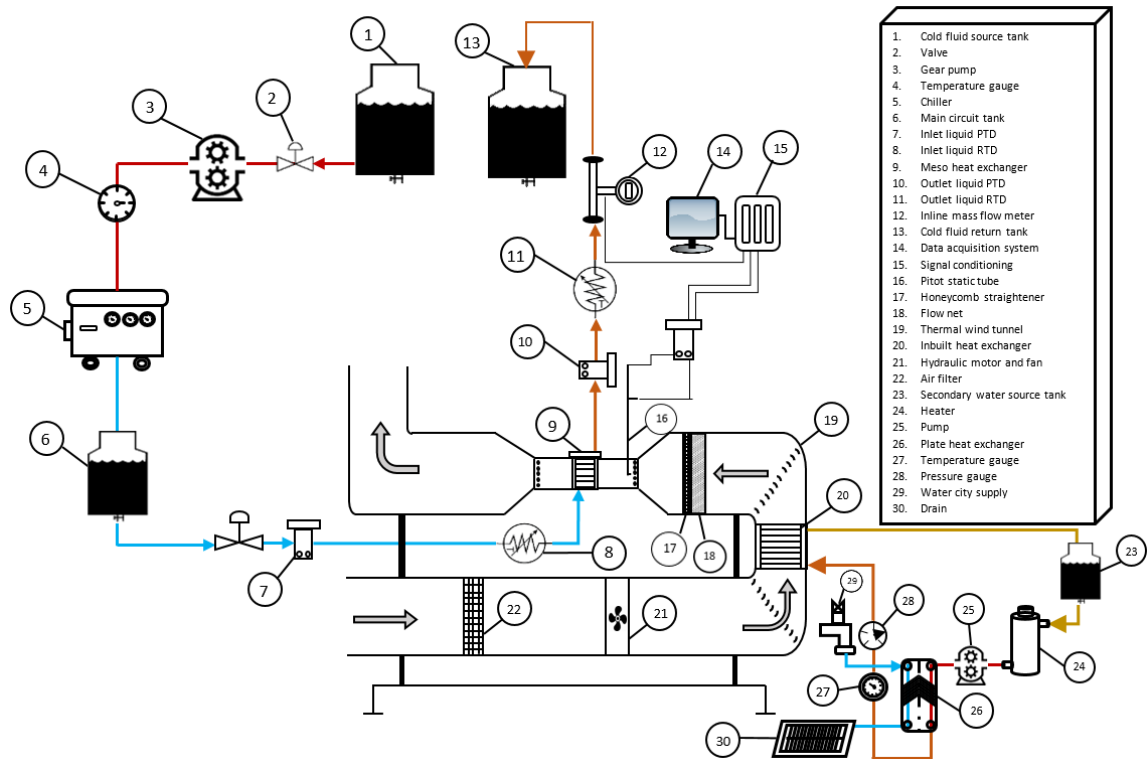
Figure 3.7. Experimental apparatus schematic diagram (cooling)

3.5. Data Acquisition System

The data acquisition system is comprised of the software, terminal block, and signal conditioner. All the readings at different measurement locations from the installed instruments such as thermocouples, PTDs, and RTDs are connected to the DAQ through their respective channels and recorded using LabView software. This system is capable of monitoring and recording 96 separate experimental parameters through its channels. In addition, DI water mass flow meter is monitored and recorded through the use of an inline Coriolis mass flow meter and its accompanied software.

3.6. Experimental Approach and Operating Conditions

The transient as well as the thermal energy storage experiments involved the compact cross flow heat exchanger in which liquid flows inside the channels and air flows perpendicular to the liquid flow. The PCM in the thermal energy storage experiments was injected and sealed as liquid under room temperature in the two upper rows between the fins. The experiments investigated the transient heat transfer in a crossflow heat exchanger for the

cases of air heating and cooling and the application of PCM as a thermal energy storage for air cooling. The operating conditions for each experiment are listed as follow.

3.6.1. Transient Air Heating Conditions

The air mass velocity in the air heating experiments was varied in a step form from an initial value to different final values. Meanwhile, the air inlet temperature, the liquid mass flow rate and inlet temperature were kept constant. The air inlet temperature was controlled using the wind tunnel inbuilt CFHX. The hot and cold city water supply heat exchange with the inlet air at room temperature provided the constant air inlet temperature to the meso heat exchanger. The heating system maintained the liquid inlet temperature at the required value. While the variable frequency pump allowed to control the inlet liquid mass flow rate. The operating conditions for the transient heating experiments can be found in Table 3.2.

Table 3.2. Air heating experimental operating conditions

DI water		Air	
Inlet temperature (°C)	**Mass flow rate (kg/s)**	**Inlet temperature (°C)**	**Mass flow rate (g/s)**
70	60	13	100 - 150
			100 - 200
			100 - 250
			100 - 300
			100 - 350

3.6.2. Transient Air-Cooling Conditions

The transient air-cooling experiments are performed at air inlet mass velocity step changes while the other conditions of air and liquid are maintained unchanged. The cooling system which its main component is the chiller supplies the cold liquid to the meso heat exchanger at a very low temperature. The supplied liquid can be DI water for the transient air-cooling experiment or 50/50 ethylene glycol-water mixture for the thermal energy storage experiment. While a variable frequency pump controls the liquid flow rate, the wind tunnel blower and its controller mange the air mass flow rate to the desired value. Meanwhile the

built-in heat exchanger regulates the air inlet temperature to its constant value. The operating conditions for the transient air cooling can be found in Table 3.3.

Table 3.3. Air cooling experimental operating conditions

DI water		Air	
Inlet temperature (°C)	**Mass flow rate (kg/s)**	**Inlet temperature (°C)**	**Mass flow rate (g/s)**
5	60	30	100 - 150
			100 - 200
			100 - 250
			100 - 300
			100 - 350

3.6.3. PCM Properties

PCM selection is an essential factor in the study of the LHTES system as the cooling energy and the time for discharging is related to the PCM amount and properties. The PCM in this study is selected based on the proposed application temperature range, automotive. In this work, the PCM selected is characterized by its high thermal storage density, nontoxicity, thermal stability, and availability. The Differential Scanning Calorimetry DSC results provided by the manufacturer shows the melting and solidification process as in Figure 3.8. This PCM is a commercial product and its detailed properties found in Table 3.4 are taken through measurements while most of them are supplied by the manufacturer [Microtek Laboratories Inc.].

Table 3.4. PCM properties

Item	Value
Type	Paraffin
Melting point [°C]	4-8
Latent heat [kJ/kg]	211
Density [kg/m^3]	760
Viscosity [m^2/s]	2.81x10^{-6}
Boiling point [°C]	252-254
Flash point [°C]	100
Thermal conductivity [W/m.K]	0.21
Specific heat [kJ/kg.°C]	2.17
Thermal cycling	Multiple
Above melting point	Liquid, colourless
Below freezing point	Solid, opaque
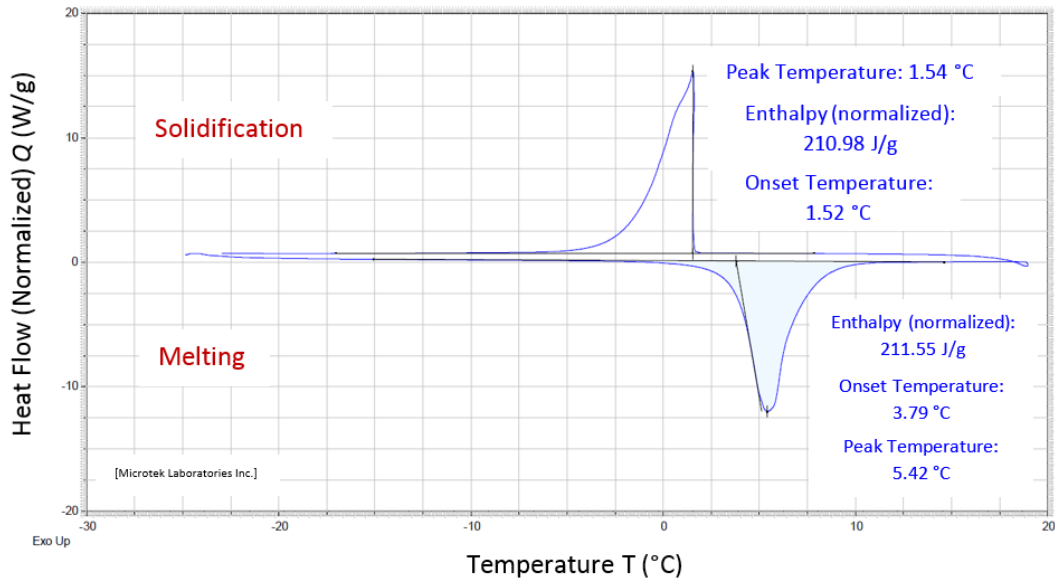
Figure 3.8. DSC results of the PCM

The operating conditions of the thermal energy storage experiments are shown in Table 3.5.

Table 3.5. PCM experimental operating conditions

Air mass flow rate change				Liquid mass flow rate change			
50/50 Ethylene glycol-water		Air		50/50 Ethylene glycol-water		Air	
Inlet temperature (°C)	Mass flow rate (g/s)	Inlet temperature (°C)	Mass flow rate (g/s)	Inlet temperature (°C)	Mass flow rate (g/s)	Inlet temperature (°C)	Mass flow rate (g/s)
-2.5	30	30	80	-3.0	20	30	80
			150		25		
			200		30		
			300		35		
					40		

3.7. Experimental Procedure

The experimental procedure for each of the four experiments is detailed in this section. All of the experiments commenced with steady state conditions. This steady state is predetermined by running trial experiments to determine the exact set positions of the heater, chiller, valves for the main DI water temperature, the mixing chamber valves of the city water in the wind tunnel, frequency of the airside blower, and the frequency of the DI water pump controller. Trial runs are also used to preset the equipment and valves according to the changes required during the experiments such as setting each of the inlet air mass flow rate that will be used for different step changes.

3.7.1. Transient Air Heating Procedure

1. Turn on the water heater from the secondary circuit and the blower of the wind tunnel. The desired water temperature and air mass flow rate are reached.
2. Start the DI water circulation by turning on the primary gear pump and adjusting its frequency to the pre-set value.
3. Achieve initial steady state conditions in which all the inlet operating conditions of air and the liquid experience no change with time.

4. Initiate the transient experiment by a sudden change in the frequency of the airside blower which results in changing the air velocity entering the test chamber.

5. Achieve the new steady state conditions after the transient change.

6. Repeat steps 3 to 5 for different mass velocity step changes as well as repeat these steps for each transient change 3 times for accuracy and repeatability confirmation.

7. Monitor and record all the data during the experiments using the data acquisition system.

3.7.2. Transient Air-Cooling Procedure

1. Start up the chiller until the set temperature of the DI water in the tank is reached.

2. Turn on the airside secondary circuit with the heater until it reaches its predetermined value.

3. Run the wind tunnel blower and set the mass flow rate and air inlet temperature to the desired values.

4. Achieve an initial steady state condition where liquid and air operating conditions are constant.

5. Apply a sudden change to the frequency of the airside blower from an initial mass flow rate to another mass flow rate value creating a step in the mass velocity.

6. Monitor the system till the new steady state conditions are achieved after the imposed change.

8. Repeat steps 4 to 6 for different mass flow rate step changes as well as repeat these steps for each transient change 3 times for accuracy and repeatability confirmation.

3.7.3. PCM With Air Mass Flow Rate Variations Procedure

The use of TES to provide extra cooling to the air when the liquid is stopped in a heat exchanger is investigated in this study. The motivation is to lower energy consumption while providing extra thermal comfort. The experiments are accomplished in 3 stages, the first stage is achieving a steady state condition, the second stage is the charging process, and the third stage is the discharging process. Meantime, all the inlet operating conditions are held constant which comprise an air inlet temperature of 30°C, a liquid inlet temperature of -2.5°C, and a liquid mass flow rate of 30g/s. These temperatures are chosen

to replicate a hot summer day where air enters a car evaporator at about 28-30°C with a very low coolant temperature to ensure the PCM is fully charged. The air mass flow rate did not experience a change with time during the experiment. However, different sets of experiments were investigated using a different air mass flow rate each time. The values of the airside mass flow rate case studied are 80, 150, 200, and 300 g/s.

The charging process is where the steady state is accomplished and the liquid in the heat exchanger reaches its set temperature value which leads to solidify the PCM at a temperature below its freezing point. This process is the charging of PCM where it transitions from liquid to solid storing energy for later use.

1. Start up the chiller until the set temperature of the 50/50 ethylene glycol-water mixture in the tank is reached.

2. Turn on the airside secondary circuit with the heater until it reaches its predetermined value.

3. Run the wind tunnel blower and set the air mass flow rate and inlet temperature to the desired values.

4. Run the variable frequency pump to the predetermined liquid mass flow rate frequency.

5. Achieve a steady state condition where liquid and air operating conditions are constant.

The positioning of several thermocouples in the airside, inside the PCM and on the surface, as well as the RTDs for the liquid side allow for data monitoring and recording through the DAQ system. The third stage is the discharging process where the PCM is melted and its stored cold thermal energy is discharged to cool the air.

The discharging process starts by shutting down the liquid mass flow rate while the airside circuit is still running. This procedure resembles the air-conditioning of a vehicle when stopping at a red light. In this case, the liquid is not cooling the air anymore, which triggers the discharging process of the energy stored in the PCM. The air outlet temperature starts rising but the PCM will work on delaying the rise in air outlet temperature by providing an extra time of cooling through its melting process. The liquid circuit is kept turned off till the PCM fully melts and transfers its stored energy to the air. Once the discharging process is complete, the liquid circuit is allowed to work, and the test is repeated for accuracy and repeatability confirmation. These 3 stages of steps are repeated each time with a different airside mass flow rate to examine the air flow rate effect on the discharging behavior of the

PCM. The data are recorded to be analyzed through the LabView software and the data acquisition system.

3.7.4. PCM With Liquid Mass Flow Rate Variations Procedure

These sets of experiments are conducted to investigate the effect of liquid mass flow rate variations on the PCM performance as a thermal energy storage. The experiments are very similar to the air mass flow rate variations however, the air mass flow rate was kept constant through all the experiments. The system started off by achieving a steady state where all the operating conditions are not changing with time. The air mass flow rate chosen was 80g/s, air inlet temperature of 30°C, and a liquid inlet temperature of -3.0°C. a set of 5 experiments were tested where the liquid mass flow rate value was different for each set as 20, 25, 30, 35, and 40 g/s.

The first stage is the charging where the cold liquid works on solidifying the liquid PCM to store the cold thermal energy for a later use. This stage starts with turning on the chiller to set the temperature of the 50/50 ethylene glycol-water in the tank. Meanwhile, the airside secondary circuit is also turned on, thus the heater provides the hot liquid that will assist in setting the airside inlet temperature to the desired value. Next the wind tunnel blower is switched on and air mass flow rate as well as its inlet temperature are allowed to reach their set values. While the liquid mass flow rate is adjusted by the variable frequency pump. Once these inlet conditions of the working fluids are achieved, a steady state condition is pursued where these parameters do not vary with time.

The last stage, which is called discharging, starts by switching off the 50/50 ethylene glycol-water pump. This process will cause a rise in the air outlet temperature and trigger the melting of the PCM to discharge its cold thermal energy to the air. The same steps in all the stages are repeated with a different 50/50 ethylene glycol-water mass flow rate each time. Additionally, each set of the five experiments is repeated 3 times for accuracy and repeatability confirmation.

CHAPTER 4

THEORETICAL BACKGROUND AND DATA REDUCTION

This chapter presents the methodology behind the transient heat transfer analysis for the crossflow heat exchanger. It also pertains to the theoretical consideration for using a PCM in a heat exchanger as a thermal energy storage. Additionally, the fundamental equations of heat transfer are demonstrated as part of this chapter analysis.

4.1. Thermophysical Properties of The Working Fluids

The thermophysical properties of air, ethylene glycol-water mixture, and DI water such as thermal conductivity, viscosity, density, etc. were evaluated using the fluid's bulk temperature. The bulk temperature of the working fluids was found using the average of both inlet and outlet temperature measurement as follows,

$$T_{a,b} = \frac{T_{a,i} + T_{a,o}}{2} \qquad \qquad 4.1$$

$$T_{DI\ water,b} = \frac{T_{w,i} + T_{w,o}}{2} \qquad \qquad 4.2$$

$$T_{g,b} = \frac{T_{g,i} + T_{g,o}}{2} \qquad \qquad 4.3$$

4.2. Key Assumptions

The objectives of the current study are to investigate and evaluate the main dimensional and dimensionless parameters that affect the transient response of a cross flow meso heat exchanger subjected to step changes in air inlet mass velocity for the cases of air heating and cooling. These parameters include both fluids outlet temperatures, heat transfer rates, airside heat transfer coefficient, Nusselt number, Colburn j factor, Reynolds number, and friction factor. Furthermore, evaluate the performance of the heat exchanger when a PCM is injected in it as a thermal energy storage. Thus, studying the effect of air mass velocity change on the discharging of the PCM in comparison to the liquid mass flow rate change.

The evaluation of the transient behavior of a compact CFHX is studied when the airside mass velocity experiences sudden variations. This evaluation is presented in terms of

parameters such as fluids dimensionless outlet temperatures, heat transfer rates, airside heat transfer coefficient, and Nusselt number. Furthermore, this section explores the thermal management aspect of the crossflow heat exchanger equipped with PCM for extended thermal cooling. It also investigates the influence of air mass flow rate on the PCM discharging process. Modeling the heat transfer for this case study requires some assumptions to be considered that are listed as in the following:

- A uniform temperature distribution of the heat exchanger body at a given time.
- The heat transfer between the test section and the surrounding can be considered negligible.
- The two fluids in the heat exchanger are assumed to be in a single phase.
- The liquid is uniformly distributed in the channels along the slab.
- The radiation effect between the heat exchanger and the air is negligible.
- Conduction heat transfer for both fluids along the direction of the fluid flow is negligible.
- The air is assumed to be dry air since the humidity contribution was found to be less than 1.5% (for air heating) and using properties of moist air for the case of air cooling.
- The potential and kinetic energies are approximated to zero.

4.3. Dimensionless Parameters

A dimensionless parameter is used to provide a generalized form of a relationship between different dimensional parameters. It is independent of any variation in the measuring unit and is preferred due to its convenience in delivering comparisons with other research works. Some of the dimensionless parameters for heat transfer and fluid flow used in this study are Reynolds number, Nusslet number, Stanton number, etc. The following is the dimensionless parameters used in this work along with a description of each.

4.3.1. Nusselt Number

Nusselt number is a dimensionless number that characterizes the enhancement in heat transfer in a fluid layer. It also represents the dimensionless form of the heat transfer

coefficient. It is defined as the ratio of convection to conduction heat transfer and can be expressed for the airside as,

$$Nu_a = \frac{h_a D_{h,a}}{k_a} \tag{4.4}$$

4.3.2. Stanton Number

It is a dimensionless number that considers the ratio of the heat transfer coefficient of the fluid to the fluid's thermal capacity. Stanton number for airside can be expressed as,

$$St_a = \frac{h_a}{G_a c_{p,a}} \tag{4.5}$$

This number is inversely proportional to the Reynolds and Prandtl numbers and also relates to the Nusselt number and the Colburn j factor.

4.3.3. Transient Dimensionless Temperature

The transient dimensionless temperature was defined by Srihari and Das [38] for each fluid at the transient time depending on the case whether air heating or air cooling as,

$$T_{w,o}^*(t) = \frac{T_{w,o}(t) - T_{a,i}(t)}{T_{w,i}(t) - T_{a,i}(t)} \qquad (heating) \tag{4.6}$$

$$T_{w,o}^*(t) = \frac{T_{a,i}(t) - T_{w,o}(t)}{T_{a,i}(t) - T_{w,i}(t)} \qquad (cooling) \tag{4.7}$$

$$T_{a,o}^*(t) = \frac{T_{a,o}(t) - T_{a,i}(t)}{T_{w,i}(t) - T_{a,i}(t)} \qquad (heating) \tag{4.8}$$

$$T_{a,o}^*(t) = \frac{T_{a,i}(t) - T_{a,o}(t)}{T_{a,i}(t) - T_{w,i}(t)} \qquad (cooling) \tag{4.9}$$

4.3.4. Dimensionless Time

The dimensionless time is defined as the heat transfer of the fluid by convection to the wall thermal capacity multiplied by time as,

$$t^* = \frac{(hA)_a}{MC} t \tag{4.10}$$

4.3.5. Colburn j Factor

The Colburn j factor for the airside is a modification of Stanton number which is utilized to characterize the heat transfer capacity of the heat exchanger and also accounts for the moderate variations of Prandtl number as,

$$j_a = St_a Pr_a^{2/3} \qquad (4.11)$$

4.3.6. Reynolds Number:

Reynolds number is a parameter that is used to distinguish the fluid flow regime such as laminar, transient, or turbulent. It is comprised of different parameters and is represented by the inertia to viscous forces of the flow as,

$$Re = \frac{\rho VZ}{\mu} \qquad (4.12)$$

The airside Reynolds number was determined using the mass velocity definition using the minimum free flow area of the air passing through the fins and slab as follows,

$$G_a = \frac{\dot{m}_a}{A_{min,a}} \qquad (4.13)$$

The mass flow rate of the air crossing the heat exchanger was found using the air velocity and area as,

$$\dot{m}_a = \rho_a V_a A_a \qquad (4.14)$$

The air velocity V was measure using Pitot static tube that was installed at the inlet of the test section. It measured the dynamic, static and total pressure which were recorded using the data acquisition system. The dynamic pressure difference is used to calculate the inlet air velocity as,

$$V_a = \sqrt{\frac{2\Delta p_{dynamic}}{\rho_a}} \qquad (4.15)$$

Therefore, airside Reynolds number can be found based on the mass velocity definition as,

$$Re_a = \left(\frac{\rho VD}{\mu}\right)_a = \frac{\frac{\rho V A_{a,min}}{A_{a,min}}D_{h,a}}{\mu_a} = \frac{\frac{\dot{m}_a}{A_{a,min}}D_{h,a}}{\mu_a} = \frac{G_a D_{h,a}}{\mu_a} \qquad (4.16)$$

4.4. Transient Heat Transfer Rate (Air Heating)

The heat transfer rate of the liquid is calculated as,

$$\dot{Q}_w = \dot{m}_w c_{p,w}(T_{w,i} - T_{w,o}) \tag{4.17}$$

The heat exchanger is assumed to behave as a lumped system which indicates that the temperature of the heat exchanger body at any point is uniform at a given time. However, this temperature is a function of time. Using this approach, the airside heat transfer rate was evaluated from applying the energy balance on the heat exchanger wall (slab+fins) as shown in Figure 4.1 for the case of air heating. Assuming the kinetic and potential energies are ≈0 and that no work is produced, the energy balance equation can be written as,

$$\dot{Q}_w - \dot{Q}_a = \frac{dE_{C.V.}}{dt} = \frac{dU}{dt} = MC\frac{dT_s}{dt} \tag{4.18}$$

$$\dot{Q}_a = \dot{Q}_w - MC\frac{dT_s}{dt} \tag{4.19}$$

Thus, the airside heat transfer rate is found from the following equation as,

$$\dot{Q}_a = \dot{m}_w c_{p,w}\left(T_{w,in} - T_{w,o}(t_{i+1})\right) - \frac{MC(T_s(t_{i+1}) - T_s(t_i))}{\Delta t} \tag{4.20}$$
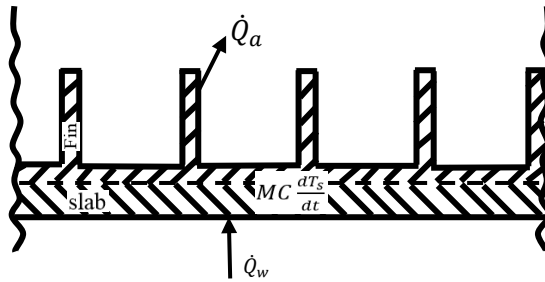
Where, i = 0, 1, 2, 3,…..,k

Figure 4.1. Thermal energy balance on the heat exchanger wall (air heating)

4.5. Transient Heat Transfer Rate (Air Cooling)

The liquid heat transfer rate is represented as,

$$\dot{Q}_w = \dot{m}_w c_{p,w}(T_{w,o} - T_{w,i}) \tag{4.21}$$

Following the same approach of lumped system to obtain the heat transfer rate for the airside, an energy balance on the heat exchanger wall was applied as illustrated in Figure 4.2 and presented as follows,

$$\dot{Q}_a - \dot{Q}_w = \frac{dE_{C.V.}}{dt} = \frac{dU}{dt} = MC\frac{dT_s}{dt} \tag{4.22}$$

$$\dot{Q}_a = \dot{Q}_w + MC\frac{dT_s}{dt} \tag{4.23}$$

Therefore, the air heat transfer rate final equation is expressed as,

$$\dot{Q}_a = \dot{m}_w c_{p,w}\left(T_{w,o}(t_{i+1}) - T_{w,i}\right) + \frac{MC(T_s(t_{i+1}) - T_s(t_i))}{\Delta t} \tag{4.24}$$

Where, $i = 0, 1, 2, 3,\ldots,k$
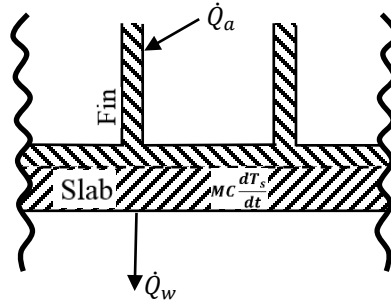
Figure 4.2. Thermal energy balance on the heat exchanger wall (air cooling)

4.6. Heat Transfer Coefficient

The heat transfer coefficient represents the heat transfer rate that occurs between a solid and a fluid for a unit area and temperature difference. There is a challenge with the current heat exchanger geometry to precisely obtain the surface temperature for the slabs and the finned areas. The obtained surface temperature is used to calculate the heat transfer coefficient. Therefore, the airside heat transfer coefficient is found through an iterative process using the fin and overall surface efficiencies.

The overall surface efficiency for airside is expressed in the following equation,

$$\eta_a = 1 - \frac{A_{fin}}{A_a}(1 - \eta_{fin}) \tag{4.25}$$

The airside heat transfer area for the slabs and fins is found from, $A_a = A_{slabs} + A_{fins}$

The expression for fin efficiency of a uniform cross section is presented by Shah and Seculic [5] and is adopted in this study as,

$$\eta_{fin} = \frac{\tanh(SL)}{SL} \tag{4.26}$$

Where,

$$S = \sqrt{\frac{2h_a}{k_{fin}t_{fin}}} \tag{4.27}$$

$$L = \frac{H_{fin}}{2} - t_{fin} \tag{4.28}$$

The surface temperature is measured using a distribution of 30 thermocouples on the inlet and outlet manifolds surfaces of the heat exchanger and the serpentine bends which are located before and after the inlet and outlet sections of the test chamber. While the air average temperature is found through the inlet an outlet grids comprised a total of 27 thermocouples inside the test section to measure the incoming and outgoing air temperature. The surface and average air temperatures are used in an iterative process to find the airside heat transfer coefficient. The following sets of equations explain the iterative process of obtaining the air heat transfer coefficient.

1. Obtain the surface and air average temperatures.
2. The overall surface efficiency is set $\eta_a = 1$ and entered in the following equation to solve for h_a as,

$$h_a = \frac{\dot{Q}_a}{\eta_a A_a(T_{s,avg}-T_{a,avg})} \; (heating) \; or \; h_a = \frac{\dot{Q}_a}{\eta_a A_a(T_{a,avg}-T_{s,avg})} \; (cooling) \tag{4.29}$$

3. The h_a from Eq. (4.29) is substituted into Eq. (4.27) to solve for S.
4. Substitute the value of S from Eq. (4.27) into Eq. (4.26) to find the fin efficiency.
5. Use the fin efficiency from step 4 and enter it into Eq. (4.25) to find the new η_a.
6. The value of the new η_a from step 5 is then to be entered into Eq. (4.29) to find h_a.
7. Repeat steps 2 to 6 using the values of η_a, h_a, and η_{Fin}, for their final values.

The resulted heat transfer coefficient can be used to obtain the dimensionless airside parameter, Nusselt number.

4.7. Transient Air Cooling With PCM

The PCM melting and solidification processes are associated with the energy provided during the charging process or the energy extracted during the discharging process by the heat transfer fluid. The thermal performance of a latent heat thermal energy storage is evaluated using the PCM absorbed thermal energy Medrano [72]. The amount of energy during a phase change process can be found as,

$$Q = M.cp_{PCM,s}\left(T_{PCM,f} - T_{PCM,initial}\right) + M.H^o{}_{PCM} + M.cp_{PCM,l}\left(T_{PCM,final} - T_{PCM,m}\right) \quad (4.30)$$

Where, M is the PCM mass, $cp_{PCM,s}$ is the PCM average specific heat between the initial and melting temperatures, $cp_{PCM,l}$ is the PCM average specific heat capacity between melting and final temperature, $T_{PCM,f}$ and $T_{PCM,m}$ are the PCM freezing and melting temperatures, $H^o{}_{PCM}$ is the PCM latent heat per unit mass, $T_{PCM,initial}$ and $T_{PCM,final}$ are the initial and final PCM temperatures during the process.

The PCM charging and discharging processes depend on the energy given by the air to the 50/50 ethylene glycol-water mixture. The temperature measurement of the air inlet and outlet thermocouple grids are used to evaluate the heat transfer for the PCM melting and solidification processes. This instantaneous energy is determined from the fluid's temperatures and mass flow rate as in the following,

$$\dot{Q}_a = \dot{m}_a c_{p_a}(T_{a,i} - T_{a,o}) \quad (4.31)$$

A dimensionless form of the airside outlet temperature can be represented using the normalized air outlet temperature as follows,

$$T_{a,norm} = \frac{(T_{a,o} - T_{a,o,initial})}{(T_{a,i} - T_{a,o,initial})} \quad (4.32)$$

The cumulative heat transfer or the energy capacity is found by integrating the instantaneous heat transfer to the air for every one second duration as,

$$Q_{a,cum.} = \sum_{i=1}^{n} Q_i dt \quad (4.33)$$

Where, *dt*=time (second), Q_i = instantaneous heat transfer, and n is the number of time intervals.

CHAPTER 5
RESULTS AND DISCUSSION

The experimental transient results of air heating and air cooling using active and passive methods through a working fluid are presented in this work. The active method is represented by the transient performance of a meso CFHX for a variation of airside mass velocity while holding all other inlet fluid conditions constant. The transient response of the heat exchanger characterized by different heat transfer and fluid flow parameters is reported for the cases of transient air heating and cooling. These parameters are presented in dimensional and dimensionless forms which comprise outlet temperatures, heat transfer rates, Reynolds number, Nusselt number, etc.

A generalized empirical correlation to predict the airside Nusselt number using experimental results is also derived. The experimental derived correlations obtained from this work are compared with the previous published work in the literature. The transient analysis provides an insight into the effect of the variation of the airside mass velocity ratio on the outlet fluids temperature response and other parameters listed in this chapter. Furthermore, the response of the compact crossflow heat exchanger to step changes in air mass velocity and the response time of each fluid to reach the steady state are discussed.

On the other hand, the passive method includes air cooling through the integration of PCM in the meso heat exchanger as a latent heat thermal energy storage. This case relates to the results of air mass flow rate effect on the PCM discharging time and extending the cooling period. The significant results of this work are presented and discussed according to the experimental findings and the predefined operating conditions.

5.1. Transient Air Heating

The experimental findings of the active air heating are discussed in the following sections. The hot DI water was flowing inside the minichannels while air flew perpendicular to the liquid flow over the slab surface between the fins. The hot DI water was used to cool the incoming air while performing step changes in air mass velocity. This resulted in a change

in the outlet response of each of the working fluids which their results are discussed in the following sections.
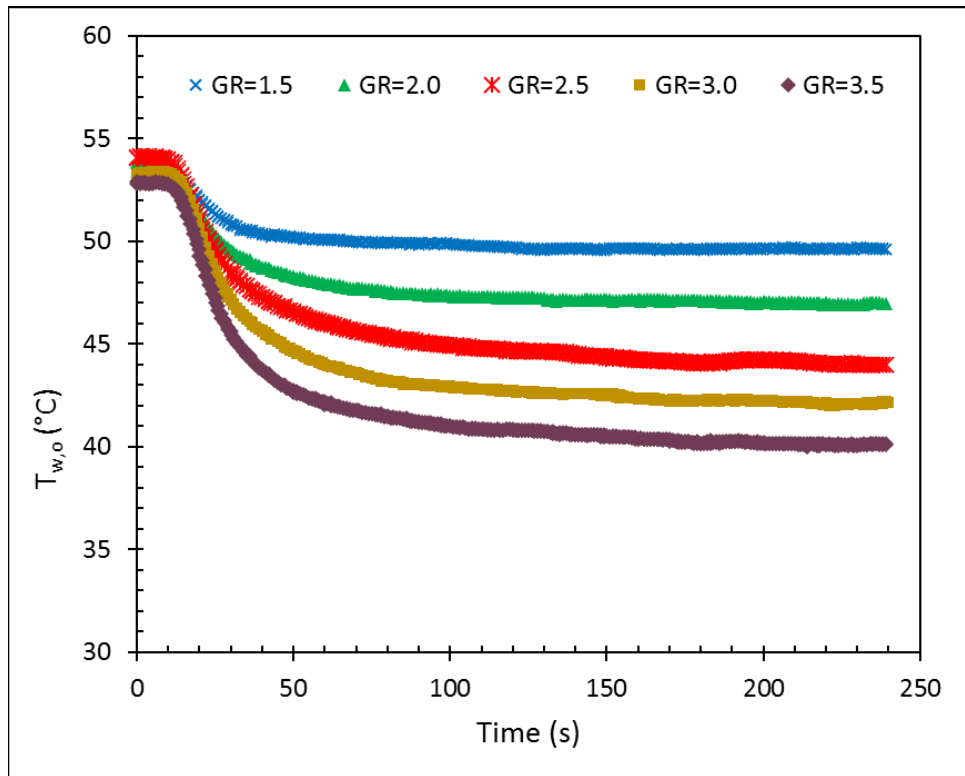
5.1.1. Exit Temperature Response with Dimensionless Time

The outlet temperature response of air and DI water in a dimensional and dimensionless form is shown in Figures 5.1 and 5.2. The non-dimensional definitions are found using equations (4.6-4.9). The two fluids outlet temperatures do not show an instantaneous response to the change in air mass velocity ratio. The delay in the outlet temperature response is called initial delay time. The delay time for the DI water is higher than the air due to many factors such as the instrument response, residence time, etc. The residence time is defined as the time the fluid takes to enter and exit the heat exchanger which is shorter for the air flow compared to the long DI water channel. The airside delay time for all the steps was found to be about 6s compared to 12s on the DI water side. It can be concluded that for the same volume of the heat exchanger, increasing the mass velocity reduces the time the fluid resides in the heat exchanger. For an air heating process, the increase in air mass velocity ratio results in shorter residence time, lower exit temperature of the fluids, higher heat transfer coefficient and heat transfer rate.

The higher the step change, the higher the decrease in the outlet temperature of the two fluids. When comparing Figure 5.2a with 5.2b at the same step change, the decrease in air outlet temperature is found higher than DI water outlet temperature reduction. The fact that air travels through a short length of the heat exchanger along with the step change imposed on the airside contribute to this difference in the outlet temperature. Additionally, the response time, which is the time it takes the fluid to undergo a change from one steady state to another, of the DI water is higher than air. It is also seen that the response time of each fluid increases with the increase in the step change however, as GR increases, the rate of increase in the response time levels off. The sudden increase in air mass velocity causes more air flow movement from inlet to outlet of the heat exchanger resulting in air outlet temperature drop. Once the DI water outlet temperature starts responding to the step change applied, the increasing tendency of air outlet temperature to drop is reduced until it reaches a final steady state.
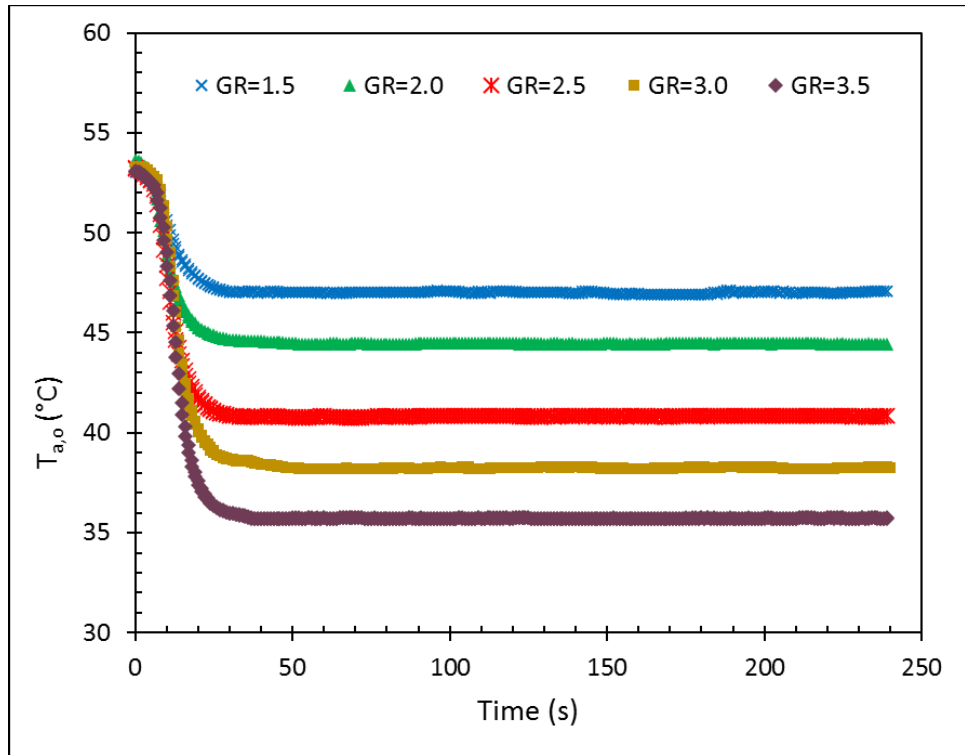
(a) Air outlet temperature

(b) DI water outlet temperature

Figure 5.1. The effect of air mass velocity ratio on outlet temperature response
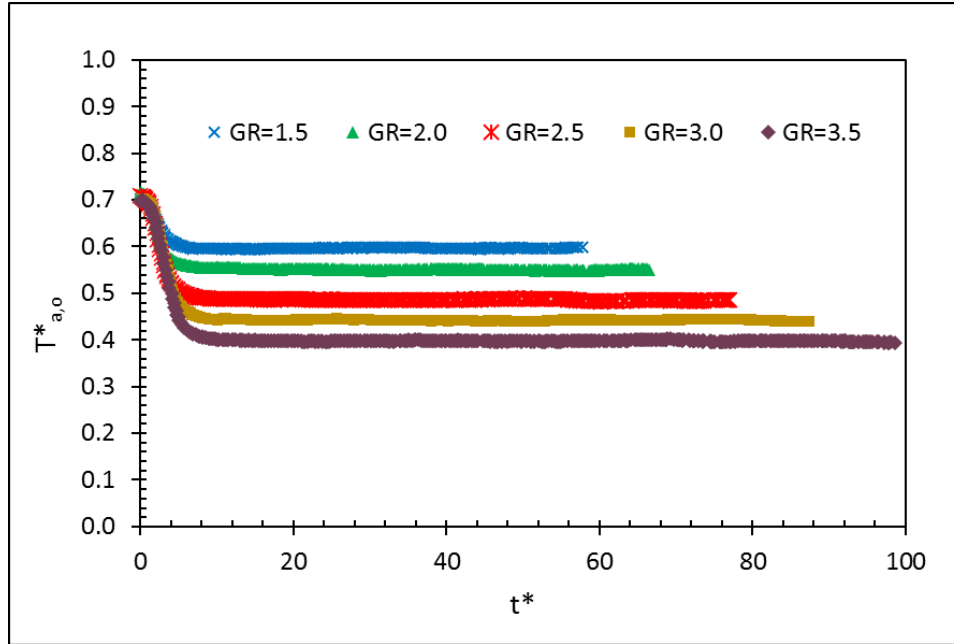
(a) Dimensionless air outlet temperature
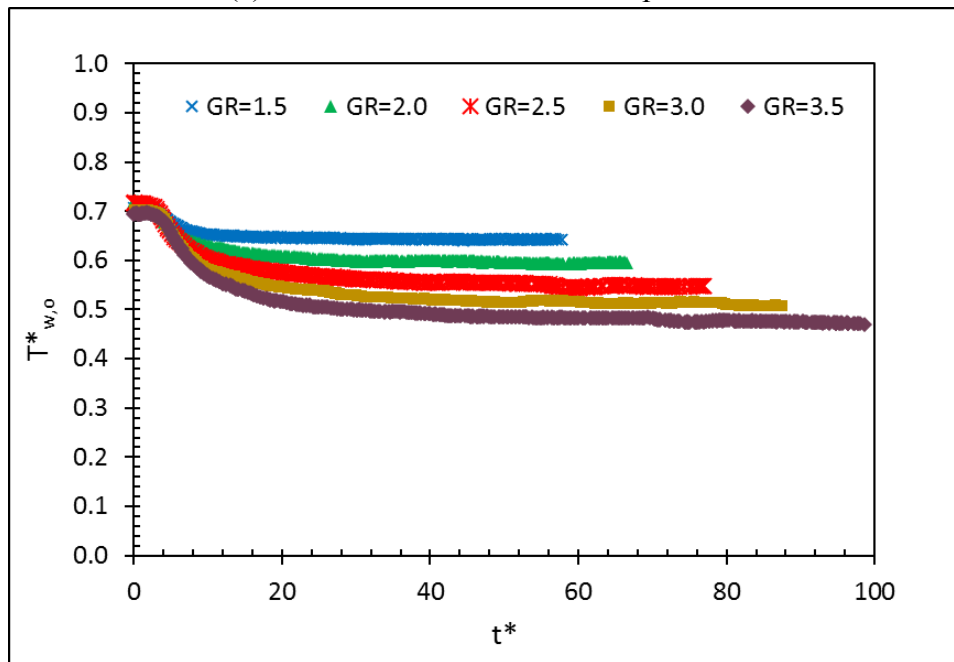
(b) Dimensionless DI water outlet temperature

Figure 5.2. Effect of air mass velocity ratio Dimensionless outlet temperature

5.1.2. Dimensionless Outlet Temperature Response with Reynolds Number

The effect of the step change variation represented by Reynolds number is demonstrated in Figure 5.3. This figure shows all the steps starting from an initial Reynolds number of about 700 since no change in inlet conditions happens and the mass flow rate of air is set

to 100 g/s at steady state. When a step change is applied to the air mass flow rate, it takes some time for the initial mass flow rate to reach its predestined value. However, the dimensionless outlet temperature continues to drop till the final steady state is reached and that is due to the ongoing heat transfer that takes place from the DI water to the heat exchanger wall then to the air. Once heat transfer balances between the two fluids at steady state, the dimensionless outlet temperature reaches its final steady state value.

It is noticed that the higher the Reynolds number, the higher the time it takes for the dimensionless outlet temperature to reach its final steady state value. The initial delay and the residence time effect contribute to the continuous change in the dimensionless outlet temperature after reaching the predestined value. When comparing Figures 5.3a with 5.3b, the DI water dimensionless outlet temperature does not possess the decreasing trend as in the airside for the transition period from an initial to a preset value of Reynolds number. The DI water has a longer initial delay time as well as residence time.
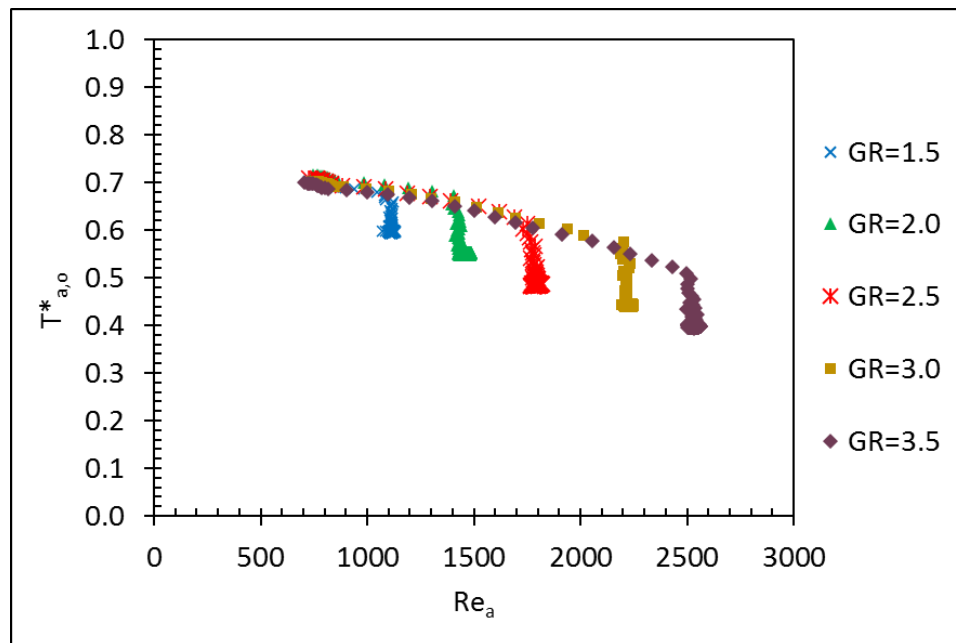
(a) Dimensionless air outlet temperature vs. Re_a
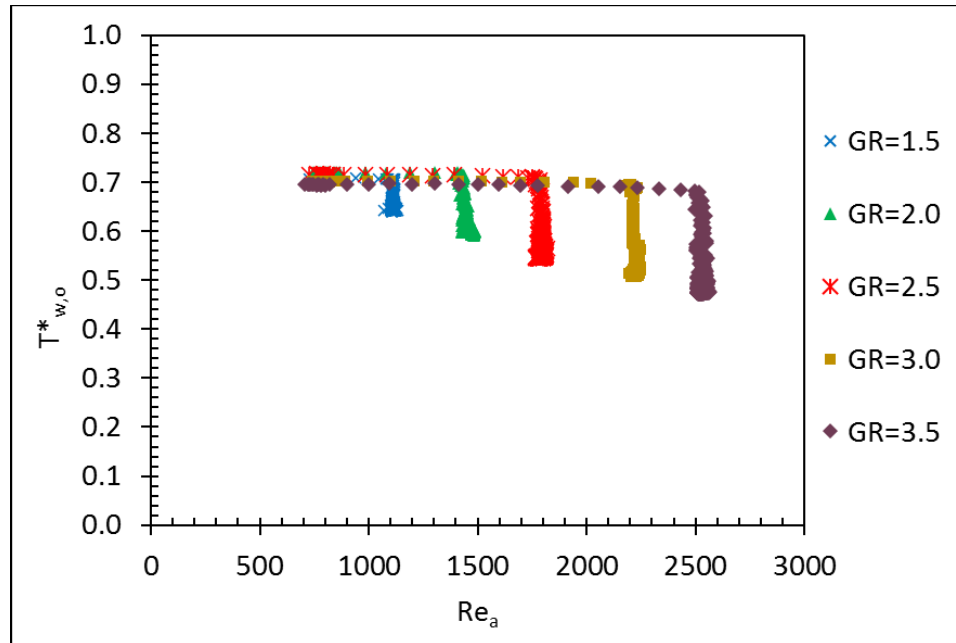
(b) Dimensionless DI water outlet temperature vs. Re_a

Figure 5.3. Dimensionless outlet temperatures with respect to Reynolds number

5.1.3. Transient Fluids Heat Transfer Rate

The heat transfer rate for the two fluids is evaluated and plotted with respect to time in Figure 5.4. Both fluids heat transfer rate increases with the increase in air flow rate, however, since the step applied is in the airside mass velocity, air behaves differently than DI water during the transient change. Initially, the two fluids heat transfer rates are balanced at the steady state. The step change applied to the air mass velocity causes an unequal delay time between the two fluids heat transfer rate and a dissimilar behavior during the transient change.

The increase in air mass velocity increases the rate of heat transfer to the air and that causes a sharp drop in the surface temperature of the wall since the air initial delay and response time is short. This explains the increase in airside heat transfer rate after the initial delay time to a high value. Then a decline in heat transfer rate is noticed since DI water outlet temperature, after its initial delay time, starts showing its response to the air mass velocity change. This response reduces the sharp rate drop of the surface temperature and increasing trend until reaching the re-balance of the two fluids heat transfer rate at the final steady state. The percentage error in comparing the two methods of finding the heat transfer rate,

where one is based on the heat exchanger wall heat transfer and the other is based on the heat transfer on the airside at the final steady state, is found to be less than 8%.
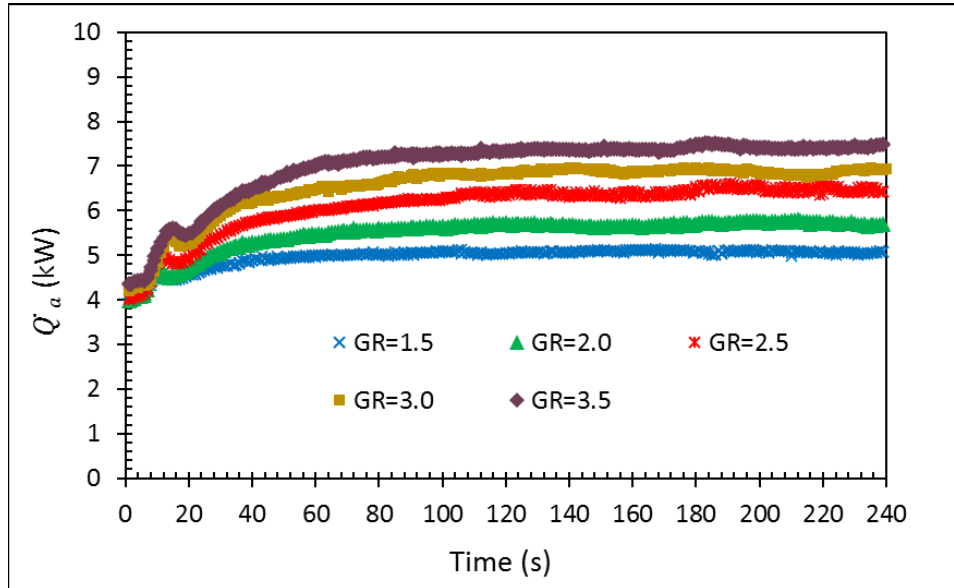
(a) Air heat transfer rate
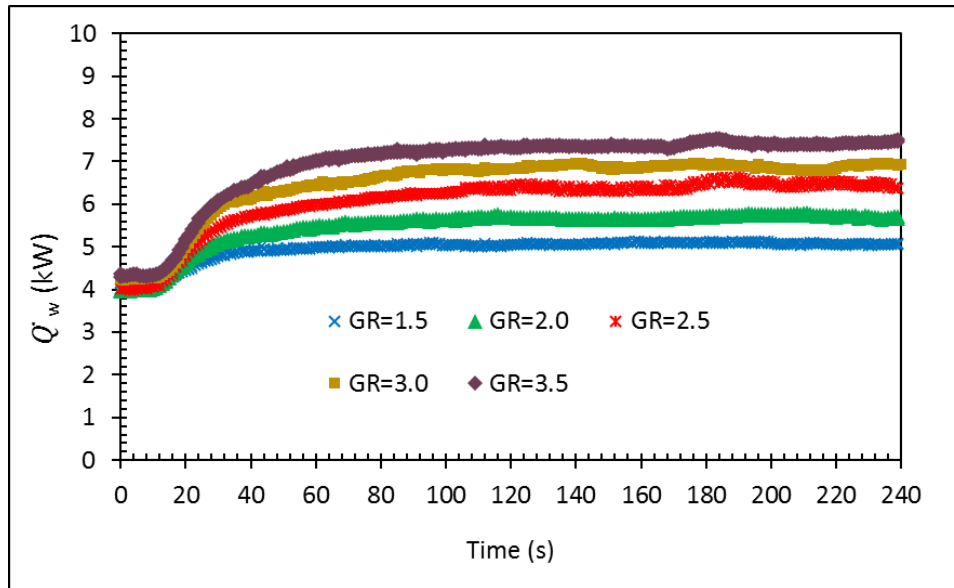
(b) DI water heat transfer rate

Figure 5.4. Effect of GR on the transient heat transfer rate

5.1.4. Transient Airside Heat Transfer Coefficient

The airside heat transfer coefficient is calculated using the iterative process discussed previously and the results are shown in Figure 5.5. The system ability to record simultaneous measurement of the air temperatures through the grids at the inlet and outlet sections across the heat exchanger provides the bulk air temperature. Along with the

surface average temperature and the air heat transfer rate, the average airside heat transfer coefficient is found. The air mass velocity step increase leads to an increase in the heat transfer coefficient and the higher the step, the higher the heat transfer coefficient. The response time of the heat transfer coefficient increases with the increase in the step change. The behavior of the airside heat transfer rate affects the trend of the heat transfer coefficient especially during the transient period. The sudden increase in air heat transfer rate in the transient region due to the increased air mass velocity and the decrease in surface temperature results in an increase in the heat transfer coefficient. However, this sharp increase is adjusted after the heat transfer rate of the two fluids balances and eventually reaches the steady state.
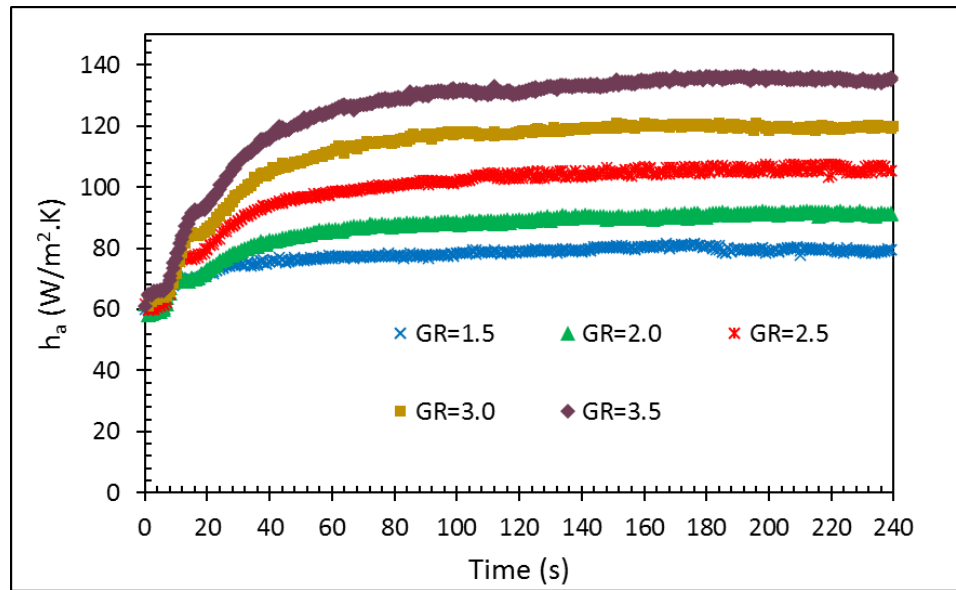
Figure 5.5. Transient airside heat transfer coefficient at different GR

5.1.5. Transient Airside Nusselt Number

Airside Nusselt number represents the dimensionless heat transfer coefficient calculated for different air mass velocity step changes and shown in Figure 5.6 with respect to changes in the dimensionless time. As expected, Nu_a increases with the increase in air mass velocity step change since the heat transfer coefficient is increased. The higher the step, the longer it takes for Nu_a to reach steady state since the response time increases with the increase in the step change. Figure 5.7 illustrates the effect of changing airside Reynolds number on Nu_a. The step increase of air mass velocity from an initial value to the predestined value happens during a finite time which is controlled by the magnitude of the step change. This

rise in air mass velocity step change leads to an increase in heat transfer rate and in turn the heat transfer coefficient. Once the air mass velocity reaches its set value and due to the heat transfer occurring between DI water, heat exchanger wall, and the air, the change in Nusselt number continues till reaching a final steady state.
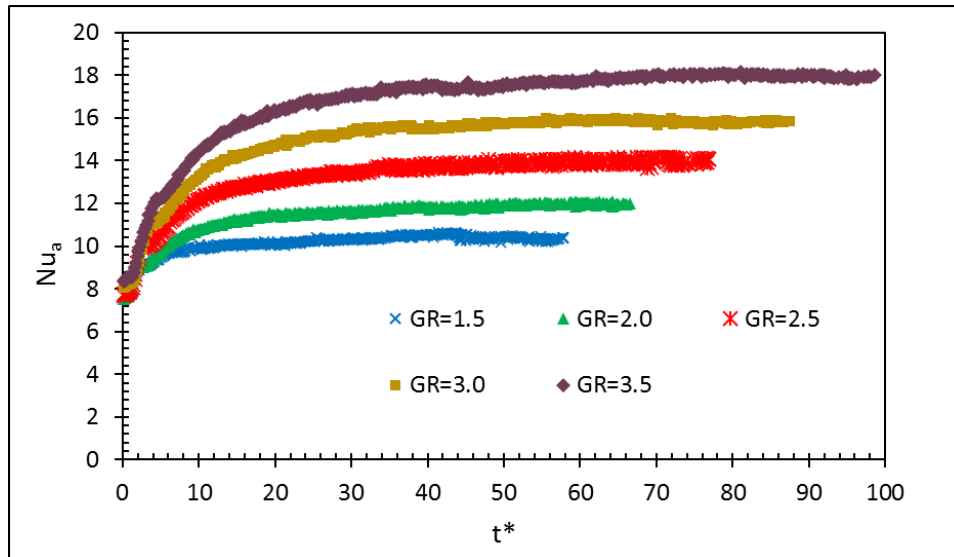
Figure 5.6. Transient Nu_a with dimensionless time
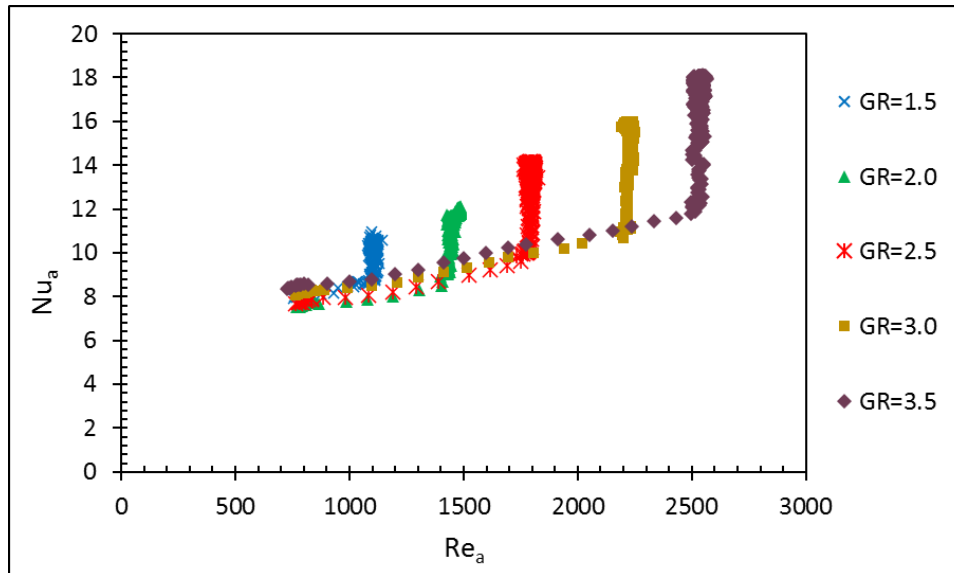
Figure 5.7. Transient Nu_a with Re_a

5.1.6. Transient Airside Colburn *j* Factor

The Colburn *j* factor is a dimensionless parameter that characterizes the heat transfer of a heat exchanger. The variation of Colburn *j* factor due to the step changes in air mass velocity is shown in Figure 5.8. Colburn *j* factor is proportional to Prandtl number and Stanton number, equation 4.11 which depends on the airside heat transfer coefficient and

60

the mass velocity of the air. The sudden increase in air mass flow rate while the other inlet conditions are constant increases the mass velocity and thus results in a sharp decrease in j_a to a lower value.
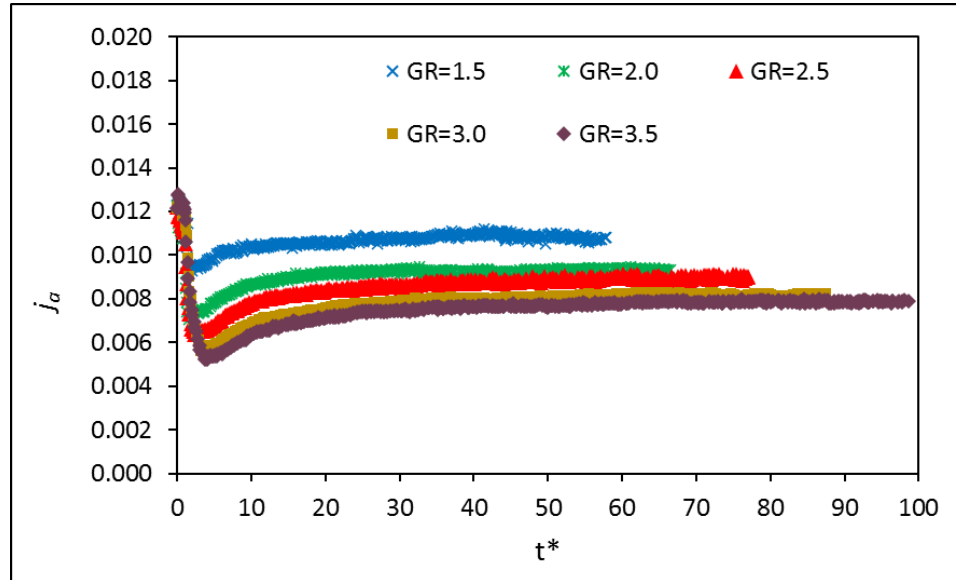
Figure 5.8. Transient j_a with dimensionless time

At first, the increase in air mass velocity is higher than the increase in the heat transfer coefficient and this results in a sharp decrease in Colburn factor j_a. This sharp decline is reduced when the heat transfer increases, and the air mass velocity reaches its set value. Therefore, the behavior of airside Colburn j factor shifts and starts increasing till the final steady state is reached. Figure 5.9 represents the changes in j_a due to the airside Reynolds number variations. This figure illustrates the time it takes for airside Reynolds number to change from an initial common value to final set values related to each airside mass velocity step change. When the air mass velocity reaches its final set value, the vertical change of each step illustrates the changes in j_a until a steady state is achieved. The response and the increase in j_a depend on the magnitude of the step change applied.
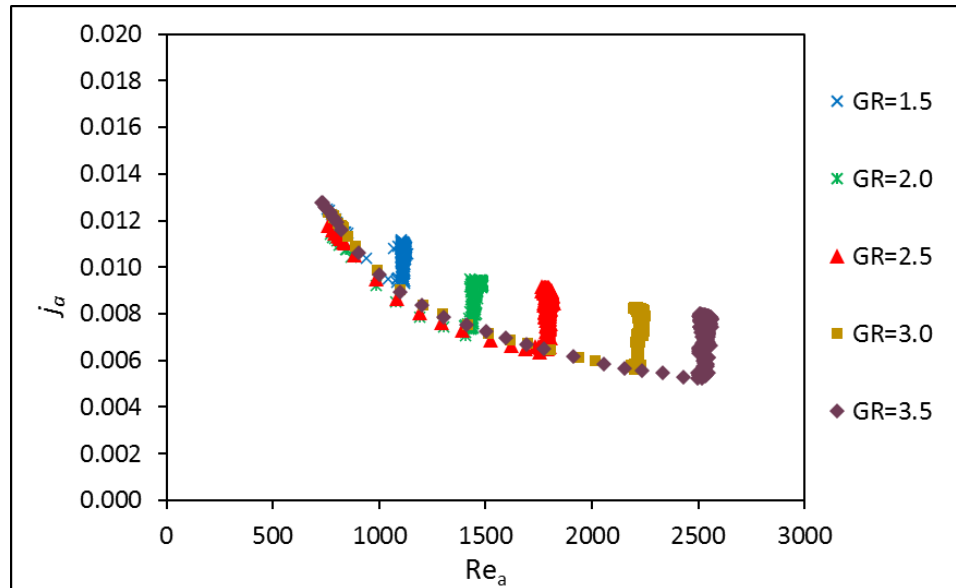
Figure 5.9. The effect of different Re_a on j_a

5.1.7. Comparison of the Current Study with the Literature

A comparison of the current results in terms of airside Nusselt number is made with previously published work found in the literature. This comparison illustrates the enhancement in heat transfer using the current meso heat exchanger compared to other heat exchangers designs.

5.1.7.1. Nu_a-Re_a Relationship Comparison

The dynamic investigation of airside in cross flow heat exchangers is scarce and rare. The discussion of important parameters influencing the heat transfer and fluid flow in airside heat transfer such as Nu is mainly found in steady state studies. Therefore, to compare the results of the current study, a steady state comparison approach was adopted. In which, the steady state results are considered and compared with available steady state data found in the literature [34, 87, and 89]. Taler [34] and [87] determined the radiator averaged airside heat transfer coefficient at steady state for a wide range of Reynolds number $150 \leq Re_a \leq 1500$. The radiator in Taler's study was a two row with two passes plate fin and tube heat exchanger having oval cross section tubes. His averaged air heat transfer coefficient results are compared to the current findings from this study at steady state as shown in Figure 5.10. While Siddiqui et al. [89] on the other hand used a three-loop compact cross flow heat

62

exchanger with 12"X12" frontal area having ethylene-glycol/water mixture and air as the working fluids.
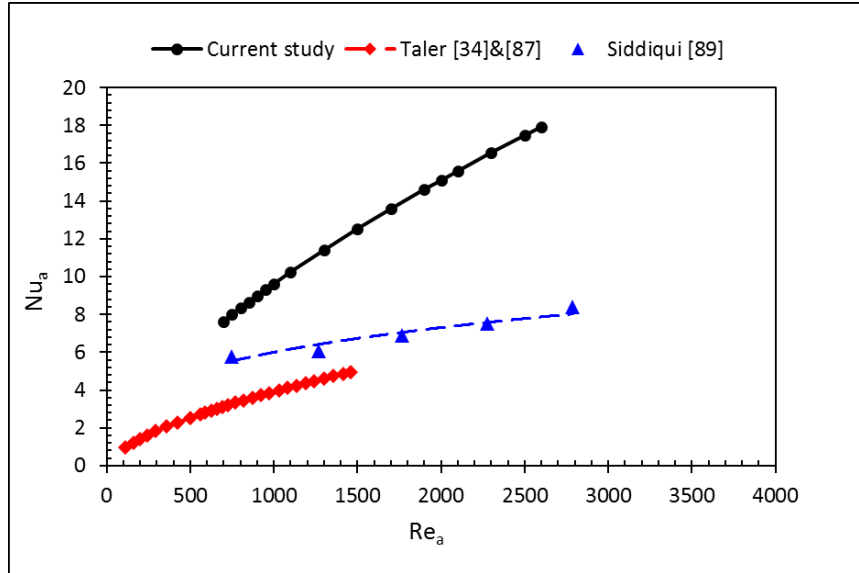
Figure 5.10. Steady state comparison of Nu_a at different Re_a

As observed from these literature studies, the differences from the current study include, heat exchanger geometries, the operating conditions, number of loops, and the working fluid. The figure demonstrates that the current study yielded higher Nu_a thus superior heat transfer rate at a range of Reynolds number. These high results in Nu_a can be attributed to the use of a flat slab which results in a uniform temperature distribution compared to using tubes. A wake region forms usually downstream of the tube which reduces the heat transfer while in the case of using a slab, only one wake region is formed compared to the multiple regions for each tube. Thus, the formation of one wake region as well as the flow of air over the flat slab where it is in contact with its surface, lead to the high heat transfer and therefore Nusselt number in the current meso heat exchanger. Additionally, the existence of the serpentine bend works on mixing and agitating the flow as it moves from an exit of a slab to the entrance of the next slab. The airside Nusselt number increases with the increase of Re_a and the variations followed a power-law relationship. A steady state correlation for the current study is found as follows,

$$Nu_a = 0.13Re_a^{0.62} \qquad (5.1)$$

63

5.1.8. Empirical Correlation for Airside Nusselt Number

In the current work, the transient heat transfer and fluid flow of a cross flow meso heat exchanger is investigated due to step changes in the airside mass velocity. Important dimensionless parameters are presented from the experimental findings. An empirical correlation for Nusselt number will be introduced in the following section which details the method of obtaining the empirical correlation equation for airside Nusselt number as a function of dimensionless time and the step change in airside mass velocity. Nusselt number characterizes the heat transfer performance by means of a dimensionless heat transfer coefficient. This characterization can be used to control the outlet fluid temperatures of the heat exchanger which is an important component of a larger thermal management system. Figure 5.11 represents the ratio of the experimental transient airside Nusselt number to the steady state Nusselt number for each step change with respect to dimensionless time. This figure demonstrates the increase in airside Nusselt number from an initial steady state to a final steady state during a finite time period. It also shows that Nusselt number is influenced by the magnitude of the step change imposed and time.
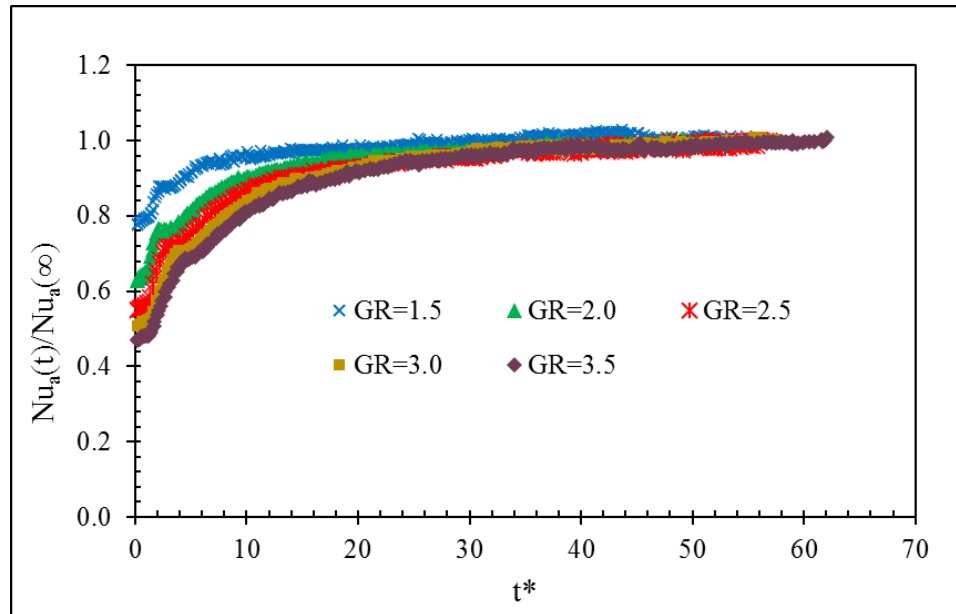

Figure 5.11. Transient to steady state Nu_a ratio at different GR

All the steps approach asymptotic value of 1 in the final steady state. At first, the effect of airside mass velocity step increase on the response of Nusselt number is stronger and gradually declines with the decreasing gradient.

Initially, the correlation of the steady state Nusselt number with air mass velocity step changes is found using the best curve fit of the steady state data for Nusselt number with different GR ratios from the experiment. The resulted curve shows that $Nu_a(\infty)$ increases with the increase in mass velocity step ratios. This increase follows a power-law relationship having a positive exponent as,

$$Nu_{a,(\infty)} = 8.00 GR_a^{0.62} \tag{5.2}$$

A generalized empirical correlation to represent $Nu_a(t)$ in terms of $Nu_a(\infty)$, and dimensionless time is shown below,

$$Nu_a(t) = Nu_a(\infty)\{1 - Ae^{-Bt^*}\} \tag{5.3}$$

The coefficients A and B are found by obtaining the correlation of $Nu_a(t)$ for each step change. These correlations are plotted with respect to the changes in air mass velocity. The transient Nusselt number correlation for each mass velocity step change is found in terms of $Nu_a(\infty)$ and t^* and are listed below,

$$Nu_a(t) = Nu_a(\infty)\left[1 - 0.23e^{-0.16t^*}\right] \tag{5.4a}$$
with $R^2=0.96$, for GR=1.5

$$Nu_a(t) = Nu_a(\infty)\left[1 - 0.37e^{-0.12t^*}\right] \tag{5.4b}$$
with $R^2=0.98$, for GR=2.0

$$Nu_a(t) = Nu_a(\infty)\left[1 - 0.45e^{-0.10t^*}\right] \tag{5.4c}$$
with $R^2=0.97$, for GR=2.5

$$Nu_a(t) = Nu_a(\infty)\left[1 - 0.52e^{-0.11t^*}\right] \tag{5.4d}$$
with $R^2=0.99$, for GR=3.0

$$Nu_a(t) = Nu_a(\infty)\left[1 - 0.56e^{-0.10t^*}\right] \tag{5.4e}$$
with $R^2=0.99$, for GR=3.5

According to the above correlations, the coefficients A and B are defined as follows,

$$A = 0.17GR^{1.02} \tag{5.5a}$$

$$B = 0.19GR^{-0.59} \tag{5.5b}$$

Where, $Nu_a(\infty)$, A, and B are dependent on the air mass velocity step change. A derived correlation from the current study as shown in equation 5.3 is used to predict the airside Nusselt number for all the step changes implied. To show the accuracy of the developed correlation, a comparison is made between the derived empirical correlation and the results from the experimental runs at different airside mass velocity ratios. Figures 5.12a to 5.12e illustrate the good agreement between the derived empirical correlation and the experimental results.
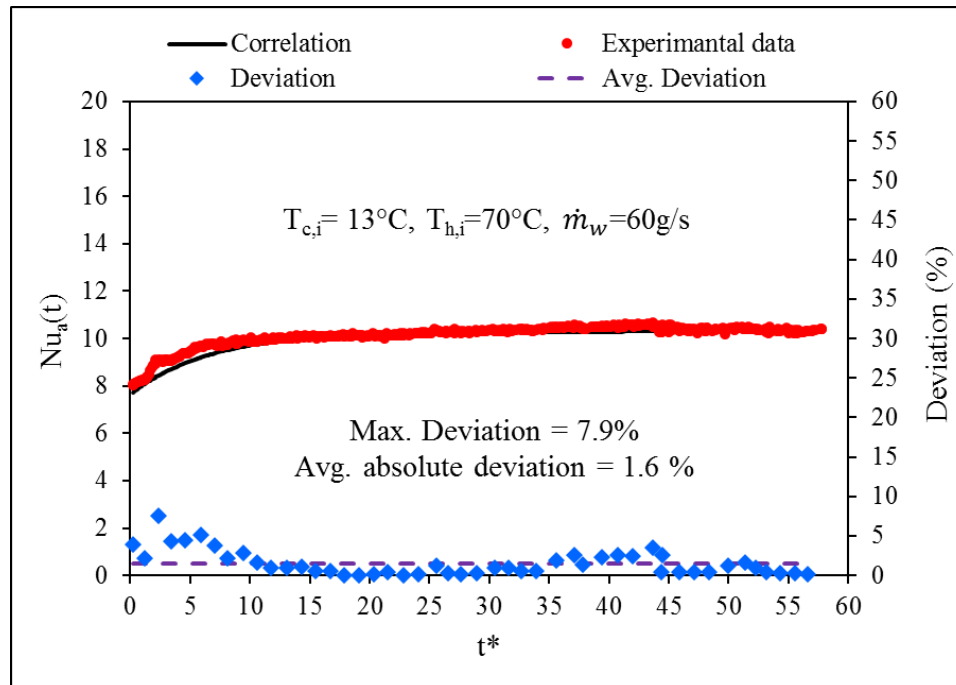
(a) Transient Nusselt number for GR=1.5
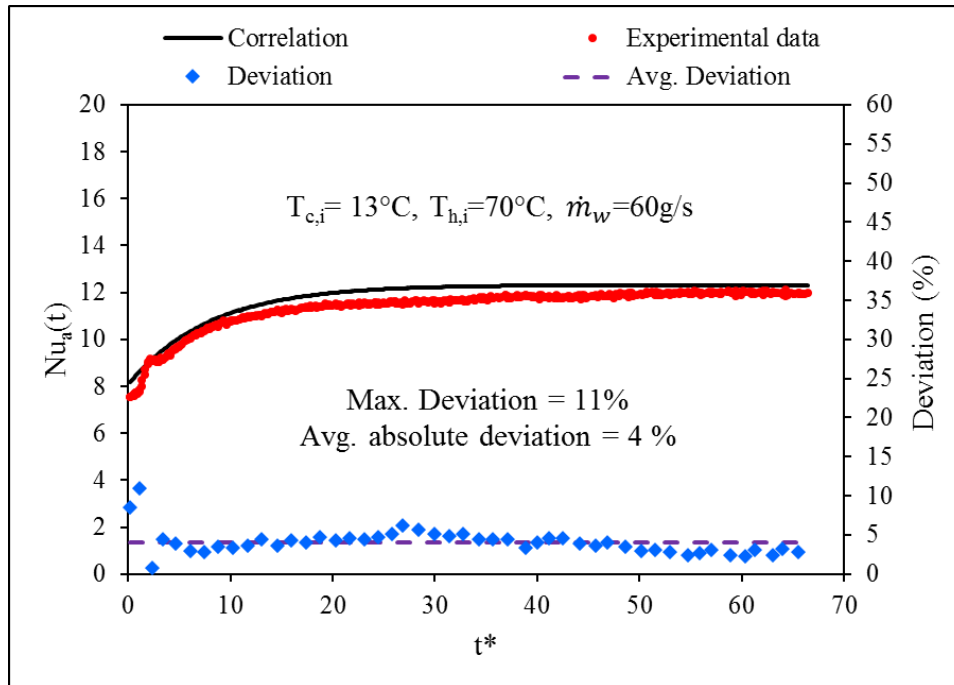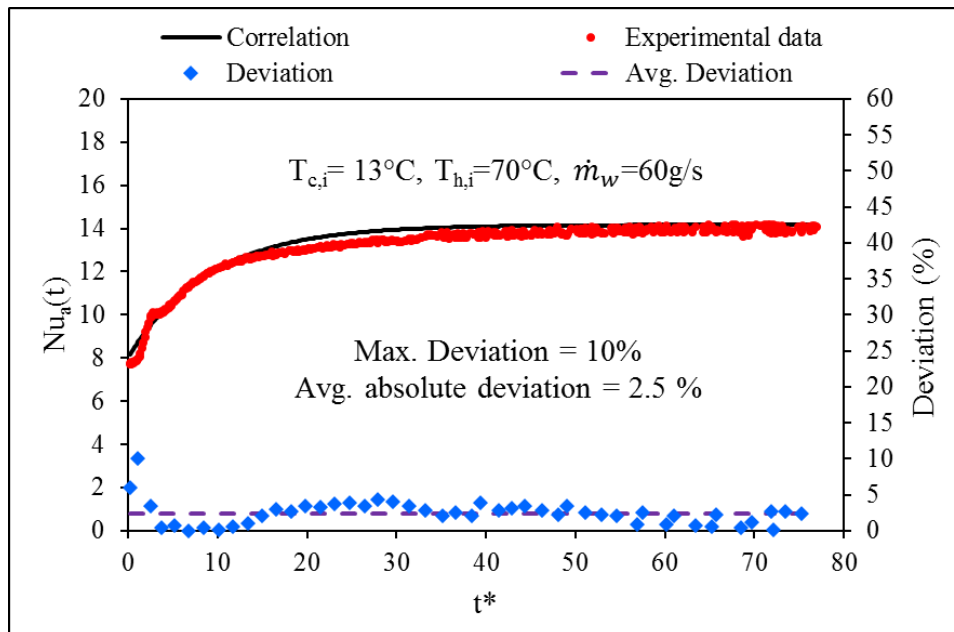
(b) Transient Nusselt number for GR=2.0

(c) Transient Nusselt number for GR=2.5
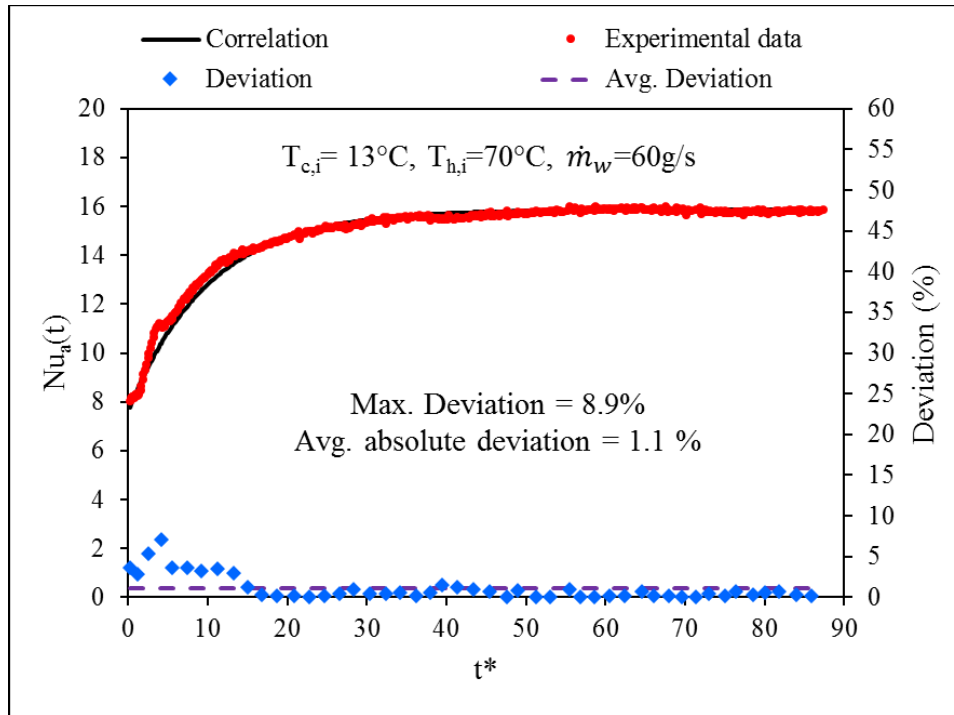
(d) Transient Nusselt number for GR=3.0
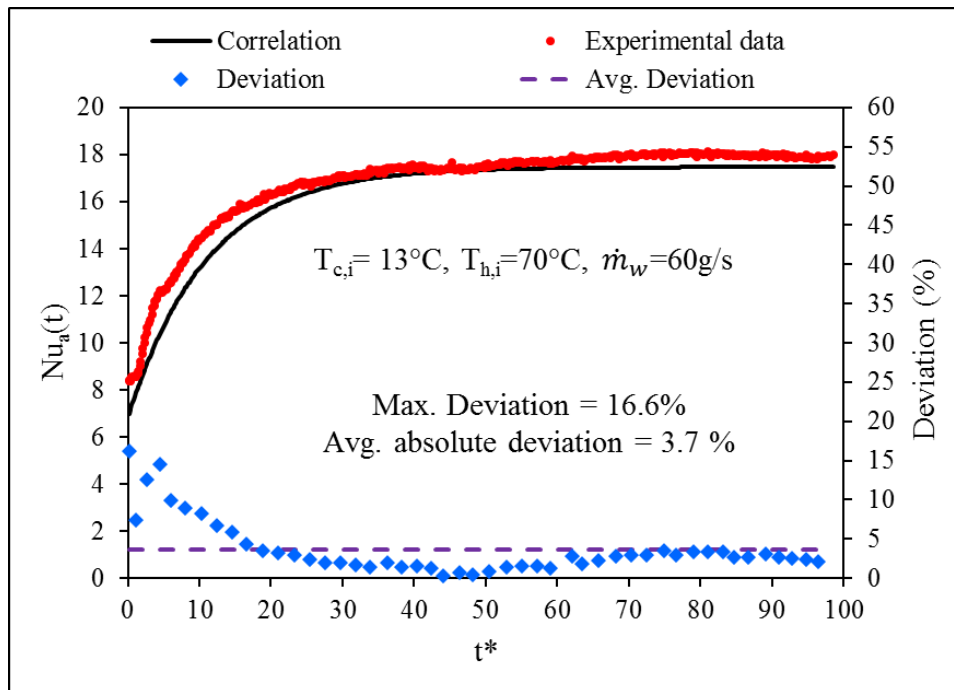
(e) Transient Nusselt number for GR=3.5

Figure 5.12. Transient Nu_a correlation for GR (a) 1.5, (b) 2.0, (c) 2.5, (d) 3.0, and (e) 3.5

The maximum and average deviations for all step changes are listed in Table 5.1.

Table 5.1. Maximum and average percentage deviation of the empirical correlation

GR	Maximum deviation %	Average absolute deviation %	$T_{a,i}$ (°C)	$T_{w,i}$ (°C)	$\dot{m}_w$ (g/s)
1.5	7.89	1.56	30	5	60
2.0	11.02	3.92	30	5	60
2.5	10.15	2.29	30	5	60
3.0	8.94	1.06	30	5	60
3.5	16.63	3.63	30	5	60

Figure 5.13 represents the derived empirical correlation for the transient Nusselt number from the experimental data for all the step changes. It is found that this correlation fits all the transient experimental data within a maximum deviation of 16.6% at an average absolute deviation of 3.7%.

$$Nu_a(t) = Nu_a(\infty)\left(1 - Ae^{-Bt^*}\right)$$

$$Nu_a(\infty) = 8.00GR^{0.62}$$

$$A = 0.17GR^{1.02}$$

$$B = 0.19GR^{-0.59}$$
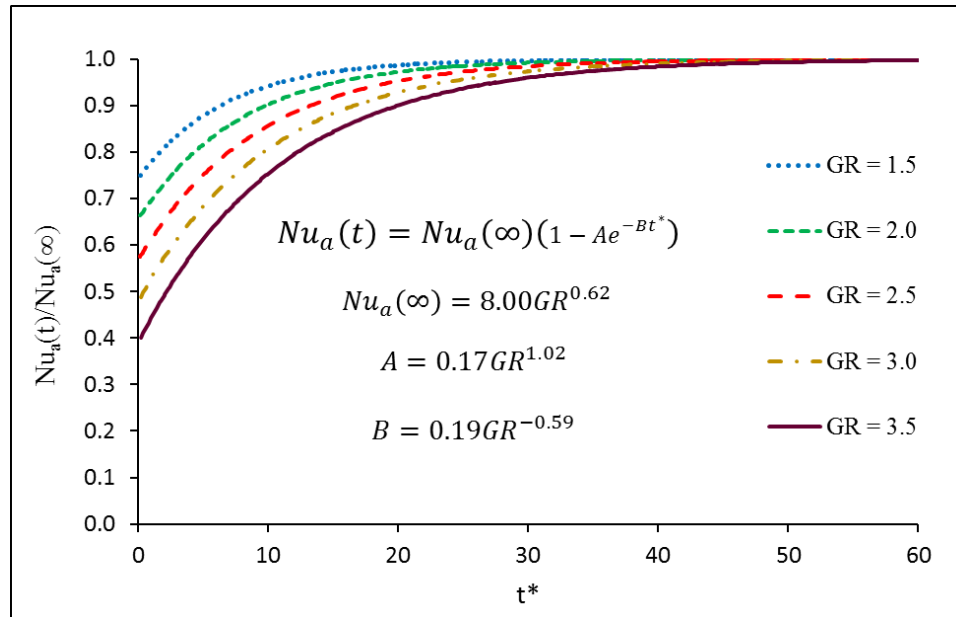
Figure 5.13. Transient Nusselt number correlations for all GRs

5.2. Transient Air Cooling

This section represents the results obtained from the transient air-cooling experiments where the airside mass velocity changes in a step form into 5 different steps. The parameters associated with the transient analysis are presented in a dimensional and non-dimensional form as follows.

5.2.1. Exit Temperature Response

The fluids' outlet temperature response is represented in both dimensional and dimensionless forms against the non-dimensional time as in Figure 5.14 and 5.15. A variation in air mass flow rate in the form of a step change leads to a mass velocity ratio of the final to the initial values. Five different inlet air mass velocity ratios are investigated (1.5, 2.0, 2.5, 3.0, and 3.5). The influence of these steps on the fluids' exit temperature response is examined. Although the working fluids do not display an instant respond, DI-water exhibited a higher delay time than air. This delay time in the outlet temperature response can be explained due to the time it takes the thermocouples and RTD to react to the change and the time it takes for the working fluids to flow through the heat exchanger. The latter is called the residence time which is found dissimilar between air and liquid due to the length of the channel compared to the depth of the airside. The delay time for the airside was found to be about 1s while for the DI-water was 5s. Since airside delay time is shorter and air travels through a short distance compared to DI-water, the air outlet temperature rise occurs before the outlet DI-water temperature increase. Thereafter, once some period of the delay time is passed, the exit temperature of the liquid starts responding to the air mass velocity variation. Air exit temperature increasing rate is minimized up until a final steady state is achieved.

Higher airside mass velocity step changes cause a rise in the fluids' outlet temperatures and a decrease in the residence time. However, both fluids dimensionless outlet temperature shows a decrease according to their definition in equations 4.6 and 4.9. It is noticed that when the air mass velocity reaches its final value, T^*_o continues to decrease up to a point where a steady state is attained. This is described as the continuous heat transfer happening between the liquid and air through the walls of the heat exchanger. A comparison of Figures 5.15a and 5.15b reveals that the fluids outlet temperature response time of the two fluids is not identical. An applied step requires a time for each fluid to reach its final steady state and this is referred to as the response time. Higher airside mass

velocity ratio results in an increase in the response time for each fluid with DI-water exhibiting greater response time than the air.
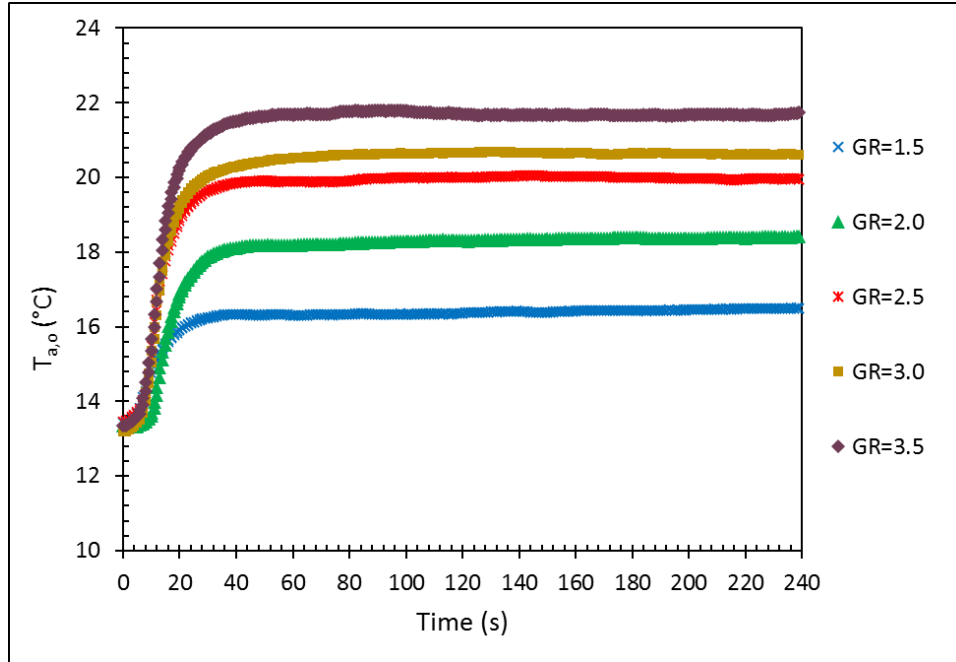
(a) Air outlet temperature
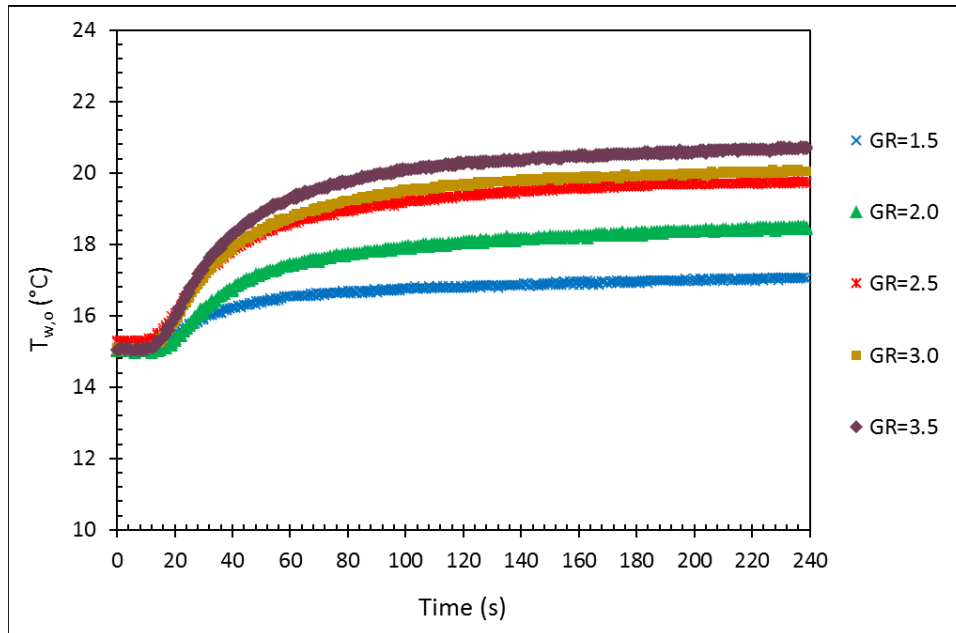
(b) DI water outlet temperature

Figure 5.14. Effect of air mass velocity ratio on outlet temperature response
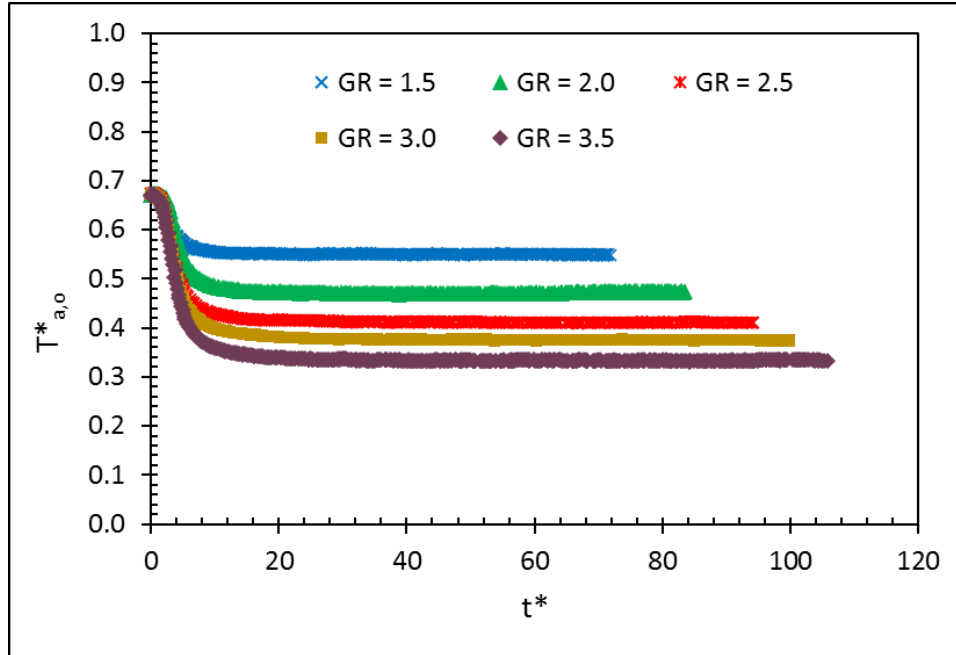
(a) Dimensionless air exit temperature
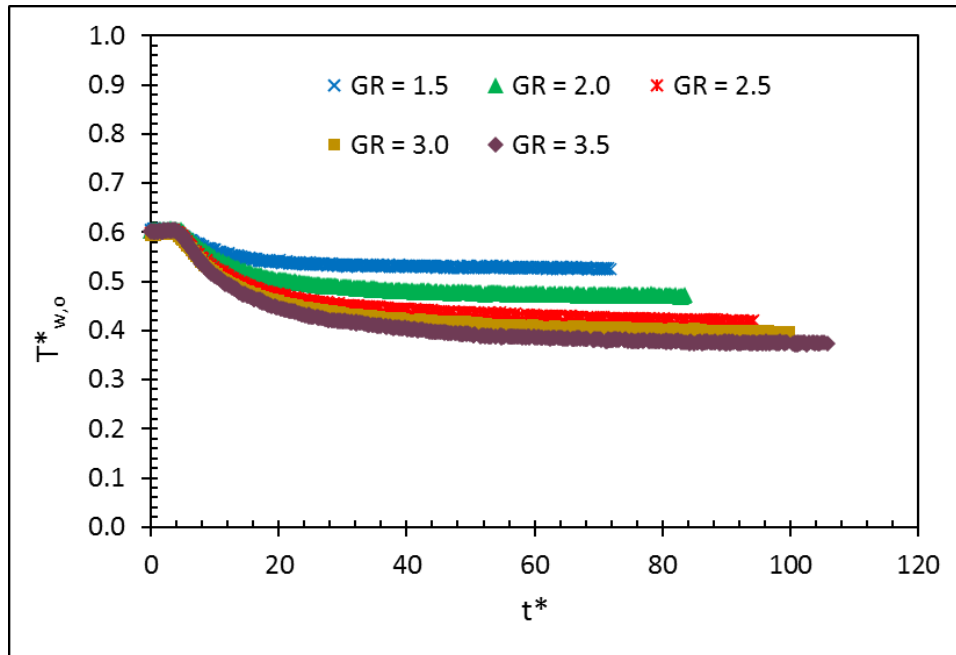
(b) Dimensionless DI water exit temperature

Figure 5.15. Effect of air mass velocity ratio on dimensionless exit temperature

5.2.2. Heat Transfer Rate

The air and DI-water heat transfer rates are presented in Figure 5.16. For the case of DI-water heat transfer rate, increasing the airside flow rate causes an increase in the DI-water outlet temperature which leads to a rise in its inlet to outlet temperature difference. Since

the DI-water operating conditions are constant, the heat transfer rate increases due to the rise in the DI-water temperature difference as shown in Figure 5.16a. At initial steady state, liquid and air heat transfer rate is the same but differs when the steps are applied. In addition to that, both fluids display a delay time in their heat transfer rate during this process. The air heat transfer rate transient behavior is different than liquid as demonstrated in Figure 5.16b. While DI-water exhibited a smooth gradual increase, air on the other hand experienced an increasing and a decreasing trend. Airside mass flow rate increase results in a sudden sharp rise in the surface temperature. Since the heat transfer rate is calculated using the energy balance in equation 4.24 which accounts for heat transfer through the walls of the heat exchanger, the airside heat transfer rate increases. As previously explained, the air exit temperature responses faster than DI-water. As DI-water begins showing a response, the sudden sharp rising trend in the surface temperature declines. After which, the heat transfer rate behavior of air and liquid develops similarly till the two achieve a final steady state. According to Fig. 5.16b, the percentage increase from the lowest to the highest step change was 36% at final steady state.
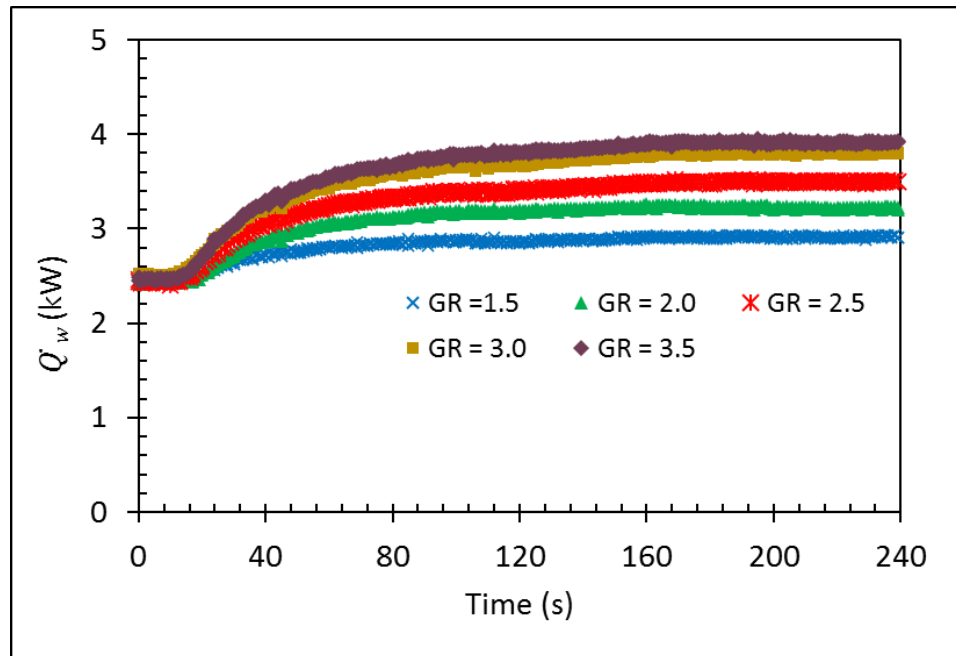
(a) DI-water transient heat transfer rate
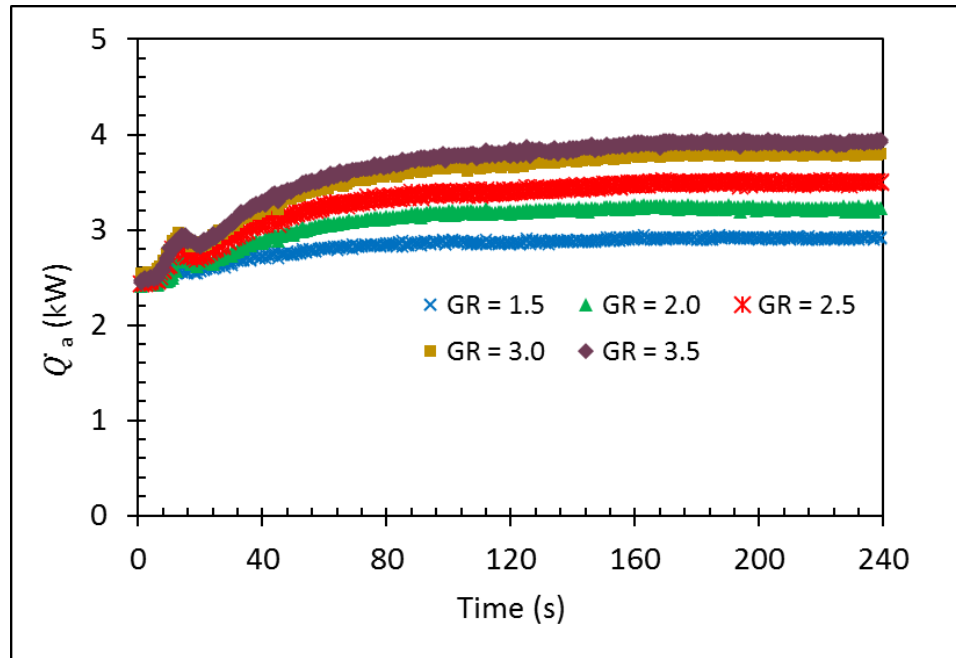
(b) Airside transient heat transfer rate

Figure 5.16. Effect of GR on the transient heat transfer rate

5.2.3. Heat Transfer Coefficient

The time dependent airside heat transfer coefficient is shown in Figure 5.17. The procedure discussed in chapter 4 is used to find the heat transfer coefficient of air at any second during the experiment. Equation 4.29 involves two temperatures, air bulk and surface temperature. The air bulk temperature is found using the two grids of thermocouples located at the entrance and exit of the test section. The thermocouples' distribution along the inlet and outlet serpentine and slab portions of the heat exchanger provided measurement for average surface temperature. The airside heat transfer coefficient is affected by the increase in the heat transfer rate. The rise in the airside mass velocity from one step to another causes a rise in the heat transfer coefficient and in its response time. The heat transfer coefficient reaches its optimal value when the steady state is achieved.
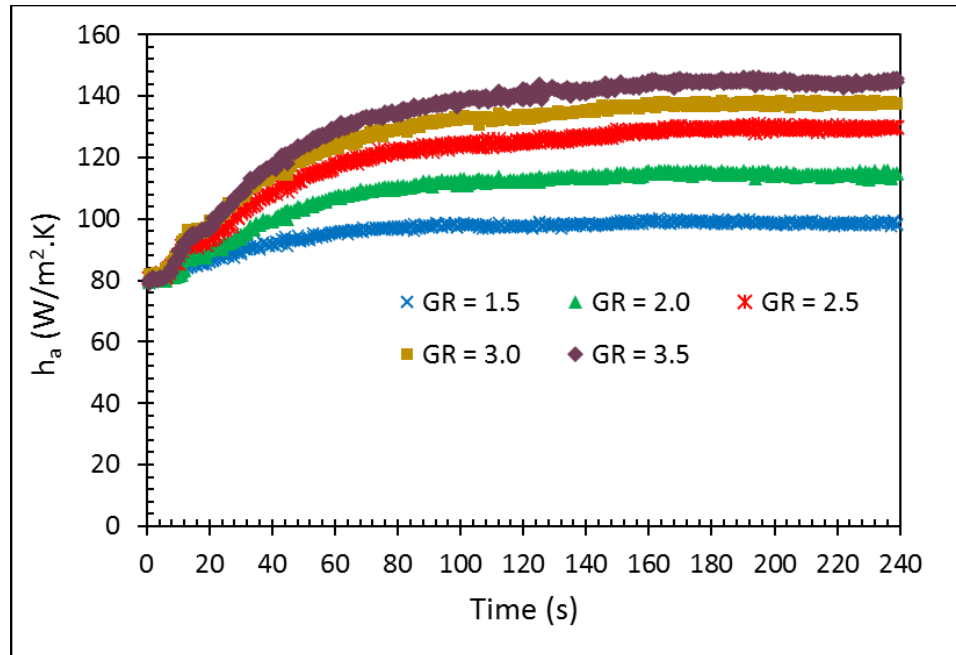
Figure 5.17. Heat transfer coefficient

5.2.4. Airside Nusselt Number

The airside transient Nusselt number is shown in Figure 5.18. The effect of varying the airside mass velocity on Nu_a behavior is presented. Airside Nusselt number is proportional to the heat transfer coefficient and an increase in air heat transfer coefficient due to the step change causes an increase in Nusselt number. Higher step changes result in higher Nusselt number values, however, the rate of change in small steps is higher than that of the larger steps. A step increase in airside mass velocity raises the heat transfer rate, heat transfer coefficient, and thus Nusselt number. The rise in Nusselt number ends when the working fluids reach their final steady state.
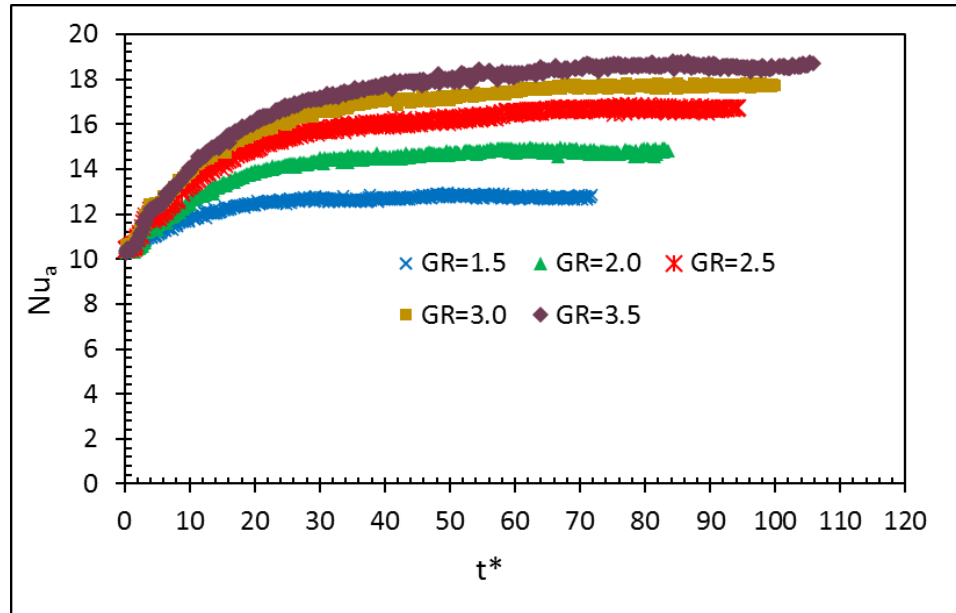
Figure 5.18. Transient Nusselt number

5.2.5. Transient Airside Colburn j Factor

The heat transfer characterized by the Colburn j-factor is presented in a dimensionless form in Figure 5.19. From Colburn j factor definition, it is found that it is inversely proportional to the increase in mass velocity. As airside Reynolds number increases, Colburn j factor values decrease. A sharp drop in j_a is noticed reaching its lowest values after which the increasing rate declines. Since air flow rate is increased and a sudden step change is applied in air mass velocity, this causes the sharp decline in j_a. The heat transfer rate on the other hand does not respond instantaneously to the change. Once the delay in heat transfer rate diminishes, the behavior of j_a is reversed and it starts increasing till reaching its final steady state.
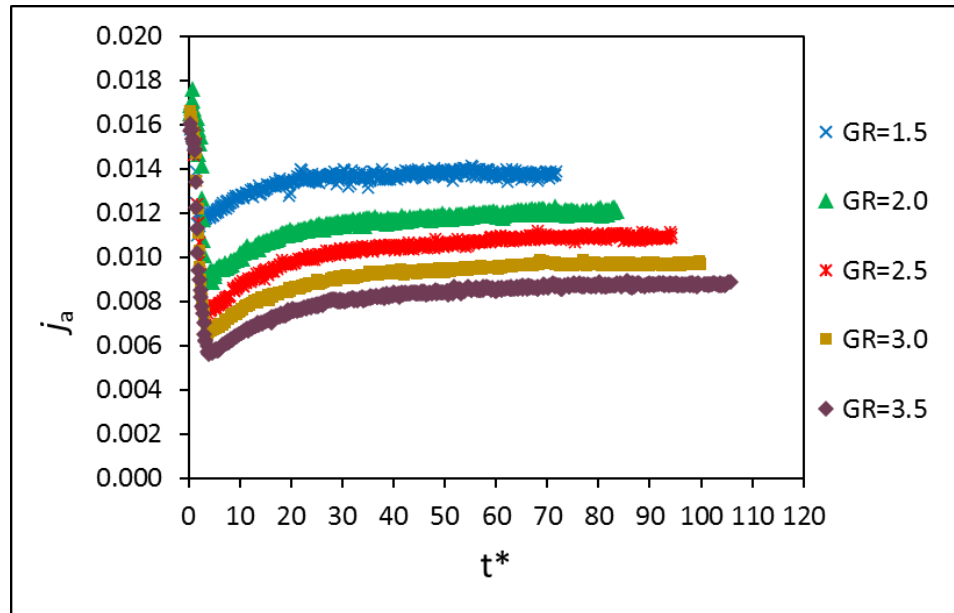
Figure 5.19. Transient airside Colburn j factor

5.2.6. Comparison of the Current Study with the Literature

The current study results are compared with the findings in the literature and presented in terms of airside Nusselt number. It represents the heat transfer improvement when using the current meso heat exchanger compared to other heat exchangers designs.

5.2.6.1. Nu$_a$-Re$_a$ Relationship Comparison

The study of compact heat exchangers with variations in the airside inlet conditions is very limited and scarce. The existing studies on airside are well presented and discussed at the steady state level. However, there is a limited work involving transient heat transfer with airside perturbations. Therefore, the dynamic response of CFHXs with airside mass velocity variations is carried out in this research. This section presents a comparison of the current experimental results at steady state with the available literature found in [90] and [91]. Figure 5.20 represents the Reynolds number effect on Nusselt number. As noticed from the figure, the current results compare well with [91]. However, some deviation is noticed due to many reasons such as: the mode of heat transfer where air heating is used in [91] compared to air cooling in this study, the heat exchanger used in the reference is composed of many tubes placed in a staggered arrangement with an outside tube diameter of 20mm and annular fins around them.

77

While the current study resulted in higher airside Nusselt number values in comparison to [90, 91]. The heat exchanger in Dasgupta et. al. [90] is a compact CFHX with a frontal area of 12"X12" and 15 slabs. DI-water and air were the working fluids with air inlet velocity between (1-5m/s) compared to (2.6-9.2m/s) in this work. The difference in size of the heat exchangers and the operating conditions contribute to the rise in airside Nusselt number. On the other hand, Tang and Yang [88] investigated air heating using a plate-finned tube heat exchanger with airside Reynolds number range of (120-480). The tested heat exchanger size was 18"X24" with 12 straight finned tube having an outside tube diameter of 0.625". It can be noted that the differences in the current experimental results from the references is attributed to the heat exchanger geometry used whether tube or mini channels, the operating conditions, and the number of slabs for the compact CFHX. All these factors quantitatively affect the Nusselt number as Reynolds number increases.
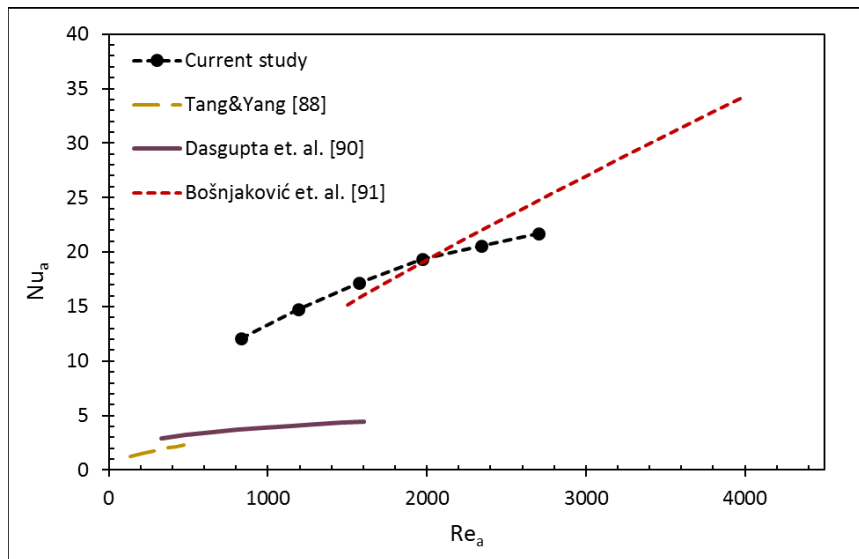
Figure 5.20. Steady state airside Nusselt number comparison

5.2.7. Empirical Correlation for Airside Nusselt Number

The following part involves a generation of an empirical correlation from the experimental data to predict the airside Nusselt number related to mass velocity step changes. The approach used to obtain the empirical correlation is discussed. The transient change in Nusselt number depends on the step magnitude. Therefore, the correlation will be presented in terms of mass velocity step and dimensionless time. The derived correlation is applied to characterize and predict the dimensionless heat transfer coefficient of a CFHX due to

variations in air mass velocity. The ratio of $Nu_a(t)/Nu_a(\infty)$ is shown in Figure 5.21 for each step change.
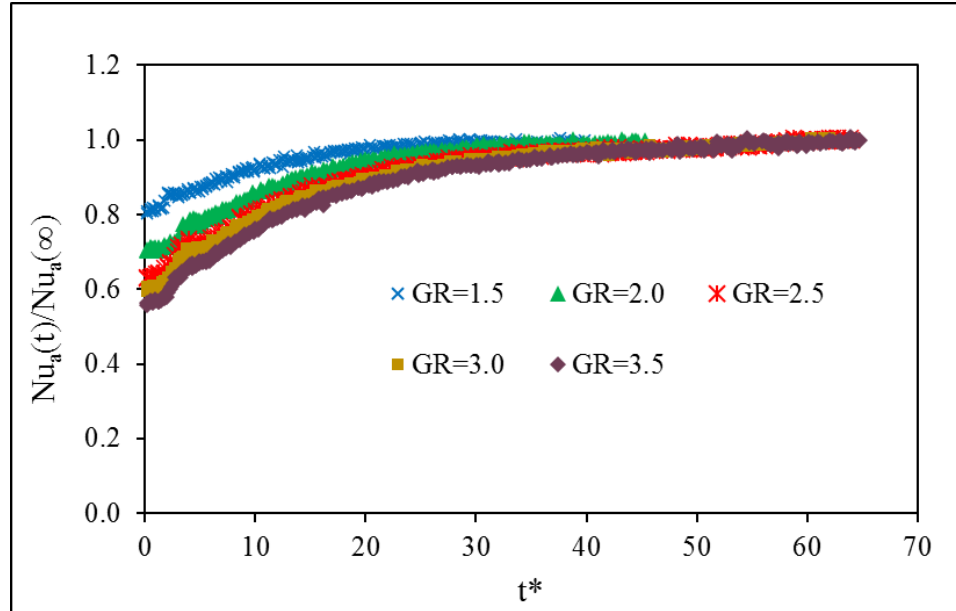
Figure 5.21. Effect of GR on transient airside Nusselt number

An increase in the ratio is seen as GR values increase during initial transient. The increase in Nusselt number follows the same trend as in the heat transfer coefficient presented in Fig. 5.17. The steady state Nu_a is considered and plotted against each GR to obtain a best curve fit that yields the equation of Nu_a steady state. A power-law relationship is the result which shows an increase in Nu_a as GR increases. The steady state Nu_a equation is as follows,

$$Nu_{a(\infty)} = 10.53 GR^{0.46} \qquad (5.6)$$

The transient Nu_a can be found using a generalized empirical equation that depends on steady state Nu_a and dimensionless time as in the following,

$$Nu_a(t) = Nu_a(\infty)\{1 - Ae^{-Bt^*}\} \qquad (5.7)$$

Where A and B are coefficients found from plotting the transient to steady state Nu_a ratio with dimensionless time for each GR. Next, the obtained coefficients from these correlations are plotted against their related GR step change Table 5.2.

Table 5.2. Transient Nu_a at each GR value

GR	$Nu_a(t)/Nu_a(\infty)$	R^2
1.5	$1 - 0.20e^{-0.10t*}$	0.985
2.0	$1 - 0.33e^{-0.08t*}$	0.992
2.5	$1 - 0.38e^{-0.07t*}$	0.995
3.0	$1 - 0.41e^{-0.07t*}$	0.997
3.5	$1 - 0.46e^{-0.06t*}$	0.998

Therefore, A and B coefficients can be found as,

$$A = 0.15GR^{0.92} \tag{5.8a}$$

$$B = 0.12GR^{-0.55} \tag{5.8b}$$

Theses coefficients are substituted in equation 5.7 to calculate the transient airside Nusselt number. The accuracy of the derived equation in predicting the experimental results for each mass velocity ratio is shown in the following Figures 5.22a-22e.
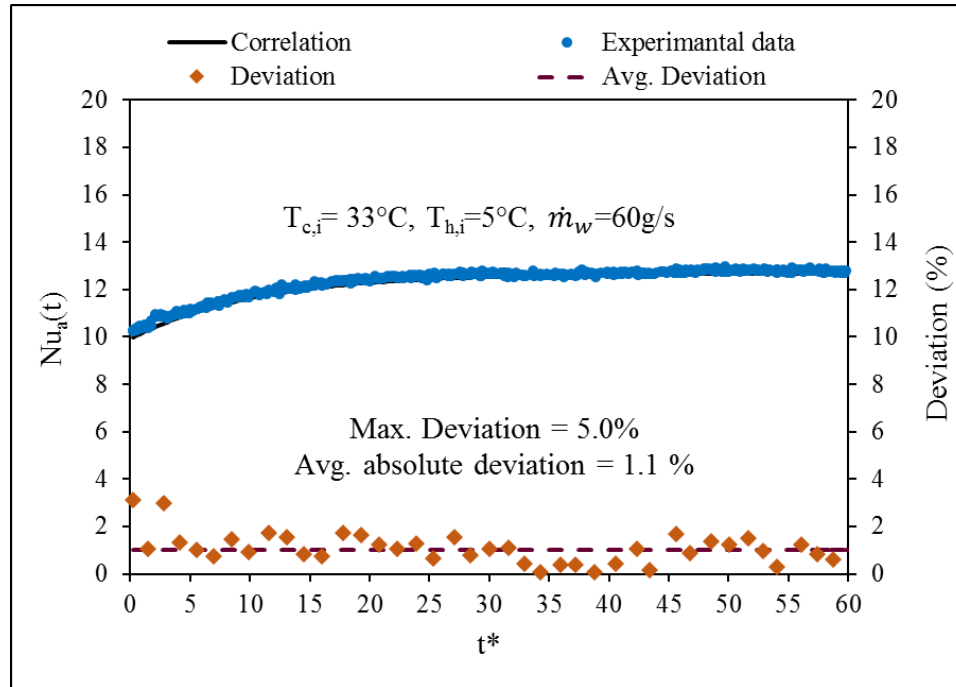
(a) Transient Nusselt number for GR=1.5
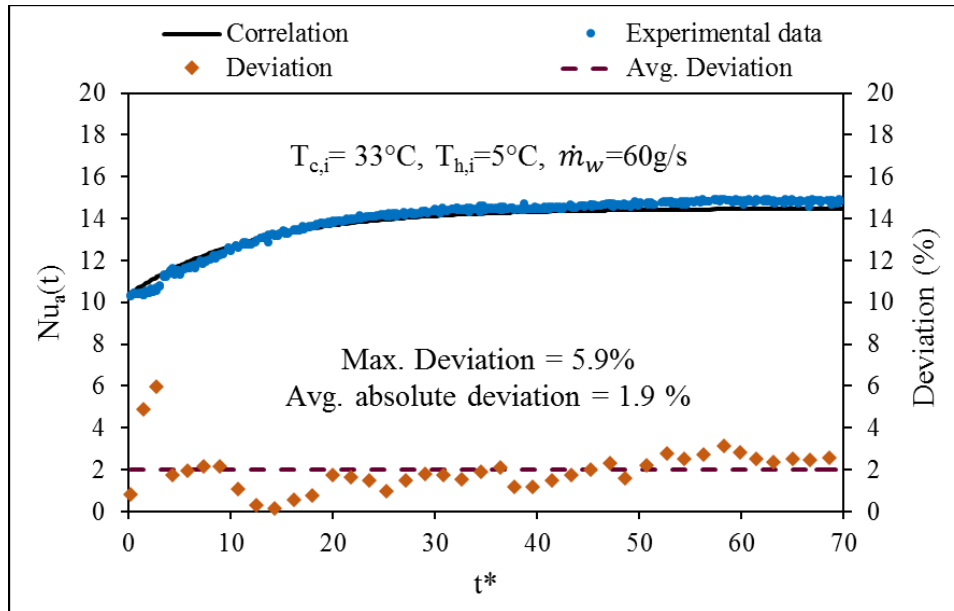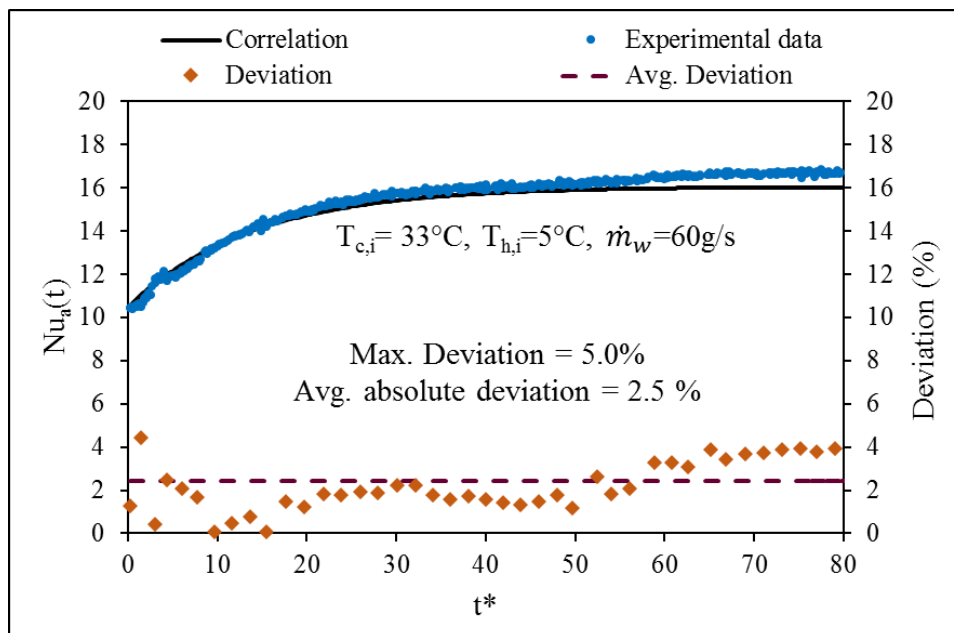
(b) Transient Nusselt number for GR=2.0

(c) Transient Nusselt number for GR=2.5
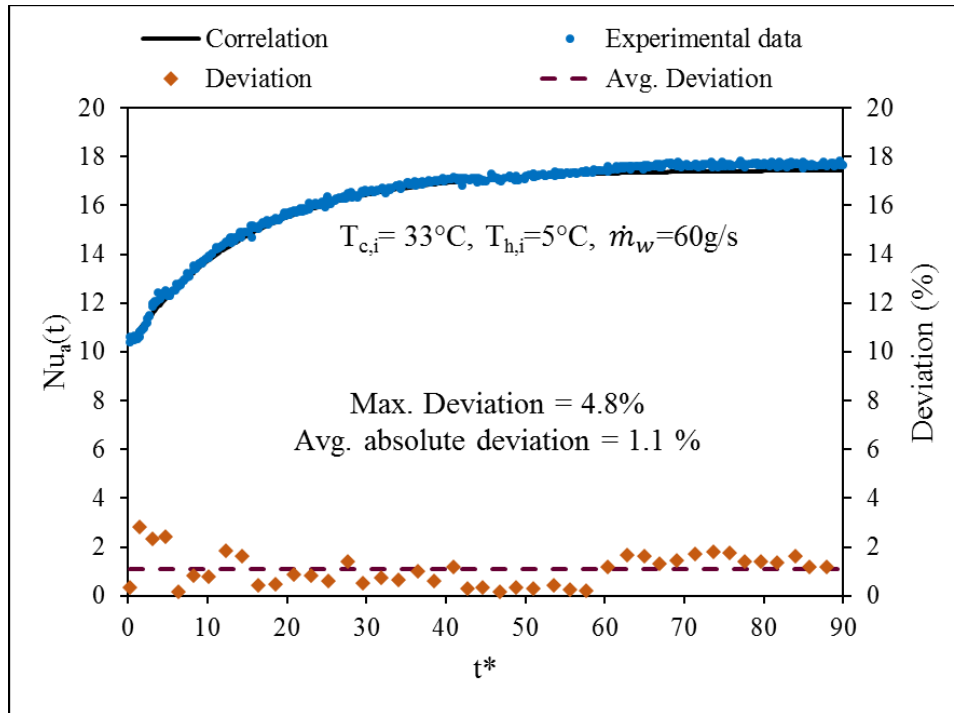
(d) Transient Nusselt number for GR=3.0
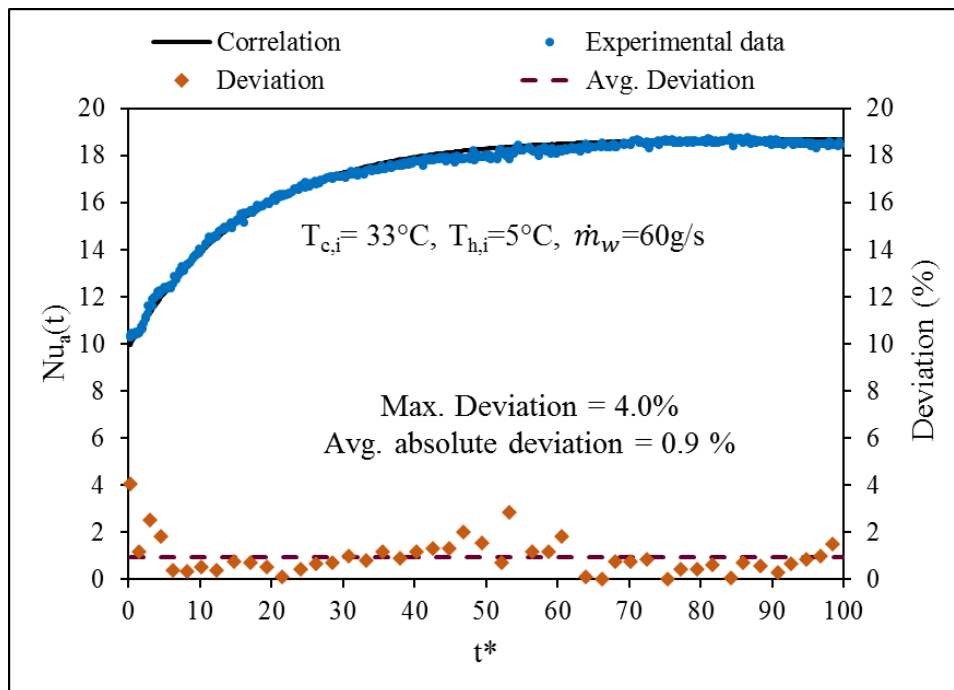
(e) Transient Nusselt number for GR=3.5

Figure 5.22. Transient Nu_a correlation for GR (a) 1.5, (b) 2.0, (c) 2.5, (d) 3.0, and (e) 3.5

Figures 5.20 (a to e) show the good prediction of the derived equation with the experimental results. The amount of deviation for each step change is displayed in Table 5.3.

Table 5.3. Maximum and average percentage deviation of the empirical correlation

GR	Maximum deviation %	Average absolute deviation %	$T_{a,i}$ (°C)	$T_{w,i}$ (°C)	$\dot{m}_w$ (g/s)
1.5	5.02	1.06	30	5	60
2.0	5.99	1.89	30	5	60
2.5	5.03	2.50	30	5	60
3.0	4.79	1.08	30	5	60
3.5	4.04	0.92	30	5	60

The derived empirical correlation of the transient airside Nusselt number at each GR is shown in Figure 5.23. The correlation to data highest deviation is found to be 5.99% at an average deviation of 1.89%.
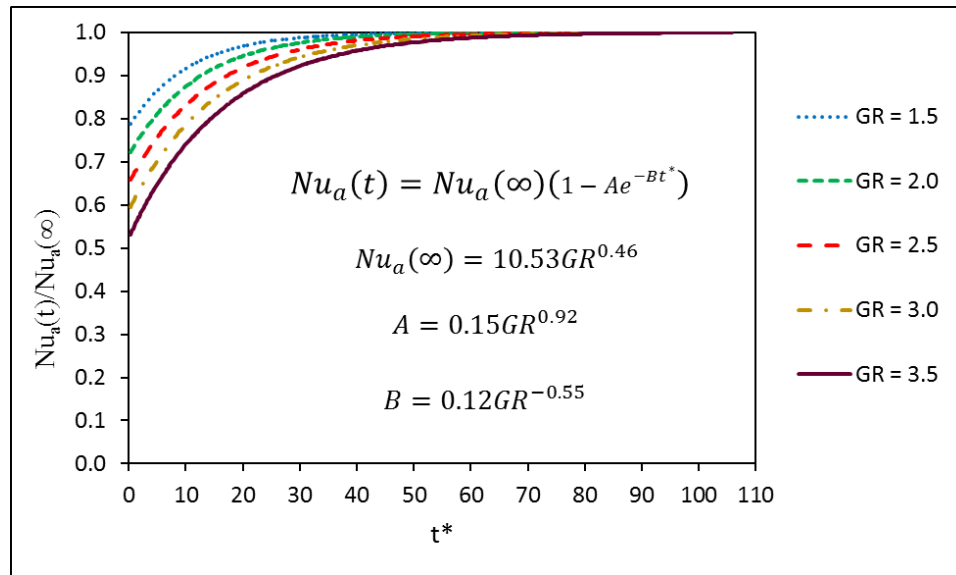
Figure 5.23. Transient to steady state Nu_a for all GRs

A set of non-linear regression equations is used to find Nusselt number. The importance of the generalized empirical correlation lies in providing a quantitative characteristic of the convective heat transfer.

5.3. Passive Air Cooling with PCM

This part demonstrates the results obtained from the experimental runs where the PCM performs as a latent heat thermal energy storage in the meso heat exchanger. Different air mass flow rate influence on the air exit temperature and other parameters during the PCM

discharging process is presented and discussed. Additionally, the coolant mass flow rate changes and the repeatability of the PCM cycle is also investigated and presented.

5.3.1. Normalized Air Exit Temperature

The thermal performance of the meso heat exchanger for air cooling is investigated using PCM to absorb and store the thermal energy. Figure 5.24 represents the effect of varying the air and 50/50 ethylene-glycol/water mixture mass flow rate on the normalized air outlet temperature with time for the PCM discharging process. The variation of the airside mass flow rate on the PCM discharging process is shown in Fig. 5.24a. Four different experimental runs are conducted considering a different airside mass flow rate for each run (80, 150, 200, and 300 g/s) with an inlet air temperature of 30°C while maintaining other fluids inlet conditions constant. For each experimental run, as the PCM is charged and the system reaches its steady state, the coolant shuts down to allow the thermal energy stored in the PCM to be discharged thus provides air cooling.

The PCM transition temperature controls the start of the melting and solidification processes. The latent heat capacity determines how much energy can be stored in the PCM. It can be noticed that the PCM discharging time is affected by the air flow rate. The heat exchange between PCM and the working fluid is longer for low air mass flow rate which results in higher cooling time. Higher airside flow rates increase the melting rate and lead to shorter air-cooling time. It is also observed that the mass flow rate effect on the discharging time diminishes at higher mass flow rates. The aforementioned results show that the air mass flow rate plays a role in the amount of the extra time of cooling provided. Fig. 5.24b represents the effect of the change in the coolant mass flow rate on the air outlet temperature as the PCM discharges its energy to the air. As seen in both figures, the PCM affects the air outlet temperature which rises when the coolant pump is turned off.

However, it is observed that the air mass flow rate has a significant effect on the air outlet temperature compared to the coolant mass flow rate change.
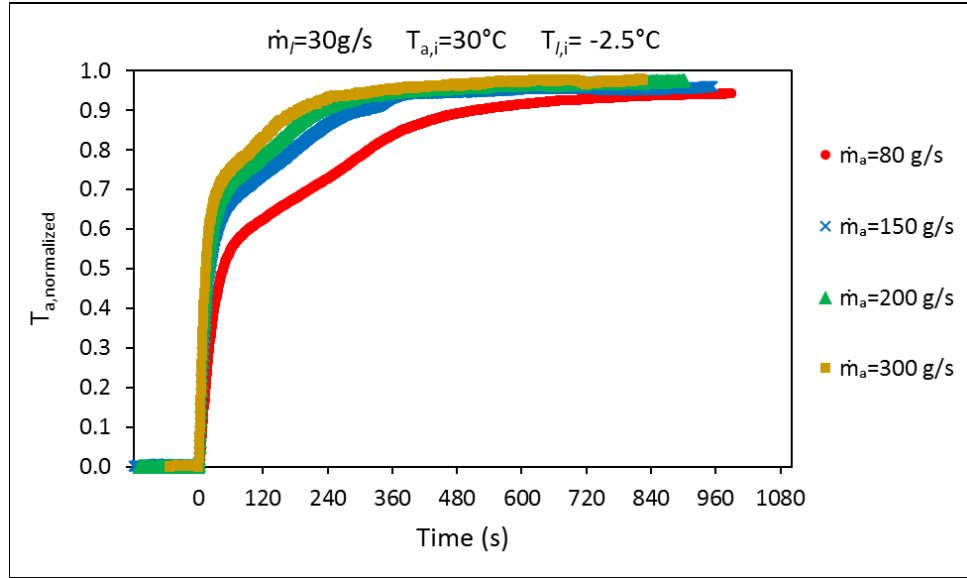
(a) Air mass flow rate variations
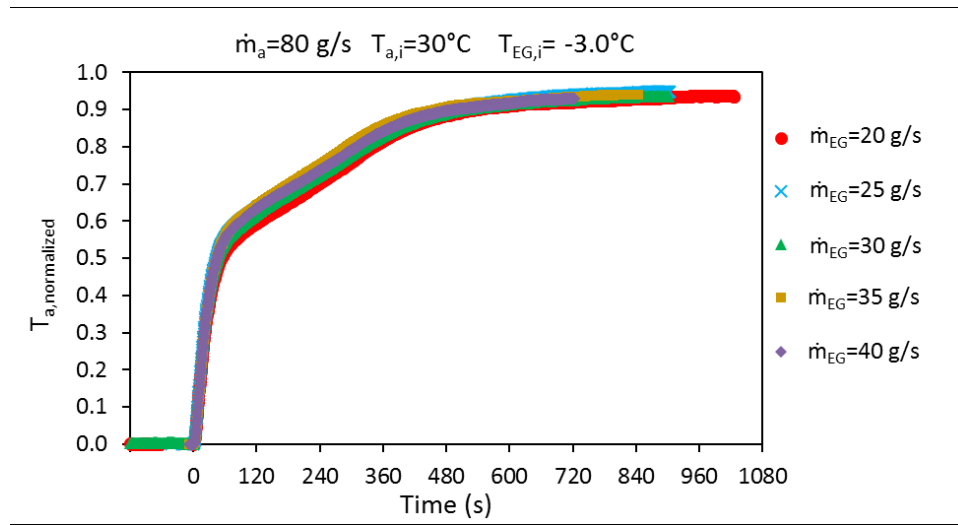
(b) 50/50 Ethylene glycol-water mass flow rate variations

Figure 5.24. Normalized air outlet temperature at different mass flow rate variations

5.3.2. Heat Transfer Rate

The transient airside heat transfer rate behavior throughout the melting process is shown in Figure 5.25 for different airside mass flow rates. Prior to the shutdown, the PCM is charged through solidification using the cold working fluid inside the channels. Meanwhile, the hot air is cooled by the liquid via the walls of the heat exchanger. After the shutdown, the PCM discharging process starts with a sharp decline in heat transfer rate. It is noted from the

figure that the increase in airside mass flow rate results in a decrease of heat transfer rate, however, this effect diminishes at higher mass flow rates.

Figure 5.26 shows heat transfer rate difference with and without PCM for air cooling. When no PCM is used, a sharp decrease in heat transfer occurs since by shutting off the coolant, the air outlet temperature increases resulting in a decrease in heat transfer rate. However, it is observed that the use of PCM extends the period of air cooling and delays the decrease in heat transfer rate. PCM works on interrupting the increase in air outlet temperature for a period of time thus providing extra time for heat transfer and cooling. It can be seen from Fig. 5.26 that the airside heat transfer rate reaches the steady state at about 500s for the case of no PCM while the use of PCM extends this period to about 800s providing extended thermal comfort. An integration of the area between the no PCM and with PCM curves in Fig. 14 shows a 120kJ of energy released from the PCM as a cold thermal energy to cool the hot air during the PCM discharging process.
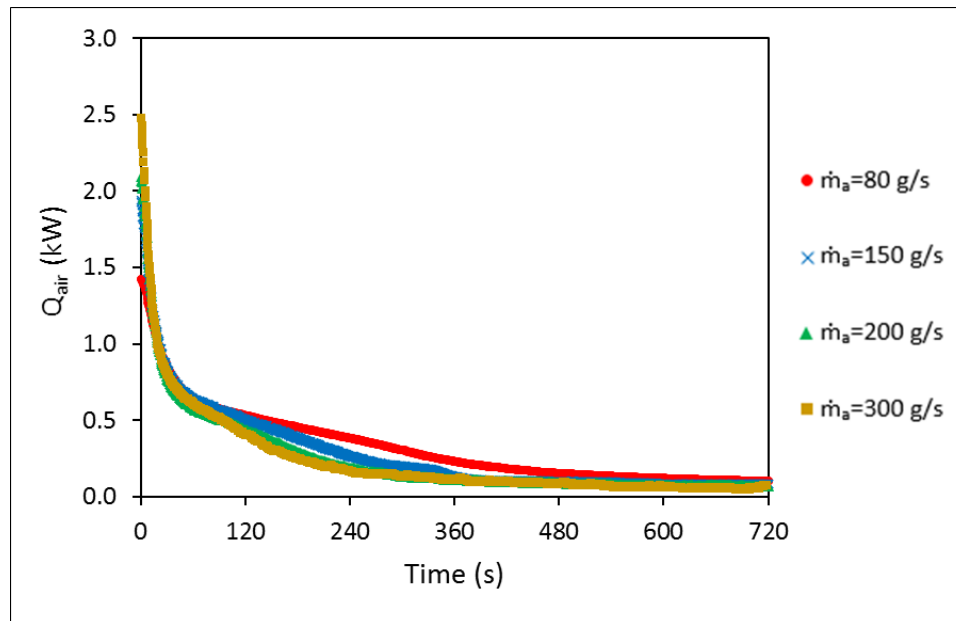
Figure 5.25. Airside heat transfer rate during the discharging process

$\dot{m}_l$=30g/s $\dot{m}_a$=80g/s $T_{a,i}$=30°C $T_{l,i}$= -2.5°C
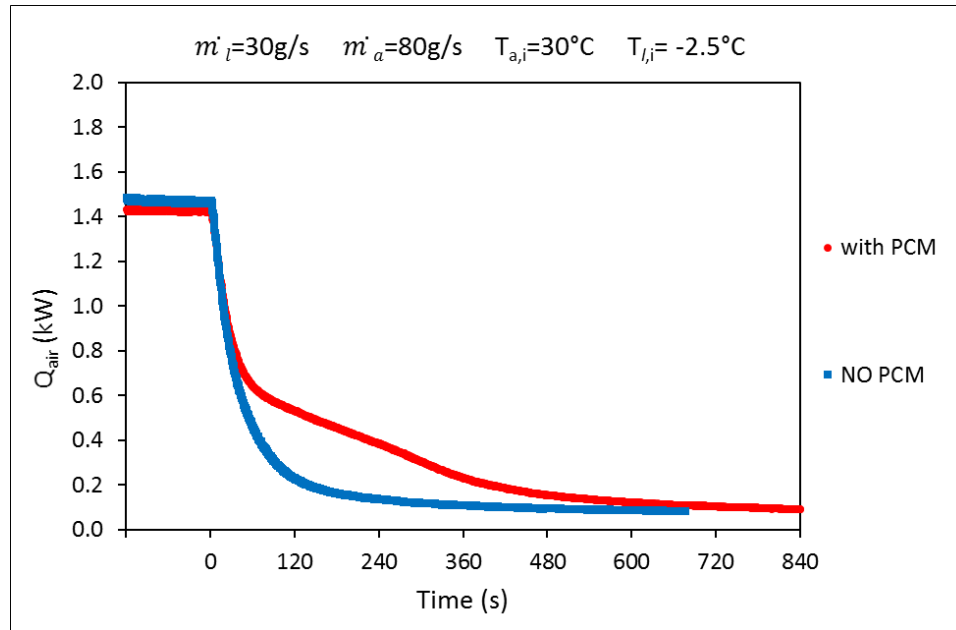
Figure 5.26. Airside heat transfer rate with and without PCM

5.3.3. Cumulative Heat Transfer

Figure 5.27 shows the results of cumulative airside heat transfer evaluated at different air mass flow rates starting at the shutdown of the liquid. It is construed from the figure that the discharging process can achieve a longer duration and higher amount of heat transfer at lower air mass flow rates. A double increase in air mass flow rates resulted in about a 29% decrease in the cumulative energy transferred to the air. During discharging, the PCM temperature increases due to the sensible heat and changes phase from solid to liquid due to latent heat of fusion. Thus, the use of PCM slows down the rise of the heat exchanger surface temperature which in turn, prolongs the period of air outlet temperature increase. This delay in the air outlet temperature rise extends the heat transfer process duration resulting in more air heat transfer release.
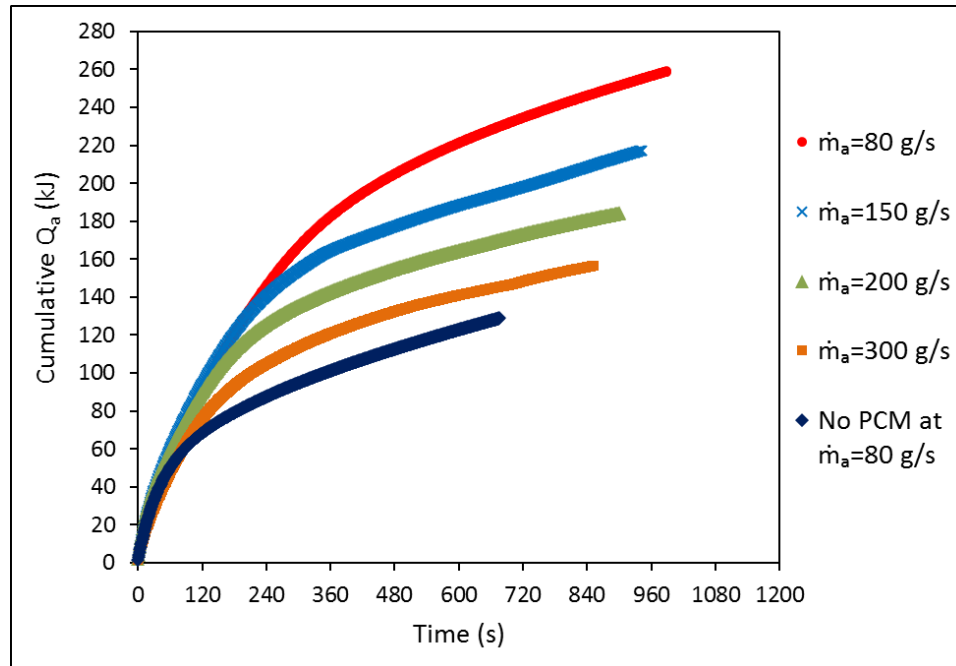
Figure 5.27. Cumulative heat transfer at different air inlet mass flow rates

5.3.4. PCM Effectiveness

The PCM effectiveness as shown in Figure 5.28 is calculated from the cumulative energy found using PCM to the cumulative energy when no PCM is used. The effectiveness evaluates the performance of the PCM in providing extra cooling relative to the case of no PCM. It is observed that the PCM effect starts increasing at coolant shutdown when the air outlet temperature increases. Effectiveness reaches an optimum value before it starts dropping as the PCM melting amount increases. Maximum effectiveness occurs at a normalized air outlet temperature of 0.8 and decreases due to the phase change completion of the PCM. This figure shows that PCM is more effective when the normalized air temperature is about 0.8 which yields the maximum cooling time PCM provides.
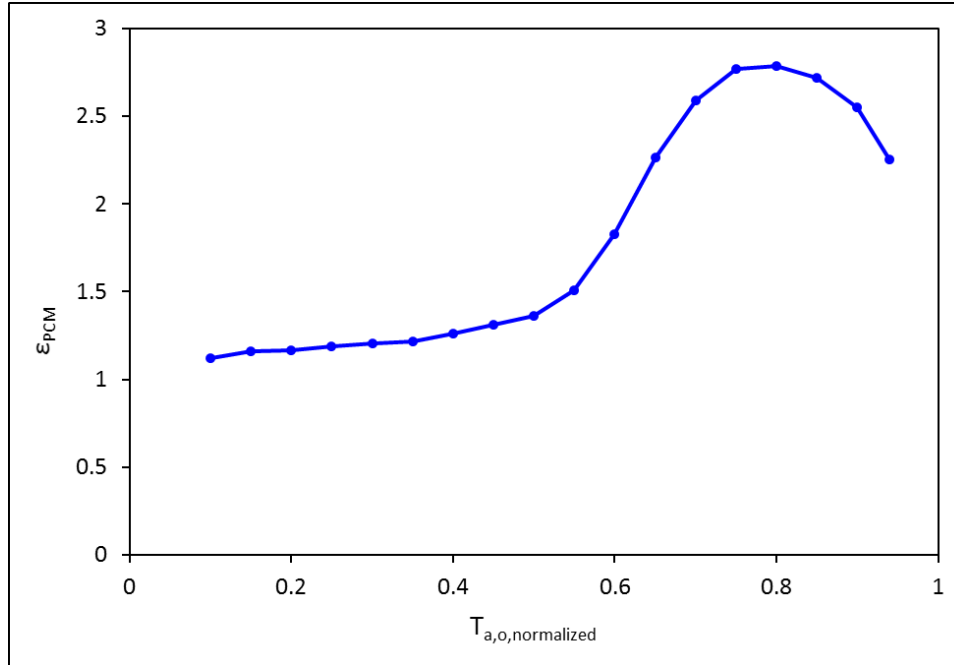
Figure 5.28. PCM effectiveness at normalized air outlet temperature

5.3.5. Air Outlet Temperature Comparison

The PCM effect on air exit temperature is shown in Figure 5.29. After the steady state is reached, the coolant pump shutdown results in a rise in the air outlet temperature. This increase in temperature triggers the PCM to discharge its stored energy and cool the air. It is seen that the use of PCM extends the cooling time to a maximum value of 272s at air outlet temperature of 27.9°C compared to no PCM. At this temperature, the no PCM case requires 172s to reach this temperature from shutdown, while it takes 444s for the PCM case. Additionally, the PCM to no PCM air outlet temperature difference reaches its maximum value after 121s from shut down. After 121s from shut down, the outlet air temperature reaches a value of 27.3°C for the case of no PCM and a value of 23.3°C for the case of PCM which gives the highest temperature difference of 4.0°C.
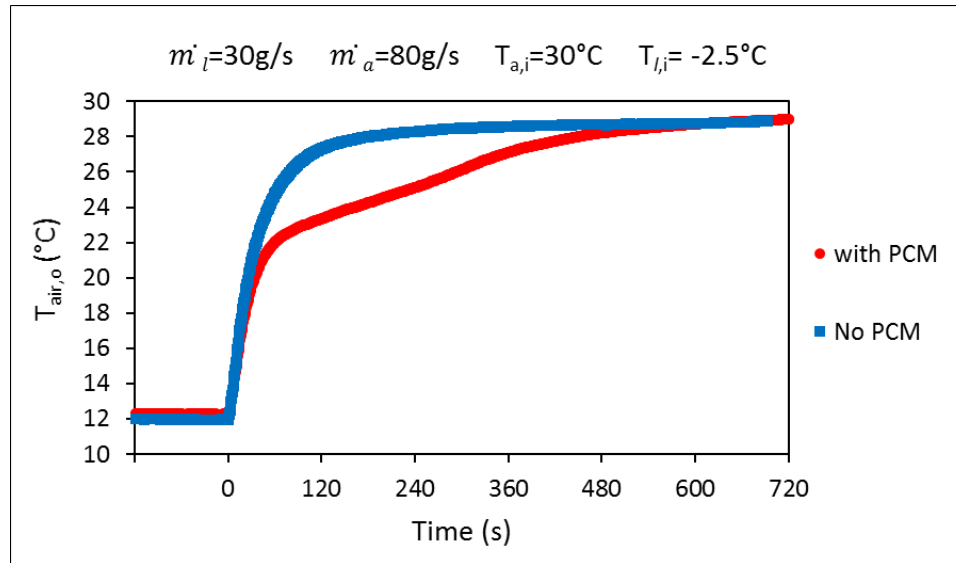
Figure 5.29. Air outlet temperature with and without P*CM*

5.3.6. Repeatability

Experiments were conducted considering the repeatability, short drive, and idle cycles of PCM charging and discharging in a vehicle. The operating conditions were used for these experiments were liquid temperature -3.0°C, air temperature 30°C, liquid mass flow rate of 30g/s, and air mass flow rate of 80g/s. The system was operated with these conditions until it reached steady state after which, the pump that supplies the liquid to the heat exchanger is turned off for a specific period of time, 60s, representing an idle cycle. The idle cycle represents charging/discharging processes and once an idle is completed, the liquid pump is turned on and the system takes few minutes to reach its steady state prior to another idle cycle.

Figure 5.30 shows the outlet air temperature for PCM charging and discharging cycles at 60s idle time. As illustrated from the figure, the air outlet temperature rises when the liquid pump is turned off. Meanwhile, the cold thermal energy stored in the PCM reduces the increasing rate of the air outlet temperature. Since the idle time is very short, not all the stored cold thermal energy is discharged. However, A very good repeatability was observed from the experimental results indicating that the PCM cold thermal energy was restored and released reasonably well during the repeated cycles. This observation can be beneficial for the case of short idle/stop in a vehicle during engine shutdown. The use of PCM works on extending the cooling time of the passenger compartment during idle times

thus provides passenger thermal comfort and can lead to energy and fuel savings. Additionally, for this 60s idle time, it takes the PCM about 1.5 minutes to be charged (i.e. while driving the car) and reached its initial steady state.
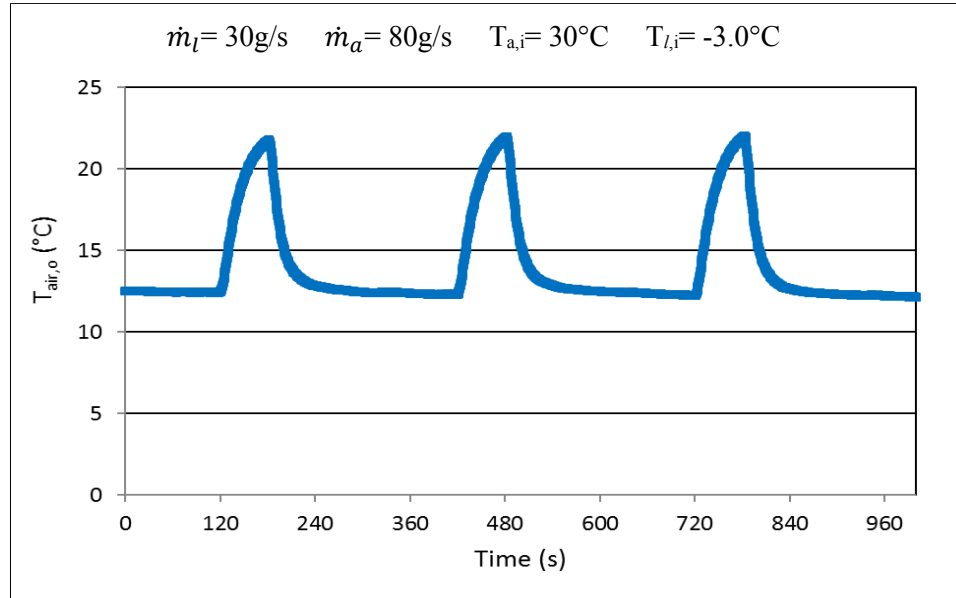
Figure 5.30. PCM repeatability for 60s cycles

The same approach is adopted each time with different idle times (30s and 45s). The system is left to reach steady state before a liquid shutdown is applied by turning off the liquid pump for periods of 30s and 45s for the different runs representing the idles. Once the idle time is completed, the liquid pump is turned on and the system is allowed to reach its initial steady state before applying another repeated cycle. Figures 5.31 and 5.32 confirm the repeatability of the PCM in different idle times during different runs.
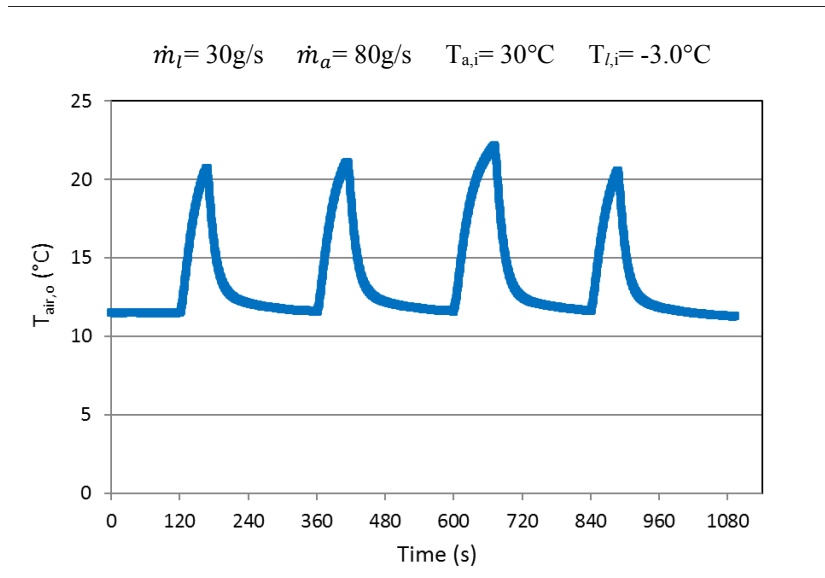
Figure 5.31. PCM repeatability for 45s cycles
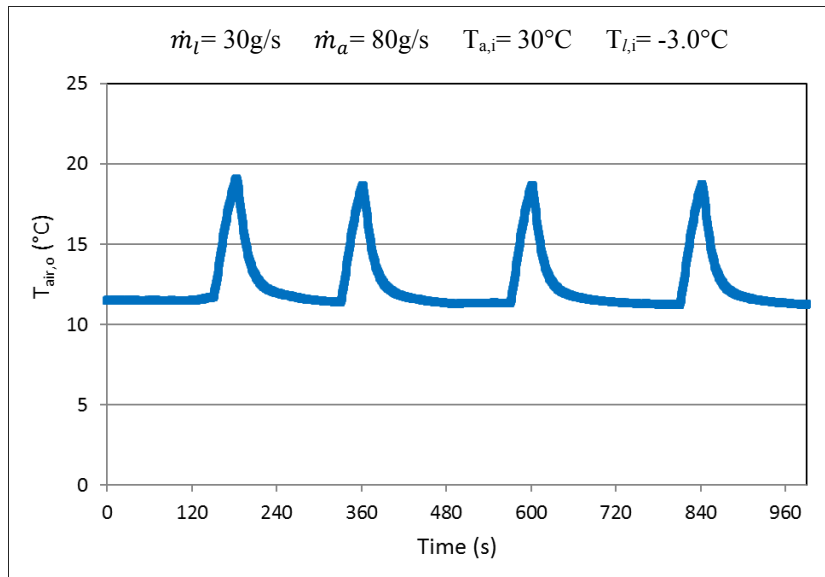
Figure 5.32. PCM repeatability for 30s cycles

CHAPTER 6

CONCLUSIONS AND RECOMMENDATIONS

The current study uses an experimental approach to reach its results and conclusions. This approach is significantly valuable yet complicated. Besides the fact that it requires a very well-equipped experimental setup, researchers must have the capabilities of problem solving and critical thinking as well as experience in solving issues while observing all the parameters of investigation. Maintain and controlling many working conditions is not easy to perform due to the many parameters and equipment involved. Test runs and presets have to be performed prior to running experiments since any small variation can affect the experimental runs. Additionally, the existence of several equipment in the system requires the researcher to be familiar of the limitation and operation of each one of them as well as trouble shooting if needed. However, the lack of experimental data in the field of transient heat transfer with airside perturbations and thermal energy storage makes it worth investigating. Experimental research provides a scientific knowledge, tests published theories, and allows the physical study of real case scenarios.

The dynamic response of a liquid-air cross flow meso heat exchanger subjected to airside mass velocity variations is experimentally investigated for the cases of active air heating and cooling. Furthermore, the effect of air mass flow rate variation is examined for the case of passive air-cooling when a PCM is injected in the meso heat exchanger acting as a thermal energy storage. Transient analysis is important to characterize the heat transfer behavior due to fluid inlet changes and to predict the outlet temperature response to maintain the thermal comfort of occupants or passengers.

6.1. Results and Discussions on Active Air Heating and Cooling

The current transient response of active air heating and cooling is studied due to a change in the air mass velocity stepping up from a common initial value to 5 different final values while maintaining the other fluids inlet conditions constant. Heat transfer and fluid flow are studied for step increases in air mass velocity for final to initial ratios of, 1.5, 2.0, 2.5, 3.0, and 3.5. The impact of the mass flow step changes is examined on the fluids outlet

temperature response, heat transfer rates, airside heat transfer coefficient, airside Nusselt number, and airside Colburn j factor. The experimental results show that the step magnitude affects the response time of each fluid and these two factors combined influence the performance of the heat exchanger as it undergoes a transient change.

The current study provides a quantitative prediction of the transient behavior of the meso heat exchanger illustrating the relationship between the changes in the input operating condition and its effect on the heat transfer and fluid flow. The findings from the experimental work are summarized in the following points,

- Both fluids outlet temperatures response is not instantaneous to the step change due to the heat stored in the wall of the heat exchanger and the time it takes for the transition to occur from an initial to a final flow rate value.

- Each fluid possesses different response time than the other which depends on the magnitude of the step change imposed.

- Higher mass velocity step changes yielded higher heat transfer rate, heat transfer coefficient, and Nusselt number with a diminishing effect at higher ratios. However, the case is not the same for outlet temperature of both fluids where they decrease with the increase of the step change.

- Air and liquid exhibited an initial delay time to the airside mass velocity ratio increase, however, DI-water exhibited higher initial delay, residence and response times compared to air.

- The step imposed on the airside mass velocity along with the shorter residence time of the air result in faster response time of air compared to the DI water.

- A generalized empirical correlation for airside Nusselt number in the form of Nusselt number with dimensionless time for different mass velocity ratios as $Nu_a(t) = Nu_a(\infty)\{1 - Ae^{-Bt^*}\}$ is derived and presented in this study for air heating and cooling.

The performance data from the experimental results as well as the presented generalized correlations provide an insight on the behavior of compact heat exchangers that can be used in practical heating system found in industries such as automotive heater core. The results from this work can be utilized to predict different parameters of the heat exchanger such

as the fluids outlet temperature response, heat transfer rates, heat transfer coefficient, etc. using the knowledge of input mass velocity ratio to be imposed. Non-linear regression equations are used in finding the generalized empirical correlation to obtain the transient dimensionless airside Nusselt number for a wide range of Reynolds number. The transient study of the crossflow heat exchanger under changes in its inlet condition from an initial steady state presents an experimental dynamic characterization of the airside. Furthermore, the current work provides a better control in maintaining the passengers thermal comfort by understanding and predicting the transient behavior of airside.

6.2. Results and Discussions on Passive Air Cooling with PCM

The second aspect evaluated is the passive air cooling with PCM as a cold thermal energy storage. An innovative PCM-air-liquid crossflow meso heat exchanger is experimentally investigated with the aim of thermal energy storage to provide extended thermal comfort during coolant shutdown in a vehicle. Fins are distributed inside the PCM and between the slabs to transfer the thermal energy between the PCM and the fluids. The effect of various mass flow rates on the PCM discharging process is examined. In addition, the air heat transfer and air outlet temperature were compared for both cases of with and without PCM. The following conclusions are reached for the passive air-cooling and are listed below,

- Higher inlet air mass flow rate resulted in a faster PCM discharging time. This effect diminishes at higher mass flow rate values.

- The use of PCM extended the cooling time by more than 4 minutes and resulted in a thermal energy release of 120 kJ during the discharging process.

- A double increase in airside mass flow rate resulted in a 29% decrease in the cumulative energy released to the air.

- The PCM effectiveness reveals that the PCM reaches its optimal performance at a normalized air outlet temperature of 0.8.

- The effect of air mass flow rate on air outlet temperature during PCM discharging process is found significant compared to the effect of liquid flow rate change.

- The PCM is found repeatable during multiple charging/discharging cycles without any deterioration in its performance.

This work is provided as a solution to the passengers' thermal comfort that is compromised during short periods of engine stops for electric and hybrid vehicles. As vehicles run and experience multiple idles, it is necessary to provide air outlet temperature control and management to the passenger cabin. The use of PCM is beneficial in providing extended cooling times without the need for energy or fuel through its storing and releasing of cold thermal energy processes.

6.3. Recommendations

The results and observations made in this study present a valuable and deep insight into the limited knowledge of transient heat transfer in compact crossflow heat exchangers. Most of the published work for heat transfer in heat exchangers is based on the steady state analysis, thus the presented study along with the derived empirical correlations provide a characterization and quantification of the behavior of the dynamic heat transfer of heat exchangers as well as the outlet temperature response of the working fluids. However, the transient active air heating and cooling study can be further extended by future researchers considering the following points,

➢ Analyzing the effect of different inlet initial steady state each time a step is imposed to reach a common final steady state.

➢ Applying step down in airside mass velocity ratios and compare the findings with the current results.

➢ Experimentally investigate the application of two variations at the same time such as air mass flow rate and temperature variations on the heat exchanger performance.

➢ Experimentally investigate the air cooling for a compact crossflow heat exchanger with liquid temperature and flow rate variations.

➢ Numerically investigate the transient heating and cooling using this study operating conditions and geometry.

The experimental investigation of a PCM in a meso heat exchanger as a thermal energy storage is rare due mainly to its complexity of controlling two working fluids along with the PCM. Adding to that, modifying the experimental setup to accommodate different

primary and secondary loops used to charge and discharge the PCM and control other fluids' operating conditions. The highly beneficial results reached from this work enrich the data base of such studies and pave the way for future researchers to advance this study further exceptional work. Some recommendations are listed below,

➢ Applying enhanced types of PCMs for better thermal performance that is characterized with higher latent heat or enhanced thermal conductivity.

➢ Numerically investigate the use of PCM in the presented heat exchanger for extended thermal comfort using cooling and heating processes.

➢ Investigating the effect of fins on the charging and discharging processes as well as the thermal properties of the PCM using different fin specifications.

➢ Introducing an infrared thermal camera to observe the melting and solidification behavior of PCM with time and obtain its temperature distribution.

➢ Studying the effect of air mass flow rate variation on the charging process and investigate different parameters that influence it.

➢ Enhancing the design of incorporating the PCM as part of the heat exchanger.

REFERENCES

1. International Energy Outlook EIA 2019 with projections to 2050. U.S. Energy Information Administration Office of Energy Analysis, U.S. Department of Energy, Washington, DC 20585, September 24, 2019, #IEO2019.

2. Canada Energy factbook-2020-2021. Natural Resources Canada, Cat. No. M136-1E, ISSN 2370-3105.

3. International Energy Agency IEA. "Cooling on the Move, the future of air conditioning in vehicles", September 2019.

4. Simion M., Socaciu L., and Unguresan P. (2016). "Factors which Influence the Thermal Comfort Inside of Vehicles, Energy Procedia, 85:472-480, ISSN 1876-6102, https://doi.org/10.1016/j.egypro.2015.12.229.

5. Shah R. K., and Sekulić D. P. (2003). "Fundamentals of heat exchanger design". Hoboken, NJ: John Wiley & Sons.

6. Siddique M., Khaled A.-R. A., and Abdulhafiz N. I., et. al. (2010). "Recent Advances in Heat Transfer Enhancements: A Review Report", International Journal of Chemical Engineering, vol. 2010, Article ID 106461, 28 pages. https://doi.org/10.1155/2010/106461.

7. Picón-Núñez M. (2012). "Heating and Cooling Systems Analysis Based on Complete Process Network". Handbook of Food Process Design. Oxford, UK: Black Well Publishing Limited. March 2012. p. 299-334. Online ISBN:9781444398274, DOI:10.1002/9781444398274.

8. Steinke M.E., and Kandlikar S. (2004). Single-phase heat transfer enhancement techniques in microchannel and minichannel flows.

9. Bergles, A.E., Jensen M.K., and Shome B. (1996). "The Literature on Enhancement of Convective Heat and Mass Transfer." Enhanced Heat Transfer 4:1-6.

10. Yang L., Jin X., Zhang Y., et. al. (2021). "Recent development on heat transfer and various applications of phase-change materials", Journal of Cleaner Production, Volume 287, 124432, ISSN 0959-6526, https://doi.org/10.1016/j.jclepro.2020.124432.

11. Elarem R., Alqahtan, T., Mellouli S., et al. (2021). "A comprehensive review of heat transfer intensification methods for latent heat storage units". Energy Storage, 3:e127. https://doi.org/10.1002/est2.127.

12. Fleischer A.S. (2015). "Thermal Energy Storage Using Phase Change Materials: Fundamentals and Applications". Springer International Publishing, L.e.E. Springer, Cham.

13. Sharma A., Tyagi V.V., Chen C.R., et. al. (2009). "Review on thermal energy storage with phase change materials and applications". Renewable and Sustainable Energy Reviews, 13(2):318-345, ISSN 1364-0321, https://doi.org/10.1016/j.rser.2007.10.005.

14. Atinafu D. G., Dong W., Huang X., et. al. (2018). "Introduction of organic-organic eutectic PCM in mesoporous N-doped carbons for enhanced thermal conductivity and energy storage capacity", Applied Energy, 211:1203-1215, ISSN 0306-2619. https://doi.org/10.1016/j.apenergy.2017.12.025.

15. Faraj Kh., Khaled M., Faraj J., Hachem F., et. al. (2020). "Phase change material thermal energy storage systems for cooling applications in buildings: A review", Renewable and Sustainable Energy Reviews, Volume 119, 109579, ISSN 1364-0321. https://doi.org/10.1016/j.rser.2019.109579.

16. Magendran S. S., Khan F. S. A., Mubarak N. M., et. al. (2019). "Synthesis of organic phase change materials (PCM) for energy storage applications: A review, Nano-Structures & Nano-Objects", Volume 20, 100399, ISSN 2352-507X. https://doi.org/10.1016/j.nanoso.2019.100399.

17. Chandel S.S., and Agarwal T. (2017) "Review of current state of research on energy storage, toxicity, health hazards and commercialization of phase changing materials", Renewable and Sustainable Energy Reviews, 67:581-596, ISSN 1364-0321. https://doi.org/10.1016/j.rser.2016.09.070.

18. Lone M. I., and Jilte R. (2021) "A review on phase change materials for different applications", Materials Today: Proceedings, Volume 46(20):10980-10986, ISSN 2214-7853, https://doi.org/10.1016/j.matpr.2021.02.050.

19. Zhou D., Zhao C.Y., and Tian Y. (2012) "Review on thermal energy storage with phase change materials (PCMs) in building applications", Applied Energy, 92:593-605, ISSN 0306-2619, https://doi.org/10.1016/j.apenergy.2011.08.025.

20. Abdul Ghani S. A., Jamari S. S., and Abidin S. Z. (2021) "Waste materials as the potential phase change material substitute in thermal energy storage system: a review", Chemical Engineering Communications, 208:5, 687-707.
DOI: 10.1080/00986445.2020.1715960.

21. Souayfane F., Fardoun F., and Biwole P. H. (2016) "Phase change materials (PCM) for cooling applications in buildings: A review", Energy and Buildings, 129:396-431, ISSN 0378-7788, https://doi.org/10.1016/j.enbuild.2016.04.006.

22. Albadr J., Tayal S., and Alasadi M. (2013) "Heat transfer through heat exchanger using Al2O3 nanofluid at different concentrations". Case Studies in Thermal Engineering, 1:1, pp.38-44.

23. Huminic G., Huminic A. (2012) "Application of nanofluids in heat exchangers: A review", Renewable and Sustainable Energy Reviews, 16(8):5625-5638, ISSN 1364-0321, https://doi.org/10.1016/j.rser.2012.05.023.

24. Ismail M., Fotowat S., and Fartaj A. (2014) "Effect of Channel Size on Heat Transfer and Pressure Drop in Thin Slabs Minichannel Heat Exchanger". International Journal of Mechanical Engineering and Mechatronics, 2: pp.33-42.

25. Moorthy P., Oumer A. N., and Ishak M. (2018) "Experimental Investigation on Effect of Fin Shape on the Thermal-Hydraulic Performance of Compact Fin-and-Tube Heat Exchangers". IOP Conference Series: Materials Science and Engineering, Volume 318, Malaysian Technical Universities Conference on Engineering and Technology 2017 (MUCET 2017) 6–7 December 2017, Penang, Malaysia. doi:10.1088/1757-899X/318/1/012070.

26. Basavarajappa S., Manavendra G., and Prakash S. B. (2020) "A review on performance study of finned tube heat exchanger" Journal of Physics: Conference Series, Volume 1473, International Conference on Thermo-fluids and Energy Systems (ICTES2019) 27-28 December 2019, Bengaluru, India.

27. Altwieb, M., Mishra, R., Aliyu, A.M., et. al. (2022) "Heat Transfer Enhancement by Perforated and Louvred Fin Heat Exchangers", Energies, 15, 400. ISSN 1996-1073, https:// doi.org/10.3390/en15020400.

28. Kuehndel J., Kerler B., and Karcher C. (2016) "Air side thermal performance of wavy fin heat exchangers produced by selective laser melting". 7th European Thermal-Sciences Conference (Eurotherm2016). Conference Series 745.

29. Erek A., Özerdem B, Bilir L, and İlken Z. (2005) "Effect of geometrical parameters on heat transfer and pressure drop characteristics of plate fin and tube heat exchangers". Applied Thermal Engineering, 25: 14–15, pp. 2421-2431.

30. Siddiqui F., Dasgupta Engr S., and Fartaj A. (2012) "Experimental investigation of air side heat transfer and fluid flow performances of multi-port serpentine cross-flow mesochannel heat exchanger". International Journal of Heat and Fluid Flow, 33:1, pp.207-219.

31. Junqi D., Jiangping C., Zhijiu C., et. al. (2007) "Heat transfer and pressure drop correlations for the wavy fin and flat tube heat exchangers". Applied Thermal Engineering, 27:11–12, pp.2066-2073.

32. Dasgupta E., Siddiqui F., and Fartaj A., (2011) "Experimental Study on Air Side Heat Transfer and Fluid Flow Characteristics of Microchannel Heat Exchanger", SAE International Journal of Materials and Manufacturing 4(1):1198-1210. https://doi.org/10.4271/2011-01-1166.

33. Waltrich P. J., Barbosa J. R., Hermes C. J.L., et. al. (2011) "Air-side heat transfer and pressure drop characteristics of accelerated flow evaporators", International Journal of Refrigeration, 34(2):484-497, ISSN 0140-7007. https://doi.org/10.1016/j.ijrefrig.2010.08.016.

34. Taler D. (2013) "Experimental determination of correlations for average heat transfer coefficients in heat exchangers on both fluid sides". Heat and Mass Transfer 49: pp.1125–1139.

35. Bunce D. (1995) "The Transient response of heat exchangers". Thesis. Rochester Institute of Technology.

36. Lachi M., Wakil N. El, and Padet J. (1997) "The time constant of double pipe and one pass shell-and-tube heat exchangers in the case of varying fluid flow rates", International Journal of Heat and Mass Transfer, 40(9):2067-2079, ISSN 0017-9310, https://doi.org/10.1016/S0017-9310(96)00274-8.

37. Yin J., and Jensen M. K. (2003). "Analytic model for transient heat exchanger response", International Journal of Heat and Mass Transfer, 46(17):3255-3264, ISSN 0017-9310, https://doi.org/10.1016/S0017-9310(03)00118-2.

38. Srihari N., and Das S. K. (2008). "Experimental and Theoretical Analysis of Transient Response of Plate Heat Exchangers in Presence of Nonuniform Flow Distribution." ASME. Journal of Heat Transfer, 130(5): 051801. https://doi.org/10.1115/1.2885153.

39. Abdallah S., and Rooke S. (1997) "Transient Response of a Serpentine Finned-Tube Cross-Flow Heat Exchanger to a Step Change in Inlet Temperature" Heat Transfer Engineering, 18:3, pp.51-60.

40. Chen H., and Chen K. (1992) "Transient response of crossflow heat exchangers with finite wall capacitance". ASME. Journal of Heat Transfer. 114:(3): pp.752–755.

41. Syed F.H., and Idem S. (2008) "Transient Performance of a Cross Flow Heat Exchanger Using Finite Difference Analysis". Proceedings of the ASME 2008 International Mechanical Engineering Congress and Exposition. Volume 10: Heat Transfer, Fluid Flows, and Thermal Systems, Parts A, B, and C. Boston, Massachusetts, USA. October 31–November 6, pp.1333-1342.

42. Gogus Y. A., and Ataer O. E., (1988) "Effect of Fins on Transient Behavior of Cross-Flow Air-Liquid Heat Exchangers". International Refrigeration and Air Conditioning Conference. Paper 67.

43. Ataer Ö. E. (2004) "An approximate method for transient behavior of finned-tube cross-flow heat exchangers". International Journal of Refrigeration, 27:5, pp.529-539.

44. Ataer Ö.E., İleri A., and Göğüş Y. (1995)"Transient behaviour of finned-tube cross-flow heat exchangers". International Journal of Refrigeration, 18:3, pp.153-160 (1995).

45. Silaipillayarputhur K., and Idem SA. (2015) "Transient Response of a Cross Flow Heat Exchanger Subjected to Temperature and Flow Perturbations". Proceedings of the ASME 2015 International Mechanical Engineering Congress and Exposition. 8A: Heat Transfer and Thermal Engineering. Houston, Texas, USA. November 13–19, V08AT10A019.

46. Silaipillayarputhur S., and Idem S. (2014) "Transient Performance of Multi-Pass Parallel and Counterflow Crossflow Heat Exchangers". IMECE2014-37030, Proceedings of IMECE, Montreal, Quebec.

47. Vaisi A., Talebi S., and Esmaeilpour M. (2011). "Transient behavior simulation of fin-and-tube heat exchangers for the variation of the inlet temperatures of both fluids", International Communications in Heat and Mass Transfer, Volume 38, Issue 7, Pages 951-957, ISSN 0735-1933, https://doi.org/10.1016/j.icheatmasstransfer.2011.04.016.

48. Pearson J.T., Leonard R.G., and McCutchan R.D. (1974) "Gain and Time Constant for Finned Serpentine Crossflow Heat Exchangers". ASHRAE Transactions 80: 2, pp.255-267.

49. Fotowat S., Askar S., and Fartaj A. (2018) "Transient response of a meso heat exchanger with temperature step variation". International Journal of Heat and Mass Transfer, 122: pp.1172-1181.

50. Askar S., Fotowat S., and Fartaj A. (2021). "Transient experimental investigation of airside heat transfer in a crossflow heat exchanger", Applied Thermal Engineering, Volume 199, 117516, ISSN 1359-4311. https://doi.org/10.1016/j.applthermaleng.2021.117516.

51. Mishra M., Das P.K., and Sarangi S., (2006). "Transient behaviour of crossflow heat exchangers due to perturbations in temperature and flow", International Journal of Heat and Mass Transfer, Volume 49, Issues 5–6, Pages 1083-1089, ISSN 0017-9310. https://doi.org/10.1016/j.ijheatmasstransfer.2005.09.003.

52. Del Valle M., and Ortega A. (2015). "Experimental Characterization of the Transient Response of Air/Water Crossflow Heat Exchangers for Data Center Cooling Systems", Proceedings of the ASME 2015 International Technical Conference and Exhibition on Packaging and Integration of Electronic and Photonic Microsystems collocated with the ASME 2015 13th International Conference on Nanochannels, Microchannels, and Minichannels. Volume 1: Thermal Management. San Francisco, California, USA. July 6–9, 2015. V001T09A021. ASME. https://doi.org/10.1115/IPACK2015-48375.

53. Gao T., Murray B., and Sammakia B. (2015) "Analysis of transient and hysteresis behavior of cross-flow heat exchangers under variable fluid mass flow rate for data center cooling applications". Applied Thermal Engineering, 84: pp.15-26.

54. Erden H. S. (2013) "Experimental and Analytical Investigation of the Transient Thermal Response of Air Cooled Data Centers". Dissertations - ALL. 43.

55. Del Valle M., Caceres C., and Ortega A. (2016) "Transient modeling and validation of chilled water based cross flow heat exchangers for local on-demand cooling in data centers" 15th IEEE Intersociety Conference on Thermal and Thermomechanical Phenomena in Electronic Systems (ITherm), pp. 727-736.
doi: 10.1109/ITHERM.2016.7517619.

56. Gao T., Sammakia B., and Geer J. (2015) "Dynamic response and control analysis of cross flow heat exchangers under variable temperature and flow rate conditions". International Journal of Heat and Mass Transfer, 81, pp.542-553.

57. Sarbu I., and Sebarchievici C. (2018) "A Comprehensive Review of Thermal Energy Storage". Sustainability, 10(1):191. https://doi.org/10.3390/su10010191.

58. Chavan S., Rudrapati R., and Manickam S., (2022) "A comprehensive review on current advances of thermal energy storage and its applications", Alexandria Engineering Journal, 61(7):5455-5463, ISSN 1110-0168.
https://doi.org/10.1016/j.aej.2021.11.003.

59. Wang W., Yang X., Fang Y., et. al. (2008) "Enhanced thermal conductivity and thermal performance of form-stable composite phase change materials by using β-Aluminum nitride", Applied Energy, 86(7–8):1196-1200, ISSN 0306-2619.
https://doi.org/10.1016/j.apenergy.2008.10.020.

60. Fan L., and Khodadadi J.M. (2011) "Thermal conductivity enhancement of phase change materials for thermal energy storage: A review". Renewable and Sustainable Energy Reviews, 15(1):24-46, ISSN 1364-0321.
https://doi.org/10.1016/j.rser.2010.08.007.

61. Teng, TP., and Yu, CC. (2012) "Characteristics of phase-change materials containing oxide nano-additives for thermal storage". Nanoscale Research Letter 7, article number 611. https://doi.org/10.1186/1556-276X-7-611.

62. Ji H., Sellan D. P., Pettes M. T., et. al. (2014) "Enhanced thermal conductivity of phase change materials with ultrathin-graphite foams for thermal energy storage". Energy and Environmental Science 7: 1185-1192.

63. Sivasamy P., Devaraju A., and Harikrishnan S. (2018) "Review on Heat Transfer Enhancement of Phase Change Materials (PCMs), Materials Today: Proceedings,

5(6):14423-14431, Part 2, ISSN 2214-7853. https://doi.org/10.1016/j.matpr.2018.03.028.

64. Al-Mudhafar A. H.N., Nowakowski A. F., and Nicolleau F. C.G.A. (2021) "Enhancing the thermal performance of PCM in a shell and tube latent heat energy storage system by utilizing innovative fins", Energy Reports, Volume 7, Supplement 2, Pages 120-126, ISSN 2352-4847, https://doi.org/10.1016/j.egyr.2021.02.034.

65. Li H., Wang N., Zhao B., et. al. (2022). "Simulation study on the effect of fins on the heat transfer performance of horizontal dual-inner-tube latent thermal energy storage heat exchangers", Journal of Energy Storage, Volume 49, 104125, ISSN 2352-152X. https://doi.org/10.1016/j.est.2022.104125.

66. Mat S., Al-Abidi A. A., Sopian K., Sulaiman M.Y., et. al. (2013) "Enhance heat transfer for PCM melting in triplex tube with internal–external fins", Energy Conversion and Management, 74:223-236, ISSN 0196-8904. https://doi.org/10.1016/j.enconman.2013.05.003..

67. Kumar N., Chavez R., and Banerjee D. (2018) "Experimental Validation of Thermal Performance of a Plate Heat Exchanger (PHX) with Phase Change Materials (PCM) for Thermal Energy Storage (TES)", 17th IEEE Intersociety Conference on Thermal and Thermomechanical Phenomena in Electronic Systems (ITherm), pages 927-934. doi: 10.1109/ITHERM.2018.8419529.

68. Kalapala L., and Devanuri J. K. (2018) "Influence of operational and design parameters on the performance of a PCM based heat exchanger for thermal energy storage – A review" Journal of Energy Storage, 20:497-519, ISSN 2352-152X. https://doi.org/10.1016/j.est.2018.10.024.

69. Lu B., Zhang Y., Sun D., et. al. (2021). "Experimental investigation on thermal behavior of paraffin in a vertical shell and spiral fin tube latent heat thermal energy storage unit", Applied Thermal Engineering, 187, Article 116575. 10.1016/j.applthermaleng.2021.116575.

70. Promoppatum P., Yao S.C., Hultz T., and Agee D. (2017) "Experimental and numerical investigation of the cross-flow PCM heat exchanger for the energy saving of building HVAC", Energy and Buildings, 138:468-478, ISSN 0378-7788. https://doi.org/10.1016/j.enbuild.2016.12.043.

71. Herbinger F., Bhouri M., and Groulx D. (2018) "Investigation of heat transfer inside a PCM-air heat exchanger: a numerical parametric study", Heat Mass Transfer 54, 2433–2442. https://doi.org/10.1007/s00231-017-2101-9.

72. Rahimi M., Ranjbar A. A., Ganji D. D., et. al., (2014) "Experimental Investigation of Phase Change inside a Finned-Tube Heat Exchanger", Journal of Engineering, volume 2014, Article ID 641954, 11 pages. doi:10.1155/2014/641954.

73. Medrano M., Yilmaz M.O., Nogués M., et. al. (2009). "Experimental evaluation of commercial heat exchangers for use as PCM thermal storage systems", Applied Energy, 86(10):2047-2055, ISSN 0306-2619. https://doi.org/10.1016/j.apenergy.2009.01.014.

74. Amagour M., Rachek A., Bennajah M., et. al. (2018). "Experimental investigation and comparative performance analysis of a compact finned- tube heat exchanger uniformly filled with a phase change material for thermal energy storage", Energy Conversion and Management, 165:137-151, ISSN 0196-8904. https://doi.org/10.1016/j.enconman.2018.03.041.

75. Koukou M. K., Vrachopoulos M. Gr., Tachos N. S., et. al. (2018). "Experimental and computational investigation of a latent heat energy storage system with a staggered heat exchanger for various phase change materials", Thermal Science and Engineering Progress, Volume 7, Pages 87-98, ISSN 2451-9049. https://doi.org/10.1016/j.tsep.2018.05.004.

76. Wang M., Wolfe E., Craig T., et. al. (2016). "Design and Testing of a Thermal Storage System for Electric Vehicle Cabin Heating", SAE Technical Paper 2016-01-0248, doi:10.4271/2016-01-0248.

77. Horvat A., Leskovar M., and Mavko B. (2006) "Comparison of heat transfer conditions in tube bundle cross-flow for different tube shapes, International Journal of Heat and Mass Transfer, 49(5–6):1027-1038, ISSN 0017-9310. https://doi.org/10.1016/j.ijheatmasstransfer.2005.09.030.

78. Mosa M. A. M. (2009) "Study of circular and elliptical tube arrays as cross flow heat exchangers". Electronic Theses and Dissertations. 8029.

79. Ismail M., Fotowat S., and Fartaj A. (2014) "Effect of Channel Size on Heat Transfer and Pressure Drop in Thin Slabs Minichannel Heat Exchanger" International Journal

of Mechanical Engineering and Mechatronics (IJMEM), Volume 2 - Year 2014 - Pages 33-42. ISSN: 1929-2724. DOI: 10.11159/ijmem.2014.004.

80. Mangrulkar C. K., Ashwinkumar D. S., Sunil C., et. al. (2019) "Recent advancement in heat transfer and fluid flow characteristics in cross flow heat exchangers" Renewable and Sustainable Energy Reviews, Elsevier, volume 113(C), pages 1-1. https://doi.org/10.1016/j.rser.2019.06.027.

81. Mohanan A. K., Prasad B.V., and Vengadesan S. (2021) "Flow and Heat Transfer Characteristics of a Cross-Flow Heat Exchanger with Elliptical Tubes", Heat Transfer Engineering, 42:21, 1846-1860, DOI: 10.1080/01457632.2020.1826742.

82. Khan Md M. (2011) "experimental investigation of heat transfer and pressure drop characteristics of water and glycol-water mixture in multi-port serpentine microchannel slab heat exchangers". University of Windsor, Electronic Theses and Dissertations. 462.

83. Quaiyum MD A., (2012) "experimental investigation of automatic transmission fluid (ATF) in an air cooled minichannel heat exchanger". University of Windsor, Electronic Theses and Dissertations. 371.

84. Ghachem K., Aich W., and Kolsi L., (2021) "Computational analysis of hybrid nanofluid enhanced heat transfer in cross flow micro heat exchanger with rectangular wavy channels", Case Studies in Thermal Engineering, Volume 24, 100822, ISSN 2214-157X, https://doi.org/10.1016/j.csite.2020.100822.

85. Paeng J.G., Kim K.H., and Yoon Y.H. (2009) "Experimental measurement and numerical computation of the air side convective heat transfer coefficients in a plate fin-tube heat exchanger. J Mech Sci Technol 23, 536–543. https://doi.org/10.1007/s12206-008-1013-5.

86. Fotowat S., (2012)"Thermal Performance Study of a Prototype Multiport Heat Exchanger". University of Windsor, Electronic Theses and Dissertations. 184.

87. Taler, D. (2005) "Prediction of heat transfer correlations for compact heat exchangers". Forsch Ingenieurwes, 69:137–150, https://doi.org/10.1007/s10010-004-0148-5.

88. Tang, S., and Yang, KT. (2005) "Thermal performance of a single-row fin-and-tube heat exchanger". Journal of Thermal Science 14, 172–180.

89. Siddiqui, F. (2011) "A Study of Cross-Flow Air Heating via a Multiport Serpentine Microchannel Heat Exchanger" University of Windsor, Electronic Theses and Dissertations 209.

90. Dasgupta, Engr., Askar, S., Ismail, M., et. al. (2012). "Air cooling by multiport slabs heat exchanger: An experimental approach". Experimental Thermal and Fluid Science, Volume 42, Pages 46-54, ISSN 0894-1777.
https://doi.org/10.1016/j.expthermflusci.2012.04.009.

91. Bošnjaković M., Muhič S., Čikić A. (2020). "Experimental testing of the heat exchanger with star-shaped fins, International Journal of Heat and Mass Transfer, Volume 149, 119190, ISSN 0017-9310.
https://doi.org/10.1016/j.ijheatmasstransfer.2019.119190row

APPENDIX A: UNCERTAINTY ANALYSIS

This chapter evaluates the uncertainties associated with the many parameters presented in this study and quantitatively evaluates the errors that can rise from different sources and affect the measured variables. Several dimensional and dimensionless parameters have been presented in the previous chapters to characterize the heat transfer and fluid flow of the meso heat exchanger for the transient air heating and cooling as well as the thermal energy storage with PCM. Errors can be due to many different sources and can affect the measurement of the main values. They can also influence the dependent parameters impacting the final results. Uncertainty analysis can point out the major sources of uncertainty in parameters for further examination. The uncertainty in experimental work is comprised of bias and precision errors [1] where the total uncertainty is the squared root of the sum of the squared values. The uncertainties in the independent parameters such as the dimensions of the meso heat exchanger, fluids temperatures, and data acquisition system components will be introduced then the dependent parameters uncertainties.

A.1. Uncertainty Evaluation Methods

The uncertainty of some of the independent parameters such as temperature measuring devices represented by RTDs, PTDs, and data acquisition components are found through the specifications provided by the manufacturer. These specifications can include linearity, hysteresis, accuracy, etc. which combined form the bias errors. On the other hand, precision errors are found from the data collection through experimental runs. Therefore, the Root Sum Square RSS method is used to obtain the bias and precision uncertainty calculation and can be found as in equations A.1 and A.2.

$$B = \pm\sqrt{B_1^2 + B_2^2 + \cdots + B_k^2} \qquad (A.1)$$

$$P = \pm\sqrt{P_1^2 + P_2^2 + \cdots + P_k^2} \qquad (A.2)$$

The overall uncertainty in this study is evaluated as per [2] and [3]. The overall uncertainty is evaluated as,

$$U_X = \pm\sqrt{B^2 + P^2} \tag{A.3}$$

The fluids properties uncertainty is found using the maximum and minimum average fluid temperature. These properties can include density, thermal conductivity, specific heat, viscosity, etc. and their uncertainty can be calculated as,

$$U_{fluid\ property} = \frac{1}{2}\left|\left[fluid\ property\ at\ T_{avg.max}\right] - \left[fluid\ property\ at\ T_{avg.min}\right]\right| \tag{A.4}$$

The uncertainty in other parameters represented by Y in the following equations which are a function of independent parameters denoted by X such as heat transfer rate, Reynolds number, Nusselt number, etc. is found using RSS method. The dependent parameters uncertainty is represented through error propagation where Y is dependent on X1, X2, etc., the uncertainty in Y is found as,

$$Y = f(X_1, X_2, X_3, \dots \dots) \tag{A.5}$$

$$U_Y = \pm\sqrt{\left(\frac{\partial Y}{\partial X_1}U_{X_1}\right)^2 + \left(\frac{\partial Y}{\partial X_2}U_{X_2}\right)^2 + \left(\frac{\partial Y}{\partial X_k}U_{X_k}\right)^2} \quad \text{(Absolute)} \tag{A.6}$$

$$\frac{U_Y}{\bar{Y}} = \pm\sqrt{\frac{\left(\frac{\partial Y}{\partial X_1}U_{X_1}\right)^2 + \left(\frac{\partial Y}{\partial X_2}U_{X_2}\right)^2 + \cdots}{[Y=f(X_1,X_2,\dots,X_k)]^2}} \quad \text{(Relative)} \tag{A.7}$$

Where, the uncertainty of the X1, X2, etc. are found using equations (A.1 – A.3).

A.2. Uncertainty in the Heat Exchanger Independent Dimensions

The heat exchanger measurements and their uncertainties are obtained using a digital caliper or supplied by the manufacturer. The digital caliper provides two sorts of errors, bias and precision. Bias errors are comprised of accuracy and resolution errors which can be found using the following expressions while precision errors are found through several measurements and taking their mean value assuming 95% confidence level with a student t distribution of 1.96 rounded to 2.

$$B_{accuracy} = \pm 2.54 \times 10^{-5} m \tag{A.8}$$

$$B_{resolution} = \frac{1}{2} B_{accuracy} = \pm 1.27 \times 10^{-5} m \tag{A.9}$$

$$B_{digital\ caliper} = \pm \sqrt{B^2{}_{accuracy} + B^2{}_{resolution}} = \pm 2.84 \times 10^{-5} m \tag{A.10}$$

$$U_X = \sqrt{B^2{}_{caliper} + P^2{}_X} \tag{A.11}$$

The main basic heat exchanger dimensions such as slab width, number of fins for each slab, fin length, channel diameter, fin height, and spacing. are measured. On the other hand, the channel diameter was not measure but its information and uncertainty are provided by the manufacturer. Additional basic dimensions include the and the channel diameter. The calculation of these measured dimensions is used in finding the dependent areas, volumes and other lengths associated to the heat exchanger. The precision error for any of the basic dimensions can be expressed as,

$$P_X = \pm t_{N,95\%} S_X \approx \pm 2 \frac{S_X}{\sqrt{N}} \quad [\, N \geq 20 \,] \tag{A.12}$$

Where X is any of the above-mentioned heat exchanger dimensions. This makes the overall uncertainty of each dimension to be written as shown in equation (A.11). An example can be shown as follows for finding the uncertainty of the slab width.

$$P_{W_{slab}} = \pm t_{N,95\%} S_{W_{slab}} \approx \pm 2 \frac{S_{W_{slab}}}{\sqrt{N}} \tag{A.13}$$

Therefore, the total uncertainty of the slab width can be found using the expression in (A.11) as,

$$U_{W_{slab}} = \sqrt{B^2{}_{caliper} + P^2{}_{W_{slab}}} \tag{A.14}$$

A.3. Uncertainty in Fins and Slab Areas

The measurements taken from the heat exchanger are used to calculate different heat exchanger parameters which can be found in the following equations.

The fin surface area and its uncertainty can be calculated using the following relationship,

$$A_{fin,HT} = 2H_{fin}\left(L_{fin} + t_{fin}\right) \tag{A.15}$$

$$U_{A_{fin,HT}} = \pm\sqrt{\left(\frac{\partial A_{fin,HT}}{\partial H_{fin}} U_{H_{fin}}\right)^2 + \left(\frac{\partial A_{fin,HT}}{\partial L_{fin}} U_{L_{fin}}\right)^2 + \left(\frac{\partial A_{fin,HT}}{\partial t_{fin}} U_{t_{fin}}\right)^2} \tag{A.16}$$

Where,

$$\frac{\partial A_{fin,HT}}{\partial H_{Fin}} = 2\left(L_{fin} + t_{fin}\right) \tag{A.17}$$

$$\frac{\partial A_{fin,HT}}{\partial L_{Fin}} = 2H_{fin} \tag{A.18}$$

$$\frac{\partial A_{fin,HT}}{\partial t_{Fin}} = 2H_{fin} \tag{A.19}$$

The fins total number comes from the number of fins per slab and the number of fin array in the heat exchanger as,

$$N_{fin,HX} = N_{fin\ array,HX}\ N_{fin,slab} \tag{A.20}$$

Its uncertainty is expressed as,

$$U_{N_{fin,HX}} = \pm\sqrt{\left(\frac{\partial N_{fin,HX}}{\partial N_{fin\ array,HX}} U_{N_{fin\ array,HX}}\right)^2 + \left(\frac{\partial N_{fin,HX}}{\partial N_{fin,slab}} U_{N_{fin,slab}}\right)^2} \tag{A.21}$$

Where,

$$\frac{\partial N_{fin,HX}}{\partial N_{fin\ array,HX}} = N_{fin,slab} \tag{A.22}$$

$$\frac{\partial N_{fin,HX}}{\partial N_{fin,slab}} = N_{fin\ array,HX} \tag{A.23}$$

Once the uncertainty in the heat transfer area of one fin as well as the uncertainty of the number of fins in the heat exchanger are calculated, the uncertainty of the heat transfer surface area of all the fins in the heat exchanger can be found as,

$$A_{fin,HT,HX} = N_{fin,HX}\ A_{fin,HT} \tag{A.24}$$

$$U_{A_{fin,HT,HX}} = \pm\sqrt{\left(\frac{\partial A_{fin,HT,HX}}{\partial N_{fin,HX}} U_{N_{fin,HX}}\right)^2 + \left(\frac{\partial A_{fin,HT,HX}}{\partial A_{fin,HT}} U_{A_{fin,HT}}\right)^2} \tag{A.25}$$

Where,

$$\frac{\partial A_{fin,HT,HX}}{\partial N_{Fin,HX}} = A_{fin,HT} \tag{A.26}$$

$$\frac{\partial A_{fin,HT,HX}}{\partial A_{fin,HT}} = N_{fin,HX} \tag{A.27}$$

While the fin frontal area equation and its related uncertainty are,

$$A_{fin,frontal} = H_{fin} \, t_{fin} \tag{A.28}$$

$$U_{A_{fin,frontal}} = \pm \sqrt{\left(\frac{\partial A_{fin,frontal}}{\partial H_{fin}} U_{H_{fin}}\right)^2 + \left(\frac{\partial A_{fin,frontal}}{\partial t_{fin}} U_{t_{fin}}\right)^2} \tag{A.29}$$

Where,

$$\frac{\partial A_{fin,frontal}}{\partial H_{fin}} = t_{fin} \tag{A.30}$$

$$\frac{\partial A_{fin,frontal}}{\partial t_{fin}} = H_{fin} \tag{A.31}$$

The total number of fins frontal area and their uncertainty can be found as,

$$A_{fin,frontal,HX} = N_{fin,HX} \, A_{fin,frontal} \tag{A.32}$$

$$U_{A_{fin,frontal,HX}} = \pm \sqrt{\left(\frac{\partial A_{fin,frontal,HX}}{\partial N_{fin,HX}} U_{N_{fin,HX}}\right)^2 + \left(\frac{\partial A_{fin,frontal,HX}}{\partial A_{fin,frontal}} U_{A_{fin,frontal}}\right)^2} \tag{A.33}$$

Where,

$$\frac{\partial A_{fin,frontal,HX}}{\partial N_{fin,HX}} = A_{fin,frontal} \tag{A.34}$$

$$\frac{\partial A_{fin,frontal,HX}}{\partial A_{fin,frontal}} = N_{fin,HX} \tag{A.35}$$

The slab frontal area with its uncertainty can be determined as,

$$A_{slab,frontal} = L_{slab,HT} \, H_{slab} \tag{A.36}$$

$$U_{A_{slab,frontal}} = \pm \sqrt{\left(\frac{\partial A_{slab,frontal}}{\partial L_{slab,HT}} U_{L_{slab,HT}}\right)^2 + \left(\frac{\partial A_{slab,frontal}}{\partial H_{slab}} U_{H_{slab}}\right)^2} \tag{A.37}$$

Where,

$$\frac{\partial A_{slab,frontal}}{\partial L_{slab,HT}} = H_{slab} \tag{A.38}$$

$$\frac{\partial A_{slab,frontal}}{\partial H_{slab}} = L_{slab,HT} \tag{A.39}$$

The heat transfer frontal area of all the slabs in the heat exchanger and its uncertainty can be shown as,

$$A_{slab,frontal,HX} = N_{slab,HT,HX}\, A_{slab,frontal} \tag{A.40}$$

$$U_{A_{slab,frontal,HX}} = \pm \sqrt{\left(\frac{\partial A_{slab,frontal,HX}}{\partial N_{slab,HT,HX}} U_{N_{slab,HT,HX}}\right)^2 + \left(\frac{\partial A_{slab,frontal,HX}}{\partial A_{slab,frontal}} U_{A_{slab,frontal}}\right)^2} \tag{A.41}$$

Where,

$$\frac{\partial A_{slab,frontal,HX}}{\partial N_{slab,HT,HX}} = A_{slab,frontal} \tag{A.42}$$

$$\frac{\partial A_{slab,frontal,HX}}{\partial A_{slab,frontal}} = N_{slab,HT,HX} \tag{A.43}$$

The sum of the areas of fins and slabs of the heat exchanger using equations A.32 and A.40 will provide the blocked area of the airflow as,

$$A_{frontal,blocked} = A_{fin,frontal,HX} + A_{slab,frontal,HX} \tag{A.44}$$

The uncertainty in the blocked frontal area is,

$$U_{A_{frontal,blocked}} = \pm \sqrt{\left(\frac{\partial A_{frontal,blocked}}{\partial A_{fin,frontal,HX}} U_{A_{fin,frontal,HX}}\right)^2 + \left(\frac{\partial A_{frontal,blocked}}{\partial A_{slab,frontal,HX}} U_{A_{slab,frontal,HX}}\right)^2} \tag{A.45}$$

Where,

$$\frac{\partial A_{frontal,blocked}}{\partial A_{fin,frontal,HX}} = 1 \tag{A.46}$$

$$\frac{\partial A_{frontal,blocked}}{\partial A_{slab,frontal,HX}} = 1 \tag{A.47}$$

The total area of one slab where there are no fins as well as its uncertainty is expressed as,

$$A_{slab,no\,fins} = 2W_{slab}\left(L_{slab,HT} - N_{fin,slab}t_{fin}\right) \tag{A.48}$$

$$U_{A_{slab,no\,fins}} = \pm \sqrt{\begin{array}{l}\left(\frac{\partial A_{slab,no\,fins}}{\partial W_{slab}} U_{W_{slab}}\right)^2 + \left(\frac{\partial A_{slab,no\,fins}}{\partial L_{slab,HT}} U_{L_{slab,HT}}\right)^2 + \\ \left(\frac{\partial A_{slab,no\,fins}}{\partial N_{fin,slab}} U_{N_{fin,slab}}\right)^2 + \left(\frac{\partial A_{slab,no\,fins}}{\partial t_{fin}} U_{t_{fin}}\right)^2\end{array}} \qquad (A.49)$$

Where,

$$\frac{\partial A_{slab,no\,fins}}{\partial W_{slab}} = 2\left(L_{slab,HT} - N_{fin,slab}t_{fin}\right) \qquad (A.50)$$

$$\frac{\partial A_{slab,no\,fins}}{\partial L_{slab,HT}} = 2W_{slab} \qquad (A.51)$$

$$\frac{\partial A_{slab,no\,fins}}{\partial N_{fin,slab}} = -2W_{slab}t_{fin} \qquad (A.52)$$

$$\frac{\partial A_{slab,no\,fins}}{\partial t_{fin}} = -2W_{slab}N_{fin,slab} \qquad (A.53)$$

The area of all the slabs where no fins are present and their uncertainty can be found as,

$$A_{slab,no\,fins,HX} = N_{slab,HT,HX}\, A_{slab,no\,fins} \qquad (A.54)$$

$$U_{A_{slab,no\,fins,HX}} = \pm \sqrt{\left(\frac{\partial A_{slab,no\,fins,HX}}{\partial N_{slab,HT,HX}} U_{N_{slab,HT,HX}}\right)^2 + \left(\frac{\partial A_{slab,no\,fins,HX}}{\partial A_{slab,no\,fins}} U_{A_{slab,no\,fins}}\right)^2} \qquad (A.55)$$

Where,

$$\frac{\partial A_{slab,no\,fins,HX}}{\partial N_{slab,HT,HX}} = A_{slab,no\,fins} \qquad (A.56)$$

$$\frac{\partial A_{slab,no\,fins,HX}}{\partial A_{slab,no\,fins}} = N_{slab,HT,HX} \qquad (A.57)$$

A.4. Uncertainty in the Heat Exchanger Areas

The frontal area of the heat exchanger is comprised of the length and height of the heat exchanger in the test section and can be calculated with its uncertainty as,

$$A_{HX,frontal} = L_{HX}\, H_{HX} \qquad (A.58)$$

$$U_{A_{HX,frontal}} = \pm \sqrt{\left(\frac{\partial A_{HX,frontal}}{\partial L_{HX}} U_{L_{HX}}\right)^2 + \left(\frac{\partial A_{HX,frontal}}{\partial H_{HX}} U_{H_{HX}}\right)^2} \qquad (A.59)$$

Where,

$$\frac{\partial A_{HX,frontal}}{\partial L_{HX}} = H_{HX} \qquad (A.60)$$

$$\frac{\partial A_{HX,frontal}}{\partial H_{HX}} = L_{HX} \qquad (A.61)$$

The minimum free flow area is found from the frontal blocked area of the heat exchanger subtracted from the frontal area of the heat exchanger. Its expression as well as uncertainty can be shown as,

$$A_{a,min} = A_{HX,frontal} - A_{frontal,blocked} \qquad (A.62)$$

$$U_{A_{a,min}} = \pm \sqrt{\left(\frac{\partial A_{a,min}}{\partial A_{HX,frontal}} U_{A_{HX,frontal}}\right)^2 + \left(\frac{\partial A_{a,min}}{\partial A_{frontal,blocked}} U_{A_{frontal,blocked}}\right)^2} \qquad (A.63)$$

Where,

$$\frac{\partial A_{a,min}}{\partial A_{HX,frontal}} = 1 \qquad (A.64)$$

$$\frac{\partial A_{a,min}}{\partial A_{frontal,blocked}} = -1 \qquad (A.65)$$

The total heat transfer surface area which includes all the fins and slabs as well as its uncertainty is expressed as,

$$A_{a,HT,HX} = A_{fin,HT,HX} + A_{slab,no\,fins,HX} \qquad (A.66)$$

$$U_{A_{a,HT,HX}} = \pm \sqrt{\left(\frac{\partial A_{a,HT,HX}}{\partial A_{fin,HT,HX}} U_{A_{fin,HT,HX}}\right)^2 + \left(\frac{\partial A_{a,HT,HX}}{\partial A_{slab,no\,fins,HX}} U_{A_{slab,no\,fins,HX}}\right)^2} \qquad (A.67)$$

Where,

$$\frac{\partial A_{a,HT,HX}}{\partial A_{fin,HT,HX}} = 1 \qquad (A.68)$$

$$\frac{\partial A_{a,HT,HX}}{\partial A_{slab,no\,fins,HX}} = 1 \qquad (A.69)$$

The airside minimum free flow area and the total heat transfer surface area are used to determine the airside hydraulic diameter as,

$$D_{a,hyd,HX} = 4W_{slab}\left(\frac{A_{a,min}}{A_{a,HT,HX}}\right) \qquad (A.70)$$

The uncertainty in airside hydraulic diameter can be found as,

$$U_{D_{a,hyd,HX}} = \pm \sqrt{\left(\frac{\partial D_{a,hyd,HX}}{\partial W_{slab}} U_{W_{slab}}\right)^2 + \left(\frac{\partial D_{a,hyd,HX}}{\partial A_{a,min}} U_{A_{a,min}}\right)^2 + \left(\frac{\partial D_{a,hyd,HX}}{\partial A_{a,HT,HX}} U_{A_{a,HT,HX}}\right)^2} \quad \text{(A.71)}$$

Where,

$$\frac{\partial D_{a,hyd,HX}}{\partial W_{slab}} = 4\left(\frac{A_{a,min}}{A_{a,HT,HX}}\right) \quad \text{(A.72)}$$

$$\frac{\partial D_{a,hyd,HX}}{\partial A_{a,min}} = 4\left(\frac{W_{slab}}{A_{a,HT,HX}}\right) \quad \text{(A.73)}$$

$$\frac{\partial D_{a,hyd,HX}}{\partial A_{a,HT,HX}} = -4W_{slab}\left(\frac{A_{a,min}}{A_{a,HT,HX}{}^2}\right) \quad \text{(A.74)}$$

A.5. Uncertainty in Data Acquisition Parts

The data acquisition system has many components such as a card, SCXI signal conditioner, and SCXI terminal block. The measurements recorded by the data acquisition system involve bias and precision errors. The following sections discusses the calculation of the uncertainties in these components.

A.5.1. Uncertainty of the Data Acquisition Card

The uncertainty in the data acquisition card is mainly to bias errors. These errors include relative accuracy, offset error, least significant bit, and differential nonlinearity. The RSS method is used to calculate the total uncertainty due to the bias errors taken from each source.

$$B_1 = Relative\ accuracy = \pm 1.5 LSB = 2.289 \times 10^{-6} V$$

$$B_2 = Offset\ error = 1.0 \times 10^{-6} V$$

$$B_3 = LSB = 1.523 \times 10^{-6} V$$

$$B_4 = Differential\ nonlinearity = 7.629 \times 10^{-7} V$$

Therefore, the total bias errors can be found as,

$$B_{DAQ,card} = \sqrt{B_1^2 + B_2^2 + B_3^2 + B_4^2} = 3.025 \times 10^{-6} V \quad \text{(A.75)}$$

A.5.2. Uncertainty of the Signal Conditioner

A signal conditioner works on proper conditioning of the signal to be interpreted by the data acquisition card. Any errors in the signal conditioner can result in errors of the

measurement data. The signal conditioner has two types of bias errors, an offset error and a differential nonlinearity error. Using the RSS method, the total bias errors by the signal conditioner can be calculated as,

$$B_1 = Offset\ error = 1.5 \times 10^{-6}V$$

$$B_2 = Differential\ nonlinearity = \pm 0.005\% FSR = 5 \times 10^{-6}V$$

$$B_{SCXI} = \sqrt{B_1^2 + B_2^2} = 5.22 \times 10^{-6}V \tag{A.76}$$

The terminal block is incorporated within the signal conditioner that considers with it the uncertainty of the terminal block since there is not enough information provided on its accuracy. The uncertainty of the DAQ system comprising the two above mentioned uncertainties can be shown as,

$$B_{DAQ} = \sqrt{B_{DAQ\ card}^2 + B_{SCXI}^2} = 6.03 \times 10^{-6}V \tag{A.77}$$

A.6. Uncertainty in Air Temperature Measurement

The air temperatures were measured using 2 grids of T-type thermocouples one at the inlet and the other at the outlet. The errors with airside temperature reading are due to the instrument errors which involves accuracy and resolution errors.

$$B_1 = Accuracy\ error = 0.5°C$$

$$B_2 = Resolution\ error = 0.1°C$$

The combined bias errors associated with the use of thermocouples are,

$$B_{thermocouple} = \sqrt{(0.1)^2 + (0.5)^2} = 0.509°C \tag{A.78}$$

The thermocouples are well calibrated at the inlet and outlet and there is no difference in calibration between them therefore, the bias error due to spatial variation is assumed to be zero. The precision error for the thermocouples is computed from the following considering a t-distribution of 1.962 according to the experimental runs.

$$U_{thermocouple} = \sqrt{B_{thermocouple}^2 + P_{thermocouple}^2} \tag{A.79}$$

$$U_{thermocouple} = \sqrt{(0.509)^2 + \left(1.962 \times \frac{S_X}{\sqrt{N}}\right)^2}\ (°C) \tag{A.80}$$

Since the thermocouples are connected to the DAQ system where the temperature reading is obtained, therefore, the total uncertainty of the air temperature can be expressed as,

$$U_T = \pm\sqrt{\left(U_{thermocouple}\right)^2 + \left(U_{DAQ}\right)^2} \qquad (A.81)$$

$$U_T = \sqrt{(0.509)^2 + \left(1.962 \times \frac{S_X}{\sqrt{N}}\right)^2 + \left(U_{DAQ}\right)^2 + \left(\frac{\partial T_a}{\partial_t} * U_t\right)^2} \; (°C) \qquad (A.82)$$

The uncertainty in the DAQ can be written in terms of temperature using the thermocouple sensitivity K as,

$$K_{thermocouple} = 43 \times 10^{-6} \; (V/°C)$$

$$U_{DAQ} = 6.03 \times 10^{-6}V = \frac{6.03 \times 10^{-6}V}{K_{thermocouple}}$$

$$U_{DAQ} = \frac{6.03 \times 10^{-6}V}{43 \times 10^{-6} \; (V/°C)} = 0.14°C \qquad (A.83)$$

The air bulk temperature depends on the inlet and outlet temperature readings and its uncertainty is found from the following equation,

$$T_{a,bulk} = \frac{T_{a,i} + T_{a,o}}{2} \qquad (A.84)$$

$$U_{T_{a,bulk}} = \pm\sqrt{\left(\frac{\partial T_{a,bulk}}{\partial T_{a,i}} U_{T_{a,i}}\right)^2 + \left(\frac{\partial T_{a,bulk}}{\partial T_{a,o}} U_{T_{a,o}}\right)^2} \qquad (A.85)$$

Where,

$$\frac{\partial T_{a,bulk}}{\partial T_{a,i}} = \frac{1}{2} \qquad (A.86)$$

$$\frac{\partial T_{a,bulk}}{\partial T_{a,o}} = \frac{1}{2} \qquad (A.87)$$

The uncertainty in the airside temperature difference is found using partial derivation and an example of that is the case of air heating as follows,

$$U_{\Delta T_a} = T_{a,o} - T_{a,i} \qquad (A.88)$$

$$U_{\Delta T_a} = \pm\sqrt{\left(\frac{\partial \Delta T_a}{\partial T_{a,o}} U_{T_{a,o}}\right)^2 + \left(\frac{\partial \Delta T_a}{\partial T_{a,i}} U_{T_{a,i}}\right)^2} \qquad (A.89)$$

Where,

$$\frac{\partial \Delta T_a}{\partial T_{a,o}} = 1 \qquad (A.90)$$

$$\frac{\partial \Delta T_a}{\partial T_{a,i}} = -1 \qquad (A.91)$$

A.7. Uncertainty in Liquid Temperatures

The liquid used in the experiments is either DI water or 50/50 ethylene glycol-water and was measure using inlet and outlet RTDs. The uncertainty in the liquid inlet and outlet temperatures is due to the uncertainty in the RTD measurement and the DAQ system. The relation showing the combined uncertainty is shown as,

$$U_{T_l} = \pm\sqrt{U_{RTD}^2 + U_{DAQ}^2 + (\frac{\partial T_l}{\partial_t} * U_t)^2} \qquad (A.92)$$

The liquid side temperatures were measured using RTDs which have bias and precision errors associated with them as illustrated below,

$$U_{RTD} = \sqrt{B_{RTD}^2 + P_{measurement}^2} \qquad (A.93)$$

The manufacturer has supplied the bias error in the RTD readings as,

$$B_{RTD} = \pm\frac{1}{10}(0.3 + 0.005|T(°C)|) \qquad (A.94)$$

While, the precision error is determined from the following,

$$P_{RTD} = \pm t_{N,95\%}S_{\bar{T}} \approx \pm 1.962 \times \frac{S_{T,RTD}}{\sqrt{N}} \qquad (A.95)$$

When it comes to the DAQ system uncertainty, the sensitivity of the RTD is used to interpret the voltage reading to °C. The RTD sensitivity is shown as,

$$K = \frac{\partial V_{RTD}}{\partial T} \qquad (A.96)$$

Where,

$V_{RTD} = I_{Excitation}R_T$

R_T is the temperature resistance relationship, $R_T = R_O(1 + AT + BT^2)$

R_o=100Ω, A=3.9080 X 10^{-3}, B=-5.8019 X 10^{-7}, $I_{Excitation}$= 100 X 10^{-6} A

Therefore,

$$K = 3.9080 \times 10^{-5} - 1.1604 \times 10^{-8}T \qquad (A.97)$$

From the above relations, the uncertainty in the DAQ system will be as follows,

$$U_{DAQ} = \pm 6.033 \times 10^{-6}V = \pm\frac{6.033 \times 10^{-6}V}{K_{RTD}}$$

$$= \pm\frac{6.033\times10^{-6}V}{3.9080\times10^{-5}-1.1604\times10^{-8}T} \; °C \qquad (A.98)$$

The liquid side bulk temperature using inlet and outlet temperatures is defined as,

$$T_{l,bulk} = \frac{T_{l,i} + T_{l,o}}{2} \tag{A.99}$$

Using the RSS method, the uncertainty in the liquid bulk temperature can be found as,

$$U_{T_{l,bulk}} = \pm \sqrt{\left(\frac{\partial T_{l,bulk}}{\partial T_{l,i}} U_{T_{a,i}}\right)^2 + \left(\frac{\partial T_{l,bulk}}{\partial T_{l,o}} U_{T_{a,o}}\right)^2} \tag{A.100}$$

Where,

$$\frac{\partial T_{l,bulk}}{\partial T_{l,i}} = \frac{1}{2} \tag{A.101}$$

$$\frac{\partial T_{l,bulk}}{\partial T_{l,o}} = \frac{1}{2} \tag{A.102}$$

The uncertainty in the liquid temperature difference is found using partial derivation for example in the case of air heating, it can be found as,

$$U_{\Delta T_l} = T_{l,o} - T_{l,i} \tag{A.103}$$

$$U_{\Delta T_l} = \pm \sqrt{\left(\frac{\partial \Delta T_l}{\partial T_{l,o}} U_{T_{l,o}}\right)^2 + \left(\frac{\partial \Delta T_l}{\partial T_{l,i}} U_{T_{l,i}}\right)^2} \tag{A.104}$$

Where,

$$\frac{\partial \Delta T_l}{\partial T_{l,o}} = 1 \tag{A.105}$$

$$\frac{\partial \Delta T_l}{\partial T_{l,i}} = -1 \tag{A.106}$$

A.8. Uncertainty in Air Pressure

Differential pressure transducers were used to measure the airside pressures. These transducers have bias errors associated with them which are given through the manufacturer. These bias errors include thermal effects which is 0.02%FS and accuracy which is 1%FS. Using the RSS method, the bias errors combined for the Pitot static tube can be found as,

$$B_{Pitot} = \pm \sqrt{B_{accuracy}^2 + B_{thermal\ effects}^2} \tag{A.107}$$

$$B_{Pitot} = \pm \sqrt{(0.01FS)^2 + (0.0002|T|FS)^2} \quad V \tag{A.108}$$

The Pitot pressure transducer measurement range is (0-1" H$_2$O). The airside bias errors in pressure difference across the heat exchanger is presented in a similar way to the bias errors in Pitot tube calculation with a range set to (0-1" H$_2$O).

$$B_{a,\Delta P} = \pm\sqrt{B_{accuracy}^2 + B_{thermal\ effects}^2} \qquad (A.109)$$

$$B_{Pitot} = \pm\sqrt{(0.01FS)^2 + (0.0002|T|FS)^2}\ \ V \qquad (A.110)$$

While the precision error in Pitot and the pressure difference across the heat exchanger is presented through the use of standard deviation, the total number of samples, and the student t-distribution as,

$$P_{Pitot} = \pm t_{N,95\%}S_{\bar{P}} \approx \pm 1.962 \times \frac{S_{Pitot}}{\sqrt{N}} \qquad (A.111)$$

$$P_{a,\Delta P} = \pm t_{N,95\%}S_{\bar{P}} \approx \pm 1.962 \times \frac{S_{a,\Delta P}}{\sqrt{N}} \qquad (A.112)$$

The total uncertainty in the airside pressures in Pitot and across the heat exchanger alone can be found using the defined bias and precision and applying the RSS method as,

$$U_{Pitot} = \sqrt{B_{Pitot}^2 + P_{Pitot}^2} \qquad (A.113)$$

$$U_{a,\Delta P} = \sqrt{B_{a,\Delta P}^2 + P_{a,\Delta P}^2} \qquad (A.114)$$

Including the DAQ system uncertainty, the overall uncertainty in the dynamic pressure and the differential pressure can be written as,

$$U_{dynamic\ pressure} = \sqrt{U_{Pitot}^2 + U_{DAQ}^2}\ \ V \qquad (A.115)$$

$$U_{diff.\ pressure} = \sqrt{U_{a,\Delta P}^2 + U_{DAQ}^2}\ \ V \qquad (A.116)$$

To convert the uncertainty of the dynamic and differential pressure from voltage to Pascal, the sensitivity of the devices is used as,

$$U_{dynamic\ pressure,(Pa)} = \pm K_{Pitot}U_{dynamic\ pressure,(V)} \qquad (A.117)$$

$$U_{diff.\ pressure,(Pa)} = \pm K_{a,\Delta P}U_{diff.\ pressure,(V)} \qquad (A.118)$$

Where, K$_{Pitot}$ = 24.49 Pa/V and K$_{a,\Delta P}$ = 125.5 Pa/V

A.9. Uncertainty in Liquid Flow Rate

The liquid mass flow rate, whether DI water or 50/50 ethylene glycol-water mixture, was measured using a Proline Promass inline Coriolis mass flow meter of the 100 series. This meter has an accuracy of ±0.1% of the measurement as per the manufacturer.

A.10. Uncertainty in the Thermal Properties

The fluid bulk temperature is used to find the fluid properties such as viscosity, specific heat, density, and thermal conductivity. The uncertainty in the viscosity of the liquid and air can be found as,

$$U_{\mu_l} = \frac{1}{2} \left| \left(\mu_l \text{ at } T_{l,b,max} \right) - \left(\mu_l \text{ at } T_{l,b,min} \right) \right| \tag{A.119}$$

$$U_{\mu_a} = \frac{1}{2} \left| \left(\mu_l \text{ at } T_{a,b,max} \right) - \left(\mu_a \text{ at } T_{a,b,min} \right) \right| \tag{A.120}$$

The uncertainty for both working fluids' density is assessed as,

$$U_{\rho_l} = \frac{1}{2} \left| \left(\rho_l \text{ at } T_{l,b,max} \right) - \left(\rho_l \text{ at } T_{l,b,min} \right) \right| \tag{A.121}$$

$$U_{\rho_a} = \frac{1}{2} \left| \left(\rho_a \text{ at } T_{a,b,max} \right) - \left(\rho_a \text{ at } T_{a,b,min} \right) \right| \tag{A.122}$$

The specific heat uncertainty of both working fluids can be written as,

$$U_{cp,l} = \frac{1}{2} \left| \left(cp_l \text{ at } T_{l,b,max} \right) - \left(cp_l \text{ at } T_{l,b,min} \right) \right| \tag{A.123}$$

$$U_{cp,a} = \frac{1}{2} \left| \left(cp_a \text{ at } T_{a,b,max} \right) - \left(cp_a \text{ at } T_{a,b,min} \right) \right| \tag{A.124}$$

The uncertainty in the thermal conductivity of both working fluids can be found from the following equations,

$$U_{k,l} = \frac{1}{2} \left| \left(k_l \text{ at } T_{l,b,max} \right) - \left(k_l \text{ at } T_{l,b,min} \right) \right| \tag{A.125}$$

$$U_{k,a} = \frac{1}{2} \left| \left(k_a \text{ at } T_{a,b,max} \right) - \left(k_a \text{ at } T_{a,b,min} \right) \right| \tag{A.126}$$

Prandtl number is a dimensionless number that can be found in the tables of fluid properties however, its uncertainty can be found using the RSS method as,

$$Pr_a = \frac{\mu_a cp_a}{k_a} \tag{A.127}$$

$$U_{Pr_a} = \pm \sqrt{ \left(\frac{\partial Pr_a}{\partial \mu_a} U_{\mu_a} \right)^2 + \left(\frac{\partial Pr_a}{\partial cp_a} U_{cp_a} \right)^2 + \left(\frac{\partial Pr_a}{\partial k_a} U_{k_a} \right)^2 } \tag{A.128}$$

Where,

$$\frac{\partial Pr_a}{\partial \mu_a} = \frac{cp_a}{k_a} \tag{A.129}$$

$$\frac{\partial Pr_a}{\partial cp_a} = \frac{\mu_a}{k_a} \tag{A.130}$$

$$\frac{\partial Pr_a}{\partial k_a} = -\frac{\mu_a cp_a}{k^2{}_a} \tag{A.131}$$

A.11. Air Mass Flow Rate Uncertainty

The air mass flow rate in the heat exchanger depends on density, velocity, and minimum free flow area. The equation to find air mass flow rate can be written as,

$$\dot{m}_a = \rho_a V_a A_{a,frontal} \tag{A.132}$$

In order to determine the air mass flow rate uncertainty, the air velocity uncertainty needs to be known. The following equations illustrate how to find the uncertainty in air velocity.

$$V_a = \pm \sqrt{\frac{2\Delta P}{\rho_a}} \tag{A.133}$$

$$U_{V_a} = \pm \sqrt{\left(\frac{\partial V_a}{\partial \Delta P_{dynamic}} U_{\Delta P_{dynamic}}\right)^2 + \left(\frac{\partial V_a}{\partial \rho_a} U_{\rho_a}\right)^2} \tag{A.134}$$

Where,

$$\frac{\partial V_a}{\partial \Delta P_{dynamic}} = \frac{1}{\sqrt{2\rho_a \Delta P_{dynamic}}} \tag{A.135}$$

$$\frac{\partial V_a}{\partial \rho_a} = -\frac{1}{2} \frac{\sqrt{2\Delta P_{dynamic}}}{(\rho_a)^{3/2}} \tag{A.136}$$

Therefore, the uncertainty in air mass flow rate can be determined from the following equation,

$$U_{\dot{m}_a} = \pm \sqrt{\left(\frac{\partial \dot{m}_a}{\partial \rho_a} U_{\rho_a}\right)^2 + \left(\frac{\partial \dot{m}_a}{\partial V_a} U_{V_a}\right)^2 + \left(\frac{\partial \dot{m}_a}{\partial A_{a,frontal}} U_{A_{a,frontal}}\right)^2} \tag{A.137}$$

Where,

$$\frac{\partial \dot{m}_a}{\partial \rho_a} = V_a A_{a,frontal} \tag{A.138}$$

$$\frac{\partial \dot{m}_a}{\partial V_a} = \rho_a A_{a,frontal} \tag{A.139}$$

$$\frac{\partial \dot{m}_a}{\partial A_{a,frontal}} = \rho_a V_a \tag{A.140}$$

A.12. Heat Transfer Rate Uncertainty

The uncertainty in the liquid heat transfer rate is found from the following expression,

$$\dot{Q}_l = \dot{m}_l c_{p,l} \Delta T_l \qquad (A.141)$$

$$U_{\dot{Q}_l} = \pm \sqrt{\left(\frac{\partial \dot{Q}_l}{\partial \dot{m}_l} U_{\dot{m}_l}\right)^2 + \left(\frac{\partial \dot{Q}_l}{\partial c_{p,l}} U_{c_{p,l}}\right)^2 + \left(\frac{\partial \dot{Q}_l}{\partial \Delta T_l} U_{\Delta T_l}\right)^2} \qquad (A.142)$$

Where,

$$\frac{\partial \dot{Q}_l}{\partial \dot{m}_l} = c_{p,l} \Delta T_l \qquad (A.143)$$

$$\frac{\partial \dot{Q}_l}{\partial c_{p,l}} = \dot{m}_l \Delta T_l \qquad (A.144)$$

$$\frac{\partial \dot{Q}_l}{\partial \Delta T_l} = \dot{m}_l c_{p,l} \qquad (A.145)$$

The air heat transfer rate depends on the liquid heat transfer rate and the heat transfer through the heat exchanger walls. The following equations present the uncertainty calculation for the heat transfer rate of the airside.

$$\dot{Q}_a = \dot{Q}_l + \dot{Q}_{wall} \qquad (A.146)$$

$$\dot{Q}_a = \dot{Q}_l + MC \frac{dT_s}{dt} \qquad (A.147)$$

$$U\dot{Q}_a = \pm \sqrt{\left(\frac{\partial \dot{Q}_a}{\partial \dot{Q}_l} \times U\dot{Q}_l\right)^2 + \left(\frac{\partial \dot{Q}_a}{\partial \dot{Q}_{wall}} \times U\dot{Q}_{wall}\right)^2} \qquad (A.148)$$

Where,

$$\frac{\partial \dot{Q}_a}{\partial \dot{Q}_l} = 1 \qquad (A.149)$$

$$\frac{\partial \dot{Q}_a}{\partial \dot{Q}_{wall}} = 1 \qquad (A.150)$$

It is worth noted that the uncertainty in the heat transfer rate of heat exchanger wall yields a very small value, therefore, the uncertainty in the air heat transfer rate can be taken as the uncertainty in the water heat transfer rate.

A.13. Reynolds Number Uncertainty

The airside Reynolds number is determined using the mass velocity and the airside hydraulic diameter.

$$Re_a = \frac{G_a D_{a,hyd}}{\mu_a} \tag{A.151}$$

The uncertainty in air mass velocity is found from the following equation,

$$G_a = \frac{\dot{m}_a}{A_{a,min}} \tag{A.152}$$

$$U_{G_a} = \pm \sqrt{\left(\frac{\partial G_a}{\partial \dot{m}_a} U_{\dot{m}_a}\right)^2 + \left(\frac{\partial G_a}{\partial A_{a,min}} U_{A_{a,min}}\right)^2} \tag{A.153}$$

Where,

$$\frac{\partial G_a}{\partial \dot{m}_a} = \frac{1}{A_{a,min}} \tag{A.154}$$

$$\frac{\partial G_a}{\partial A_{a,min}} U_{A_{a,min}} = -\frac{\dot{m}_a}{\left(A_{a,min}\right)^2} \tag{A.155}$$

The uncertainty in Reynolds number can be calculated as,

$$U_{Re_a} = \pm \sqrt{\left(\frac{\partial Re_a}{\partial G_a} U_{G_a}\right)^2 + \left(\frac{\partial Re_a}{\partial D_{a,hyd}} U_{D_{a,hyd}}\right)^2 + \left(\frac{\partial Re_a}{\partial \mu_a} U_{\mu_a}\right)^2} \tag{A.156}$$

Where,

$$\frac{\partial Re_a}{\partial G_a} = \frac{D_{a,hyd}}{\mu_a} \tag{A.157}$$

$$\frac{\partial Re_a}{\partial D_{a,hyd}} = \frac{G_a}{\mu_a} \tag{A.158}$$

$$\frac{\partial Re_a}{\partial \mu_a} = -\frac{G_a D_{a,hyd}}{(\mu_a)^2} \tag{A.159}$$

A.14. Uncertainty in Airside Heat Transfer Coefficient

The uncertainty in the airside heat transfer coefficient can be calculated from the following equations in which air heating is taken into consideration as an example,

$$h_a = \frac{\dot{Q}_a}{\eta_a A_a (T_{s,avg} - T_{a,avg})} \tag{A.160}$$

$$U_{h_a} = \pm \sqrt{\left(\frac{\partial h_a}{\partial \dot{Q}_a} U_{\dot{Q}_a}\right) + \left(\frac{\partial h_a}{\partial \eta_a} U_{\eta_a}\right)^2 + \left(\frac{\partial h_a}{\partial A_a} U_{A_a}\right)^2 + \left(\frac{\partial h_a}{\partial T_{s,avg}} U_{T_{s,avg}}\right)^2 + \left(\frac{\partial h_a}{\partial T_{a,avg}} U_{T_{a,avg}}\right)^2} \quad \text{(A.161)}$$

Where,

$$\frac{\partial h_a}{\partial \dot{Q}_a} = \frac{1}{\eta_a A_a (T_{s,avg} - T_{a,avg})} \quad \text{(A.162)}$$

$$\frac{\partial h_a}{\partial \eta_a} = -\frac{\dot{Q}_a}{\eta^2{}_a A_a (T_{s,avg} - T_{a,avg})} \quad \text{(A.163)}$$

$$\frac{\partial h_a}{\partial A_a} = -\frac{\dot{Q}_a}{\eta_a A^2{}_a (T_{s,avg} - T_{a,avg})} \quad \text{(A.164)}$$

$$\frac{\partial h_a}{\partial T_{s,avg}} = -\frac{\dot{Q}_a}{\eta_a A_a (T_{s,avg} - T_{a,avg})^2} \quad \text{(A.165)}$$

$$\frac{\partial h_a}{\partial T_{a,avg}} = \frac{\dot{Q}_a}{\eta_a A_a (T_{s,avg} - T_{a,avg})^2} \quad \text{(A.166)}$$

The uncertainty in the overall surface efficiency can be found from the following equations,

$$\eta_a = 1 - \frac{A_{fin}}{A_a}(1 - \eta_{fin}) \quad \text{(A.167)}$$

Where,

$$\frac{\partial \eta_a}{\partial A_{HT,Fin,HX}} = \frac{\eta_{Fin} - 1}{A_{HT,a,HX}} \quad \text{(A.168)}$$

$$\frac{\partial \eta_a}{\partial A_{HT,a,HX}} = \frac{A_{HT,Fin,HX}(1 - \eta_{Fin})}{(\eta_{Fin})^2} \quad \text{(A.169)}$$

$$\frac{\partial \eta_a}{\partial \eta_{Fin}} = \frac{A_{HT,Fin,HX}}{A_{HT,a,HX}} \quad \text{(A.170)}$$

The uncertainty in the fin efficiency can be found as,

$$\eta_{Fin} = \frac{\tanh(SL)}{SL} \quad \text{(A.171)}$$

$$U_{\eta_{Fin}} = \pm \sqrt{\left(\frac{\partial \eta_{Fin}}{\partial S} U_S\right)^2 + \left(\frac{\partial \eta_{Fin}}{\partial L} U_L\right)^2} \quad \text{(A.172)}$$

Where,

$$\frac{\partial \eta_{Fin}}{\partial S} = \frac{SL\,sech^2(SL) - \tanh(SL)}{S^2 L} \quad \text{(A.173)}$$

$$\frac{\partial \eta_{Fin}}{\partial L} = \frac{SL\,sech^2(SL) - \tanh(SL)}{L^2 S} \quad \text{(A.174)}$$

A.15. Uncertainty in Airside Nusselt Number

Airside Nusselt number is a dimensionless form of the heat transfer coefficient. The definition of airside Nusselt number and its uncertainty is determined as in the following,

$$Nu_a = \frac{h_a D_{a,hyd}}{k_a} \tag{A.175}$$

$$U_{Nu_a} = \pm \sqrt{\left(\frac{\partial Nu_a}{\partial h_a} U_{h_a}\right)^2 + \left(\frac{\partial Nu_a}{\partial D_{h,a}} U_{D_{a,hyd}}\right)^2 + \left(\frac{\partial Nu_a}{\partial k_a} U_{k_a}\right)^2} \tag{A.176}$$

Where,

$$\frac{\partial Nu_a}{\partial h_a} = \frac{D_{a,hyd}}{k_a} \tag{A.177}$$

$$\frac{\partial Nu_a}{\partial D_{h,a}} = \frac{h_a}{k_a} \tag{A.178}$$

$$\frac{\partial Nu_a}{\partial k_a} = -\frac{h_a D_{a,hyd}}{k^2{}_a} \tag{A.179}$$

A.16. Uncertainty in Colburn *j* Factor

The Colburn-j factor is a function of Stanton number and Prandtl number. In order to estimate the uncertainty in Colburn-j factor, the uncertainty in Stanton number is found first as in the following,

$$St_a = \frac{h_a}{G_a c_{p,a}} \tag{A.180}$$

$$U_{St_a} = \pm \sqrt{\left(\frac{\partial St_a}{\partial h_a} U_{h_a}\right)^2 + \left(\frac{\partial St_a}{\partial G_a} U_{G_a}\right)^2 + \left(\frac{\partial St_a}{\partial c_{p,a}} U_{c_{p,a}}\right)^2} \tag{A.181}$$

Where,

$$\frac{\partial St_a}{\partial h_a} = \frac{1}{G_a c_{p,a}} \tag{A.182}$$

$$\frac{\partial St_a}{\partial G_a} = -\frac{h_a}{G^2{}_a c_{p,a}} \tag{A.183}$$

$$\frac{\partial St_a}{\partial c_{p,a}} = -\frac{h_a}{G_a c_{p,a}{}^2} \tag{A.184}$$

Now, Colburn-j factor uncertainty is calculated as,

$$j_a = St_a Pr_a^{2/3} \tag{A.185}$$

$$U_{j_a} = \pm \sqrt{\left(\frac{\partial j_a}{\partial St_a} U_{St_a}\right)^2 + \left(\frac{\partial j_a}{\partial Pr_a} U_{Pr_a}\right)^2} \tag{A.186}$$

Where,

$$\frac{\partial j_a}{\partial St_a} = Pr_a^{\frac{2}{3}} \tag{A.187}$$

$$\frac{\partial j_a}{\partial Pr_a} = \frac{2}{3} St_a Pr_a^{-1/3} \tag{A.188}$$

The equations presented in this appendix relate to the main parameters discussed in this study. In some calculations, the air heating equations are considered as an example of the uncertainty calculation due to the presence of different modes such as heating and cooling. In general, the uncertainty is found higher for lower airside mass velocity. Table A.1 represents the main parameters for air heating experiments in their percentages of nominal values.

Table A.1. Air heating parameters uncertainty

Parameters	Uncertainty (%)
Air mass flow rate ($\dot{m}_a$) (kg/s)	2.8-1.4
$T_{a,i}$ (°C)	4
$T_{w,i}$ (°C)	0.24
Mass flow rate of water, ($\dot{m}_w$) (kg/s)	0.1
Heat transfer rate ($\dot{Q}_a$) (kW)	1.5-0.9
Heat Transfer coefficient (h_a) (kW/m².K)	2.8-2.9
Nusselt number (Nu_a)	3.2-3.4
Colburn factor (j_a)	4.2-3.6

Table A.2 represents the uncertainty in percentages of the main parameters nominal value for the case of air cooling with and without PCM.

Table A.2. Air cooling parameters uncertainty

Parameter	Uncertainty (%)
Air mass velocity G_a (kg/m^2.s)	3.2-2.1
Air inlet temperature $T_{a,i}$ (°C)	1.8
DI-water inlet temperature $T_{w,i}$ (°C)	3.0
DI-water mass flow rate ($\dot{m}_w$) (kg/s)	0.1
Airside heat transfer rate ($\dot{Q}_a$) (kW)	2.4-1.5
Airside heat Transfer coefficient (h_a) (kW/m^2.K)	5.5-5.6
Airside Nusselt number (Nu$_a$)	5.7-5.8
Air outlet temperature $T_{a,o}$ (°C)	4.0-2.4

REFERENCES

1. Figliola R.S., and Beasley D.E. (2011) "Theory and Design for Mechanical Measurements", 5th edition, John Wiley and Sons, Inc., New York, USA.

2. Editorial (1991). "Journal of Fluids Engineering: Policy on reporting uncertainties in experimental measurements and results." Transactions of the ASME, Journal of Fluids Engineering 113: 313-314.

3. Editorial (1993). "Journal of Heat Transfer: Policy on reporting uncertainties in experimental measurements and results." Transactions of the ASME, Journal of Heat Transfer 115: 5-6.

APPENDIX B: MAIN SYSTEM EQUIPMENT

The experimental work performed in this study comprises many system components that are used for controlling, heating, cooling, measuring, or monitoring certain parameters such as temperature, pressure, flow rate, etc. The following is pictures of some of these main components.

B.1. Inline Immersion Heater

This 20kW heater is used to heat the main DI water for the air heating experiments. The heated DI water is allowed to pass to the test section where the meso heat exchanger is located. It is provided with a temperature control panel to achieve the desired final DI water temperature Figure B.1.

(a)   (b)

Figure B. 1. (a) Heater and (b) Heater controller

B.2. Gear pump

The main liquid whether DI water or 50/50 ethylene glycol-water mixture flows through the connected pipes from a heater or a chiller to the test section heat exchanger by means of a gear pump. This pump is supplied with a variable frequency controller that allows to preset and control the liquid flow rate via a frequency change Figure B.2.
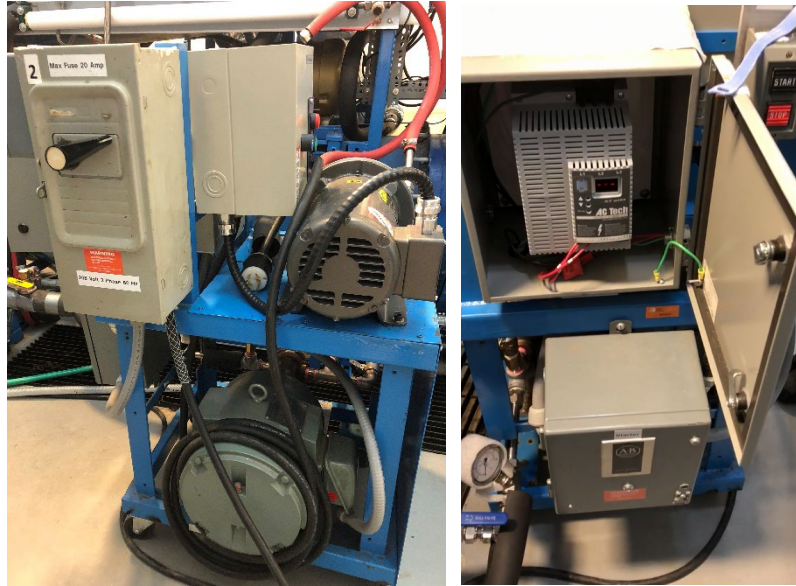
Figure B. 2. Gear pump

B.3. Chiller

A 10-ton chiller is used in the main liquid circuit for air cooling experiments Figure B.3. The main purpose is to provide a low temperature liquid to cool the airflow and solidify the PCM. It is equipped with built-in controller that allows to set the desired liquid temperature.

Figure B. 3. Chiller

B.4. Blower

A blower provided at the inlet section of the wind tunnel is used to force the air flow through the thermally insulated tunnel to the test section. The blower is operated by an electrically powered hydraulic pump. A frequency controller provides a wide range of air velocities that can be achieved. The flexibility in changing from one velocity to another allows to perform air mass velocity step changes required for the transient experiments. Figure B.4 shows the blower with its pump located at the middle lower section of the wind tunnel.

Figure B.4. Air blower and controller

B.5. Instrument Calibration

The test facility is equipped with many measuring instruments that are selected to be compatible with the DAQ system. The experiments involved many thermocouples and RTDs to measure the liquid and air temperature at the inlet and outlet of the test section, the surface temperature of the meso heat exchanger, and the PCM temperature. These thermocouples and RTDs were carefully removed from the test section and calibrated using a precision dry block calibrator to ensure accurate reading values. The values obtained from the calibrator are entered into the LabView software that is used in the National instrument data acquisition system. once the calibration is complete, the thermocouples and RTDs are carefully placed back into their preset locations. The calibration device is shown in Figure B.5.

Figure B.5. Precision dry block calibrator

B.6. Thermal Conductivity Analyzer

The manufacturer of the PCM provides some information on the properties of the material, however, some required properties were measured. The thermal conductivity of the PCM was directly measured using a C-Therm thermal conductivity analyzer with an accuracy of better than 5% as shown in Figure B.6.

Figure B.6. Thermal conductivity analyzer

B.7. Differential Scanning Calorimetry (DSC)

The PCM melting and solidification temperatures, latent heat of fusion, heat flow, and other information is provided through the use of the TA-DSC2500. Different tests have been run in collaboration with the Chemistry department at the University of Windsor to confirm the reported data by the supplier. An initial sample weight of 2.24 mg was tested in small fully sealed crucible at (2, 10, 40, 60, 100) °C/min with a temperature range of 20 to 40°C to ensure the complete melting and solidification of the PCM sample. The sample weight then reduced to 1.06mg for more accurate results using smaller °C/min range. The peak and onset temperatures for the melting and freezing loops were measured and recorded. Figure B.7 shows the DSC machine that is used with the tray that holds the sample crucibles.
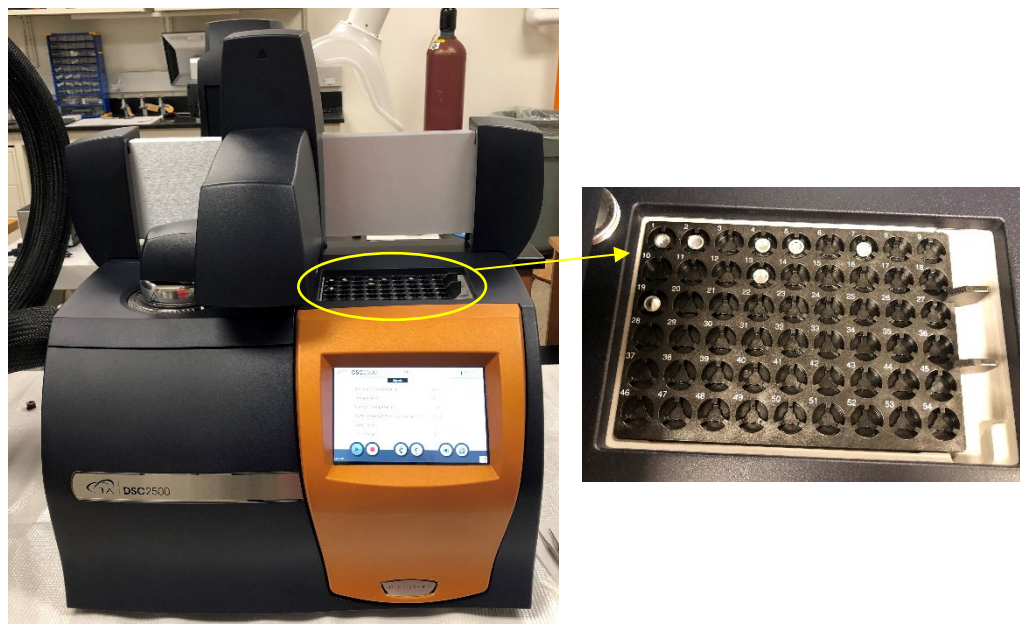
Figure B.7. TA DSC2500 (Curtesy of the Chemistry and Biochemistry Department)

APPENDIX C: PERMISSION/COPYRIGHTED MATERIAL

Letter of permission/ Journal of Applied Thermal Engineering

Letter of permission/Microtek Laboratories Inc.

VITA AUCTORIS

NAME: Serena Askar

PLACE OF BIRTH: Baghdad, Iraq

YEAR OF BIRTH: 1986

EDUCATION: University of Technology, BASc., Baghdad, Iraq, 2007

                   University of Windsor, MASc., Windsor, ON, Canada, 2011

                   University of Windsor, Ph.D., Windsor, ON, Canada, 2022